EVOLUTION OF OFFSHORE DREDGE PITS WITH APPLICATIONS TO THE BLACK SEA

by
Arzu Gözde Samancı
B.S. in C.E., Boğaziçi University, 2002

Submitted to the Institute for Graduate Studies in
Science and Engineering in partial fulfillment of
the requirements for the degree
of Master of Science

Graduate Program in Civil Engineering
Boğaziçi University
2005

EVOLUTION OF OFFSHORE DREDGE PITS WITH APPLICATIONS TO THE BLACK SEA

APPROVED BY:

Assoc. Prof. Emre Otay ....
(Thesis Supervisor)

Assoc. Prof. Osman Börekçi ....

Prof. Yalçın Yüksel ....

DATE OF APPROVAL: ....

When the solution is simple, God is answering.

Albert Einstein

ACKNOWLEDGEMENTS

I would like to thank to Dr. Otay for inspiring me to start this graduate program and for trusting and guiding me till the end of my study. I would like to thank to Dr. Börekçi for commenting on my study and helping me when I got into trouble. I would like to thank to Dr. Yalçın for his valuable comments on my study. I also would like to thank to Dr. Jette, Dr. Perlin and Dr. Stive for helping me when I asked for their help.

Anıl, I am very glad that we worked together. Thank you for your continuing support till the last day of my study. I would like to thank to Bilge, Cenk and Yavuz for everything we shared as a team and as friends.

Ercan, Sevinç, Zeynep and my family. Your presence has always been the greatest support to me.

ABSTRACT

EVOLUTION OF OFFSHORE DREDGE PITS WITH APPLICATIONS TO THE BLACK SEA

The present work investigates planform and profile evolutions of the dredge pits at the inner shelf. The governing equations are derived from the Bailard & Inman (1981) bed-load sediment transport equations, which are extended to account for the longshore gradients in the bathymetry caused by the dredge pit. The evolution of the pit is numerically modeled with a set of unsteady, nonlinear, partial differential equations. Long-term numerical test runs using a large range of wave and pit characteristics have lead to a number of dimensionless parameters, which control the fate of the dredge pit. The dredge pit is found to diffuse in the longshore and cross-shore directions at different backfilling rates, depending on wave and pit characteristics. The sensitivity analyses reveal that the Ursell number, relative wave length, and pit flatness control the half life of the pit. Under shore-normal waves, the dredging contour is found to diffuse symmetrically about the center of the pit. Under oblique waves, the pit migrates alongshore against the wave. To simulate long-term evolution of dredge pits under real field conditions, waves with varying height, period, angle and duration are used from statistics of the southwestern Black Sea. The half life of the backfilling is found to be on the order of decades, which is much shorter than the half life computed using a monochromatic wave with the average statistical wave parameters for the entire simulation. This result indicates that most of the backfilling occurs not during average wave conditions, but during seldom extreme waves.

ÖZET

AÇIK DENİZ TARAMA ÇUKURLARININ EVRİMİ VE KARADENİZ’E UYARLAMALARI

Bu çalışmada, surf bölgesinden uzakta (10m-30m) açılan tarama çukurlarının plan ve profildeki evrimi incelenmiştir. Bailard ve Inman (1981) sürüntü taşınım modeli, kıyıya paralel yöndeki zemin eğimin etkilerini içerecek şekilde yeniden geliştirilmiştir. Çukurun evrimi, değişken, doğrusal olmayan bir kısmi differensiyal denklemler setinin sayısal olarak çözülmesiyle modellenmiştir. Geniş kümeler halinde tanımlanan dalga ve çukur özellikleri ile yapılan uzun dönemli sayısal testler sonucu, çukurun evrimini kontrol eden bir grup boyutsuz parametre tanımlanmıştır. Tarama çukurunun planda ve profilde yayıldığı gözlemlenmiştir. Dolma hızı, dalga ve çukur özelliklerine bağlı olarak değişmektedir. Hassasiyet testlerine göre, Ursell sayısı, göreli dalga boyu ve çukur yassılığının çukurun yarılanma ömrünü kontrol ettiği belirlenmiştir. Kıyıya dik gelen dalgaların etkisi altında tarama kontürü, çukur ekseni etrafında simetrik bir şekilde yayılmaktadır. Kyıya açılı dalgalar çukurun dalgaya doğru kıyıya paralel yönde ilerlemesine sebep olmaktadır. Tarama çukurlarının uzun vadede gerçek dalga iklimi altındaki evrimi, güneybatı Karadeniz için geçerli istatistiklerden elde edilen değişken dalga yüksekliği, peryodu, açısı ve süresi kullanılarak modellenmiştir. Çukurun yarılanma ömrünün onyıllar mertebesinde olduğu gözlemlenmiştir. Bu süre, bu bölge için ortalama dalga özelliklerine sahip tekil bir dalganın devamlı etkisi altında gözlemlenen yarılanma ömründen çok daha kısadır. Bu sonuç, dolmanın çoğunun ortalama dalga koşulları altında değil de daha nadir aşırı dalga koşulları altında olduğunu göstermektedir.

TABLE OF CONTENTS

LIST OF FIGURES

LIST OF TABLES

LIST OF SYMBOLS/ABBREVIATIONS

A	Ratio of a_1 to a_2
a_1	Coefficient for the first order part of wave orbital velocity at bottom for second-order Stokes wave
a_2	Coefficient for the second order part of wave orbital velocity at bottom for second-order Stokes wave
C	Wave celerity from linear wave theory
C_0	Deep water wave celerity
C_g	Group velocity
c_f	Drag coefficient for the bed
D	Sediment diameter
d_p	Depth of the pit
E	Total average wave energy per unit surface area
F_p	Flatness of the pit
f	Darcy-Weisbach friction coefficient
g	Gravitational acceleration
H	Wave height
H_0	Deep water wave height
h	Water depth
h_d	Water depth before dredging at the dredging contour
$\hat{i}$	Unit vector in x-direction
$\vec{i}_t$	Time dependent immersed weight sediment transport rate
$\left\langle i_x \right\rangle$	Time averaged immersed weight bed-load sediment transport rate in x-direction
$\left\langle i_y \right\rangle$	Time averaged immersed weight bed-load sediment transport rate in y-direction
$\hat{j}$	Unit vector in y-direction
K	Constant of proportionality in immersed weight sediment transport rate equation

$\vec{k}$	Wave number vector
k_x	x-component of the wave number vector
k_y	y-component of the wave number vector
L	Wave length
L_0	Deep water wave length
L_p	Length of the pit
L_r	Relative wave length, L_0/h_d
m	Beach slope
N	The volume concentration of the sediment in the bed-load layer
p	Porosity of sediment
$\vec{q}$	Volumetric sediment transport rate
q_x	Longshore component of the sediment transport rate
q_y	Cross-shore component of the sediment transport rate
s	Specific gravity of sediment
$\mathbf{T}$	Granular-fluid stress tensor
T	Shear stress per unit area on bottom plane
T_{g_x}	Gravity component of T_{xz}
T_{g_y}	Gravity component of T_{yz}
T_{xz}	Component of granular-fluid stress tensor in the x-direction on the xy-plane
T_{yz}	Component of granular-fluid stress tensor in the y-direction on the xy-plane
T_0	Magnitude of the velocity-induced bed stress
T_{50}	Half life of the dredge pit
t	Time
$\vec{U}$	Granular fluid velocity vector
U_R	Ursell number
u	Cross-shore component of the steady current
$\vec{u}$	Total velocity vector
$\overline{u}$	Mean velocity vector
$\tilde{u}$	Oscillatory velocity vector
u_m	Amplitude of the wave orbital velocity at bottom
v	Longshore component of the steady current
W_p	Width of the pit

w	Total expended fluid power
x	Cross-shore direction showing onshore
x_s	Distance of the shoreline from the origin of the x-axis
y	Longshore direction showing to the right of an observer on the shore looking to the sea
Z_0	Thickness of the bed-load layer
α	The angle $\vec{k}$ makes with the y-axis (positive in the ccw direction), i.e. wave angle
α_0	Deep water wave angle
β	Bottom slope in the cross-shore direction
γ	Bottom slope in the longshore direction
$\vec{\nabla}_H$	Horizontal differential operator
δ	Direction of the flow above the bed-load layer from the x-axis
ε_b	Bed-load efficiency
θ	Direction of the steady current from the x-axis
κ	Breaker index
ν	Kinematic viscosity
ρ	Density of water
ρ_s	Dry density of the granular material
τ_b	Bed shear stress
ϕ	Internal friction angle of the granular material
ψ	Wave skewness
ω	Angular frequency
$\langle \; \rangle$	Time averaging operator
CEM	Coastal Engineering Manual
EBP	Equilibrium beach profile

1. INTRODUCTION

Planning and management of seabed resources will be of utmost importance in the near future. Apart from being used as an aggregate for concrete, it is predicted that sand will be massively mined for beach restorations, construction of artificial islands, and other recreational and/or landscaping purposes. Thus, in order to satisfy the need for such large amounts of sand, dredging at the inner shelf will be required. However, it is important to be able to predict the natural consequences of offshore dredging. This issue has two aspects: engineering and ecological aspects. Engineering aspects are considered mainly to consist of coastal erosion due to the backfilling of the pit, and due to the changes in wave field. The ecological effects, like the impact of dredging on the habitat, are not in the scope of this thesis.

In this study, the main goal is to predict the fate of a dredge pit depending on wave climate, water depth, and pit dimensions. The questions that require answers are: How does the pit evolve in time? Does backfilling occur? If yes, how fast does it occur, and where does the sand come from? Which is more preferable: backfilling of the pit or remaining of the pit as it is?

In order to be able to answer these questions, a tool is needed to quantitatively analyze and predict the sediment transport in the inner shelf. An engineering approach to deal with the problem is required. Factors controlling sediment transport include waves, currents, sediment characteristics and the bathymetry in the vicinity of the pit. The sediment transport in this region is highly complicated by the presence of turbulence due to bed forms such as ripples and bars, superposition of waves, and wave-current interactions.

The idea here is to construct an analogy between the evolution of the deformation of the dredging contour and the evolution of the shoreline in response to a beach fill project, which can be modeled by a relatively simple equation proposed by Pelnard-Considére (1956).

Among the available mathematical models, the time averaged immersed weight bed-load sediment transport model of Bailard and Inman (1981) was chosen. Their formulation is modified to account for the sediment transport due to the longshore bottom slopes caused by the presence of the pit. Since an analytical solution to the mathematical model was not available, a numerical model based on finite differences is constructed. By running the model for various cases, the answers to the questions listed above are sought. Some practical conclusions are drawn regarding the processes associated with the evolution of a dredge pit at the inner shelf.

2. BACKGROUND

The aim of this chapter is to review the necessary material to solve the problem defined. First, a review of some concepts that needs to be considered to handle the problem is provided. Then, existing studies on the morphological evolution of the dredge pit are summarized. Lastly the choice of the mathematical model employed is discussed.

2.1. Review of Relevant Concepts for Modeling Sediment Transport in the Inner Shelf

Sediment transport in the marine environment is still a subject of research, and due to the complex mechanisms involved, its theory is not well established yet. There are various techniques to measure the sediment transport in the field. However, they are expensive, and can not be repeated for the desired conditions. The laboratory experiments help to understand the processes, but they can only mimic the real situation to some limited extent. Scale effects are a big problem for sediment transport modeling under laboratory conditions. Another method is mathematical modeling. Mathematical models should be calibrated using experimental and observational data. Thus, approaches to model the sediment transport involve a proper combination of the above listed methods.

In general, there are two approaches to sediment transport modeling: the tractive force approach and the energetics approach. Sediment transport is defined as a function of bed shear stress in the former, and as a function of wave energy dissipation in the latter. For practical purposes, sediment transport is investigated by dividing it into a longshore and a cross-shore component; a decomposition obviously non-existent in nature. For detailed information about sediment transport one can refer to Fredsøe and Deigaard (1992), Coastal Engineering Manual, CEM, (2002), and Dean and Dalrymple (2004).

The continental shelf is the region beginning from the point of significant bed slope change and ending at the beginning of the steeper continental slope. The coastal shelf is subdivided into inner-, mid-, and outer zones in practice. However, mostly there are no geomorphic features on the shelf suggesting this division. One can find various depth limit suggestions for the inner shelf. In this work it is considered to be the region beginning from the closure depth and extending to a depth about 25-30 m where dredging operations can still be considered as being feasible.

Bailard and Inman (1981) derived equations for the time-averaged rate of bed-load transport rates induced by the time-varying motion of water particles and steady currents over a planar bed sloping in the cross-shore direction. Bagnold's energetics based sediment transport model for streams (Bagnold, 1963, 1966) was used as a basis. Bailard (1981) derived a total load sediment transport model. It is an extension of his work with Inman that accounts also for the suspended load sediment transport. This model predicts the local near-bottom sediment transport rates as a function of the near-bottom water velocity vector. Each mode of the sediment transport vector consists of a velocity-induced component parallel to the instantaneous velocity vector, and a gravity induced component directed downslope. Bailard and Inman (1981) further simplified their general formulation by differentiating between weak and strong longshore currents, relative to the wave orbital velocity. They deduced that this model was probably only applicable to plane bed conditions, because it was derived from linear momentum equilibrium and does not incorporate the effects of the phase-dependent sediment suspension associated with the vortex generation over the vortex ripple crest. They limited their model within the surf zone because near and within the surf zone the bed is mostly plane. Transition from ripples to plane bed occurs as the flow becomes stronger. Fredsøe and Deigaard (1992) define the transition criterion as the Shields number being around 0.8-1. There are other studies, mostly experimental, trying to define this transition. In those studies, the sediment is cohesionless and the bed load transport behaves as a granular-fluid shear layer.

There are two principal assumptions in the derivation of the time-averaged rate of bed-load sediment transport model by Bailard and Inman (1981):

- Instantaneous sediment transport rate is directly proportional to and responds immediately to the instantaneous energy dissipation rate (quasi-steadiness).
- The drag coefficient is constant.

The equilibrium beach profile (EBP) concept plays an important role in beach evolution. A very brief description would be to define it as that shape, a beach of specific grain size tries to attain under specific wave conditions, at which no net sediment transport occurs. Although changes in the wave parameters result in a new EBP, observations show that beaches indeed attain a dynamic equilibrium state. There are various studies about EBP's, however, there is no commonly accepted theory describing the physics of the process. Some theories are based on the wave energy dissipation; others are based on the local balance of forces acting on a sediment grain. For a review of EBP's, the reader may want to refer to Dean(1991), Inman et al. (1993), Larson et al. (1999), and Dean and Dalrymple (2004).

Inman et al. (1993) and Larson et al. (1999) divided the EBP into two parts: a bar-berm profile, extending from the berm crest to the breaking bar, and a shorerise profile, extending seaward from the breaking bar. The physical explanation for this division is that under breaking waves, the sediment transport is controlled by the intense turbulence due to breaking, and both bed-load and suspended sediment loads are significant. Under non-breaking waves, offshore of the breaking zone, the expected dominant transport mode is the bed-load transport. Inman et al. (1993) fitted two different parabolas to each region of the measured profiles and united them by the breaking bar. Larson et al. (1999) state, for profiles in equilibrium that the break point acts as a singularity and no sediment is transported into and out of the surf zone.

Another important concept related to the sediment transport is the depth of closure. Dean and Dalrymple (2004) give the definition of the depth of closure as:

> "The offshore depth beyond which profiles taken over time at a given site coincide is known as the depth of closure. Seaward of this depth, although the waves can move sediment, the net sediment transport does not result in significant changes in mean water depth."

However, thinking that the bottom sediment do not move offshore of the closure depth, would be a misconception. It only means that no net movement of sediment occurs till the equilibrium is disturbed.

The N-line model of Perlin and Dean (1983) was developed to simulate bathymetric changes in response to coastal structures. Initially, this model was implemented to model the evolution of the dredge pit. However, their sediment transport equations are found to be insufficient to cover the sediment movement throughout the inner shelf. They employed a fixed longshore distance vs. fixed depth grid with variable cross-shore distance, which is more convenient in order to track the contour change However, the wave equations and sediment transport formulations in literature are based on a grid system with fixed cross- and longshore grids, where depth varies from grid to grid. Thus, modification of the equations to be solved is necessary to handle variable grid spacing in cross-shore direction. In addition, the model cannot represent bars, since every depth contour must be single-valued.

In the past decade, researches have concentrated mostly on suspended sediment transport, mainly due to the difficulty of measuring the bed-load transport (Kleinhans, 2002) and due to the presence of the rippled beds, which cannot be modeled under sheet flow conditions.

2.2. State of the Art on Evolution of Dredge Pits

Kobayashi (1982), employing the tractive force approach, developed a model for the bed-load sediment transport on a gentle slope due to oscillatory flow and investigated the infilling of small-scale, symmetric trenches over horizontal bottoms. He assumed that suspended sediment is negligible in the absence of currents. The depth of the trench is assumed to be small compared with its width and with the water depth. Refraction of the waves is not taken into account and the wave orbital velocities are calculated using linear wave theory. He reasoned his choice of linear wave theory by saying that the dominant backfilling occurs due to the presence of the slope. The model was compared with two different field observations, where the water depth varies between 11-33 meters. He said that his model results are in qualitative agreement with the observations.

In order to predict the maintaining dredging volume for various channels, Van Rijn (1986) proposed a two-dimensional vertical mathematical model for suspended sediment transport by currents and waves. His model represents convection, diffusion, settling and sediment pick-up. The effect of the wave refraction on the sedimentation is found to be relatively small when the angle between the current and the channel axis is larger than 60°. The influence of the wave height variations over the channel on the sedimentation of the channel is found to be relatively small. Thus he concluded that a constant wave height can be assumed outside and inside the channel. The model is developed for non-breaking waves. The water depth outside the channel is assumed to be uniform.

Jensen et al. (1999) investigated the sediment transport across long, straight channels, such as navigational channels and pipeline trenches, under the effect of oblique currents. Later, Jensen and Fredsøe (2001), developed this approach further into a two-dimensional mathematical model to investigate the morphological evolution of small-scale excavations under the effect of phase-resolved oscillatory flow, i.e. the model is not based on time-averaged transport rates. Their model accounts both for the bed-load and the suspended load transports, and bed-load transport takes the effect of the gravity into account. Their purpose was to describe the backfilling of trenches through relevant non-dimensional parameters. The currents come perpendicular to the channel axis.

Sand Pit is a recent project founded by the EC Fifth Framework Program trying to answer coastal zone management questions related to the large-scale sand mining projects for the benefit of the end-users, such as policy makers and dredging engineers. The study aims to develop more sophisticated models to simulate the transport at the middle and lower shoreface. Through this, the aim is to model offshore sand pits. For further information about the project one may visit their website (http://sandpit.wldelft.nl).

In coastal engineering, it is accepted that the sediment transport is significant in a region extending from the outer break point shoreward to the beach, called the surf zone. The causes of the intense sediment transport in this region are the breaking waves and their associated currents. The region seaward of the break point up to a depth about 20-30 m is called the inner shelf, where bottom friction has again strong influence on sediment transport.

2.3. Selection of the Transport Model for the Present Study

The bed-load sediment transport model of Bailard and Inman (1981) is chosen as the formula to be used in this thesis to model the sediment transport. It can handle the transport in the inner shelf while most other sediment transport models consider only the surf zone.

The formulation of Bailard and Inman (1981) is considered to be the most transparent one among other bed-load sediment transport models. The effects of the gravity and the flow on the variation of sediment transport rates can be visualized easily.

Bailard and Inman (1981) differentiated between the bed-load sediment transport and the suspended sediment transport. Since seaward of breaking zone, bed-load is expected to dominate the suspended load; it allows us to consider only the bed-load. Another advantage of this choice over some other models is that it gives the magnitude and the direction of the transport at the same time.

The presence of ripples might cause fluctuations from the observations. As mentioned before, the model assumes quasi-steady bottom conditions, an assumption that can not explain the sediment suspension due to the vortex ripples. For the average wave conditions of the Southwest Black Sea, small ripples might be expected on the inner shelf. However, it is assumed that these ripples are sufficiently small for average wave conditions, and thus they have no effect on the sediment transport. For the more severe wave conditions, it is assumed that the transition from rippled bed to the plane bed conditions has already occurred.

3. DERIVATION OF BED-LOAD SEDIMENT TRANSPORT EQUATIONS

In this chapter the Bailard and Inman (1981) formula will be modified to include the effect of a longshore bottom slope, and the velocity moments will be incorporated into the model. The equation of conservation of mass and the sediment transport equations together define a mathematical model for the proposed problem.

3.1. Extension of Bailard and Inman (1981) Bed-Load Transport Equation for Longshore Sloping Bottoms

Bailard and Inman (1981) developed a mathematical model for the bed-load transport for a beach sloping in the cross-shore direction. They assumed that the longshore gradient of depth is zero. However, a pit has gradients of depth in both directions. The equations need to be modified to account for the local longshore slopes. In the following pages, some modification will be made to the bed-load sediment transport equations of Bailard and Inman (1981).

The problem geometry is shown in Figure 3.1. Initially, the x-axis (cross-shore) is sloping downwards with an angle *β,* the y-axis (longshore) is sloping to the right of an observer looking from the shore with an angle *γ*, and the z-axis is directed upwards. The origin is located at the top of the bed-load layer. The direction of the flow makes an arbitrary angle of δ to the x-axis. The equation of motion for steady-state fully developed granular flow in vectorial form is:

$$(\rho_s - \rho)N\vec{g} + \nabla\vec{\mathrm{T}} = 0 \qquad (3.1)$$

where N is the volume concentration of the sediment in the bed-load layer, $\vec{\mathrm{T}}$ is the granular-fluid stress tensor, ρ_s is the dry density of the granular material and ρ is the density of water.

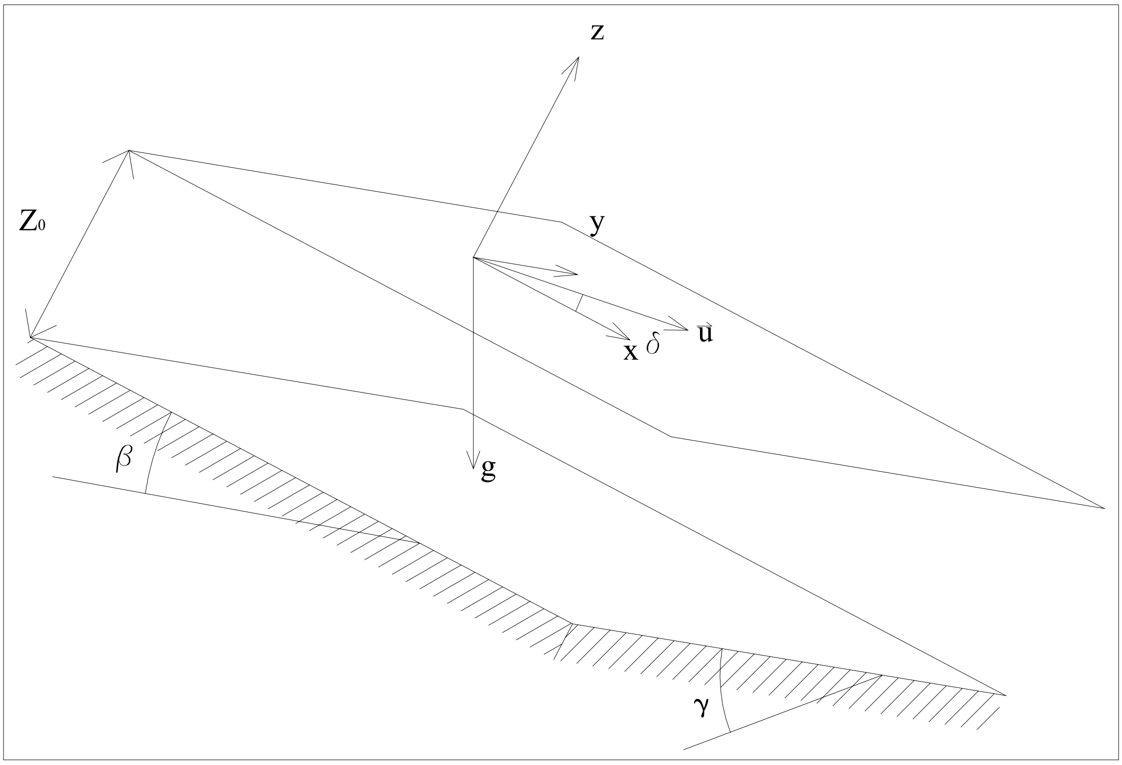

Figure 3.1. Definition sketch showing the bed-load layer

The boundary conditions at the top (z=0) and at the bottom (z=-Z_0) of the bed-load layer are given through Equations (3.2)-(3.5).

at *z=0*

$$T_{xz} = T_0 \cos\delta \tag{3.2}$$

$$T_{yz} = T_0 \sin\delta \tag{3.3}$$

$$T_{zz} = 0 \tag{3.4}$$

at $z=-Z_0$

$$\frac{|T|}{-T_{zz}} = \tan\phi \tag{3.5}$$

where T_0 is the magnitude of the velocity-induced bed stress, T is the shear stress per unit area on the bottom plane (x-y plane), T_{xz} is the component of granular-fluid stress tensor in the x-direction on a plane perpendicular to the z-axis (x-y plane), and ϕ is the internal friction angle of the granular material.

Integrating Equation (3.1) over the bed load layer, results in the following shear stresses on the x-y plane. The components of the weight are found by first assuming a plane sloping in x-direction only, and resolving it to its components: one in the x-y' plane, and one perpendicular to it. Then the whole setup is rotated about the x-axis by an angle of γ. The component of gravity perpendicular to x-y plane found previously is resolved further to its components since the y-z plane has been rotated, Figure 3.2. However, initially the bed is assumed to be sloping in the direction of flow as in Figure 3.1.

$$T_{xz} = -(\rho_s - \rho) g \sin\beta \int_0^{-Z_0} N dz + T_0 \cos\delta \tag{3.6}$$

$$T_{yz} = -(\rho_s - \rho) g \cos\beta \sin\gamma \int_0^{-Z_0} N dz + T_0 \sin\delta \tag{3.7}$$

$$T_{zz} = (\rho_s - \rho) g \cos\beta \cos\gamma \int_0^{-Z_0} N dz \tag{3.8}$$

where Z_0 is the thickness of the bed load layer.

The shear stress on the x-y plane is defined as in Equation (3.9). Thus, the shear stress at the base of the bed-load layer is given in Equation (3.10).

$$\vec{T} = T_{xz}\hat{i} + T_{yz}\hat{j} \tag{3.9}$$

$$\left.\vec{T}\right|_{z=-Z_0} = \left(T_{g_x} + T_0 \cos\delta\right)\hat{i} + \left(T_{g_y} + T_0 \sin\delta\right)\hat{j} \tag{3.10}$$

where

$$T_{g_x} = -(\rho_s - \rho) g \sin\beta \int_0^{-Z_0} N dz \tag{3.11}$$

$$T_{g_y} = -(\rho_s - \rho) g \cos\beta \sin\gamma \int_0^{-Z_0} N dz \tag{3.12}$$

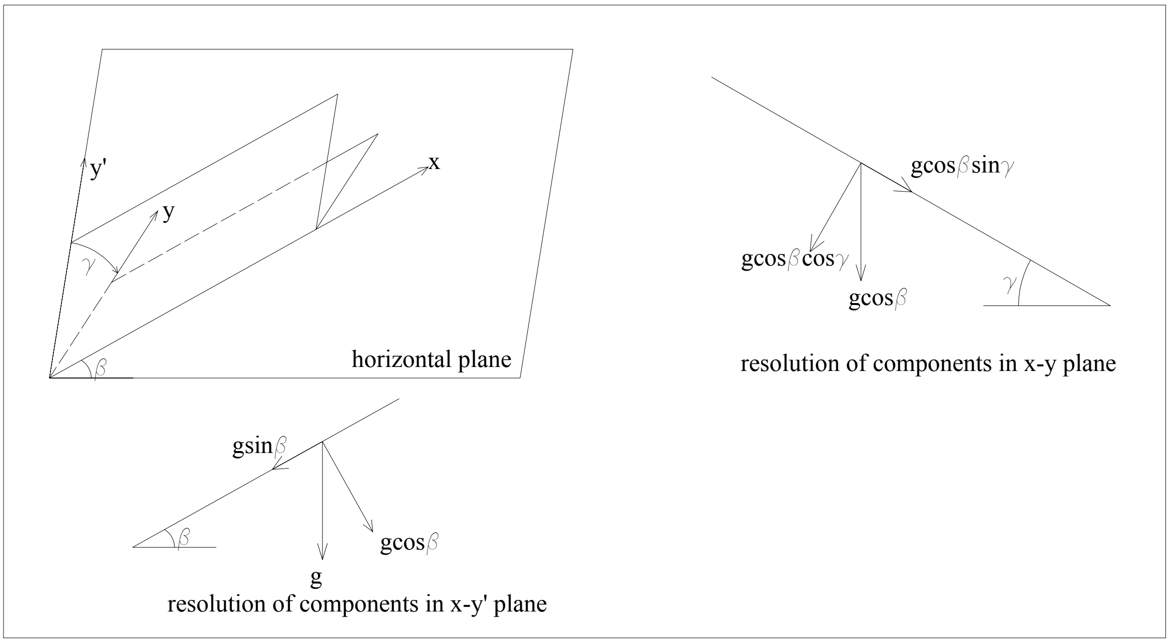

Figure 3.2. Definition of x-y plane and resolution of the weight and into its components

In order to obtain the magnitude of the shear stress on the x-y plane, Equation (3.10) is squared expanded.

$$|T|^2 = T_0^2 \left[\left[\frac{T_{g_x}}{T_0}\right]^2 + \left[\frac{T_{g_y}}{T_0}\right]^2 + 1 + 2\frac{T_{g_x}}{T_0}\cos\delta + 2\frac{T_{g_y}}{T_0}\sin\delta \right] \tag{3.13}$$

Assuming that $T_0 \gg T_{g_x}$ and $T_0 \gg T_{g_y}$, we can approximate Equation (3.13) by

$$|T|^2 = T_0^2 (\frac{T_{g_x}}{T_0}\cos\delta + \frac{T_{g_y}}{T_0}\sin\delta + 1)^2 \tag{3.14}$$

The magnitude of the shear stress on the x-y plane becomes

$$\left|T\right| \simeq T_{g_x}\cos\delta + T_{g_y}\sin\delta + T_0 \tag{3.15}$$

Equations (3.5), (3.8), (3.11), (3.12), and (3.15) can be combined in order to give

$$T_0 = -\left(\rho_s - \rho\right) g \cos\beta \left[\cos\gamma \tan\phi - \tan\beta \cos\delta - \sin\gamma \sin\delta\right] \int_0^{-Z_0} N dz \tag{3.16}$$

Bagnold (1963, 1966) defined the immersed weight sediment transport rate $\vec{i}_t$ to be a fraction of the total expended fluid power, *w*, that is

$$\left|\vec{i}\right| \propto w \tag{3.17}$$

$$w = T_0 \left|\vec{u}\right| \tag{3.18}$$

For a bed sloping in the cross-shore direction only, the immersed weight sediment transport is defined as:

$$\vec{i}_t = -\left(\rho_s - \rho\right) g \cos\beta \int_0^{-Z_0} N\vec{U} dz \tag{3.19}$$

where $\vec{U}$ is the granular fluid vector velocity

Since the component of the weight normal to the bottom is different for the present case, a bed sloping in both cross- and longshore directions, the modified immersed weight sediment transport $\vec{i}_t^*$ is defined as in

$$\vec{i}_t^* = -\left(\rho_s - \rho\right) g \cos\beta \cos\gamma \int_0^{-Z_0} N\vec{U} dz \tag{3.20}$$

Equations (3.16), (3.18), and (3.20) are combined to give the magnitude of $\vec{i}^*$

$$\left|\vec{i}_t^*\right| = \frac{w\varepsilon_b}{\left(\tan\phi - \dfrac{\tan\beta}{\cos\gamma}\left(\vec{u}/\left|\vec{u}\right|\cdot\hat{i}\right) - \tan\gamma\left(\vec{u}/\left|\vec{u}\right|\cdot\hat{j}\right)\right)} \tag{3.21}$$

where the bed-load efficiency $\varepsilon_b = \left(-\int_0^{-Z_0} N\left|\vec{U}\right|dz\right)\Big/\left(-\left|\vec{u}\right|\int_0^{-Z_0} Ndz\right)$. The bed-load efficiency is assumed to the same in both directions.

The direction of the immersed weight transport rate can be approximated by the ratio $T/\left\|T\right\|_{z=-Z_0}$.

$$\frac{T}{|T|} = \frac{\vec{u}}{\left|\vec{u}\right|}\left[1 - \frac{\tan\beta}{\tan\phi\cos\gamma}\left(\frac{\vec{u}}{\left|\vec{u}\right|}\cdot\hat{i}\right) - \frac{\tan\gamma}{\tan\phi}\left(\frac{\vec{u}}{\left|\vec{u}\right|}\cdot\hat{j}\right)\right] + \frac{\tan\beta}{\tan\phi\cos\gamma}\hat{i} + \frac{\tan\gamma}{\tan\phi}\hat{j} \tag{3.22}$$

When the magnitude and the direction of $\vec{i}_t^*$ are combined, the outcome is

$$\begin{gathered}\vec{i}_t^* = \frac{w\varepsilon_b}{\left(\tan\phi - \dfrac{\tan\beta}{\cos\gamma}\left(\vec{u}/\left|\vec{u}\right|\cdot\hat{i}\right) - \tan\gamma\left(\vec{u}/\left|\vec{u}\right|\cdot\hat{j}\right)\right)} \\ \left(\frac{\vec{u}}{\left|\vec{u}\right|}\left[1 - \frac{\tan\beta}{\tan\phi\cos\gamma}\left(\frac{\vec{u}}{\left|\vec{u}\right|}\cdot\hat{i}\right) - \frac{\tan\gamma}{\tan\phi}\left(\frac{\vec{u}}{\left|\vec{u}\right|}\cdot\hat{j}\right)\right] + \frac{\tan\beta}{\tan\phi\cos\gamma}\hat{i} + \frac{\tan\gamma}{\tan\phi}\hat{j}\right)\end{gathered} \tag{3.23}$$

Assuming that $T_0 = \rho c_f \vec{u}\cdot\vec{u}$ and further assuming that $\tan\phi \gg \tan\beta$ and $\tan\phi \gg \tan\gamma$ yields

$$\vec{i}_t^* \simeq \frac{\rho c_f \varepsilon_b}{\tan\phi}\left(\left|\vec{u}\right|^2\vec{u} + \frac{\tan\beta}{\tan\phi\cos\gamma}\left|\vec{u}\right|^3\hat{i} + \frac{\tan\gamma}{\tan\phi}\left|\vec{u}\right|^3\hat{j}\right) \tag{3.24}$$

However, unlike in a stream, in marine environment the bed slope is in the negative x-direction, as shown in Figure 3.2. Thus:

$$\vec{i}_t^* \simeq \frac{\rho c_f \varepsilon_b}{\tan\phi}\left(\left|\vec{u}\right|^2\vec{u} - \frac{\tan\beta}{\tan\phi\cos\gamma}\left|\vec{u}\right|^3\hat{i} + \frac{\tan\gamma}{\tan\phi}\left|\vec{u}\right|^3\hat{j}\right) \tag{3.25}$$

Averaging the equation above over a wave period gives the time-averaged bed-load sediment transport model on a bottom sloping in two-directions.

$$\left\langle \vec{i}_t^{\,*} \right\rangle = \frac{\rho c_f \varepsilon_b}{\tan\phi}\left(\left\langle |\vec{u}|^2\, \vec{u} \right\rangle - \frac{\tan\beta}{\tan\phi\cos\gamma}\left\langle |\vec{u}|^3 \right\rangle \hat{i} + \frac{\tan\gamma}{\tan\phi}\left\langle |\vec{u}|^3 \right\rangle \hat{j} \right) \tag{3.26}$$

For comparison purposes, the model of Bailard and Inman (1981), derived for cross-shore slope only, is shown in given below.

$$\left\langle \vec{i}_t \right\rangle = \frac{\rho c_f \varepsilon_b}{\tan\phi}\left(\left\langle |\vec{u}|^2\, \vec{u} \right\rangle - \frac{\tan\beta}{\tan\phi}\left\langle |\vec{u}|^3 \right\rangle \hat{i} \right) \tag{3.27}$$

The time averaging procedure is defined as $\left\langle f \right\rangle = \frac{1}{T}\int_t^{t+T} f\,dt$.

Equation (3.27) reveals that the original sediment transport equation consists of a wave induced component in the direction of the velocity vector $\vec{u}$, and a gravity component in the downslope, i.e. offshore, direction. The same pattern is valid for the modified version, described in Equation (3.26). However, since there are slopes in both directions, there is an additional component transporting sediment down the longshore slope. For both formulations, in order to achieve equilibrium on the beach, it is obvious that the wave induced transport has to be non-zero for non-zero bed slopes, a condition that can not be fulfilled with linear waves, since for linear waves the velocity moment $\left\langle |\vec{u}|^2\, \vec{u} \right\rangle$ is zero. This issue will be handled in detail later when the velocity moments are evaluated.

As shown in Figure 3.3, we assume that the velocity vector is composed of a steady, $\bar{u}$, and a time-varying, $\tilde{u}$, component

$$\vec{u} = \left(\bar{u}\cos\vartheta + \tilde{u}\cos\alpha\right)\hat{i} + \left(\bar{u}\sin\vartheta + \tilde{u}\sin\alpha\right)\hat{j} \tag{3.28}$$

However, inserting Equation (3.28) into Equation (3.26) is mathematically not very convenient. In order to simplify, Bailard and Inman (1981) considered two separate cases, one with weak longshore currents and one with strong longshore currents. Throughout this study, it is assumed that the waves are stronger than the currents, an assumption fairly valid for many beaches, especially at the inner shelf. From now on, only this case will be considered. Bailard and Inman (1981), following Liu and Dalrymple (1978), approximated the time averaged quantities in the equation above as

$$\begin{aligned}\left\langle \left|\vec{u}\right|^{2}\vec{u}\right\rangle \simeq &\left[\left\langle \tilde{u}^{3}\right\rangle \cos\alpha+\left\langle \tilde{u}^{2}\right\rangle \left(u+2u\cos^{2}\alpha+2v\sin\alpha\cos\alpha\right)\right]\hat{i}\\ &+\left[\left\langle \tilde{u}^{3}\right\rangle \sin\alpha+\left\langle \tilde{u}^{2}\right\rangle \left(v+2v\sin^{2}\alpha+2u\sin\alpha\cos\alpha\right)\right]\hat{j}\end{aligned} \tag{3.29}$$

$$\left\langle \left|\vec{u}_{t}\right|^{3}\right\rangle \simeq \left\langle \left|\tilde{u}\right|^{3}\right\rangle +3\left\langle \left|\tilde{u}\right|\tilde{u}\right\rangle \left(u\cos\alpha+v\sin\alpha\right) \tag{3.30}$$

where $u=\tilde{u}\cos\theta$ and $v=\tilde{u}\sin\theta$.

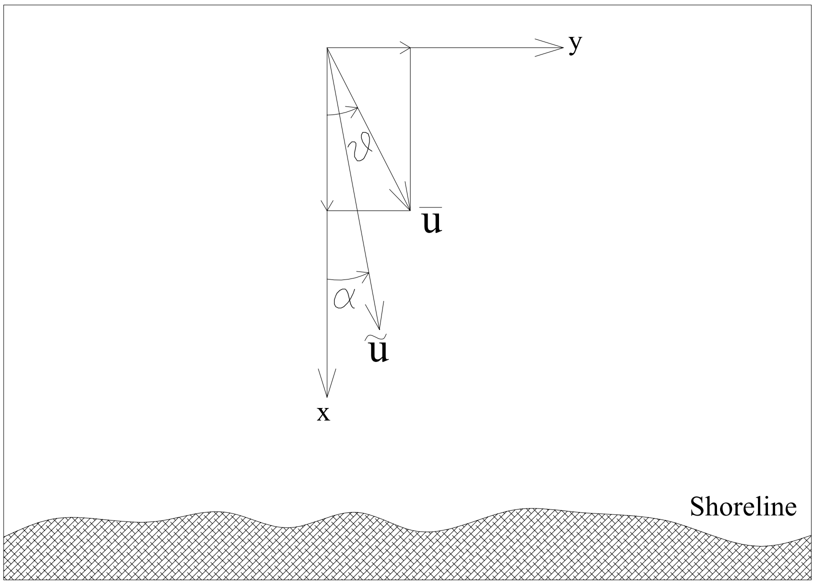

Figure 3.3. Definition of the total velocity

Substituting these approximations into the time-averaged immersed weight bed-load transport equation, Equation (3.25), and resolving it into its longshore and cross-shore components yields:

$$\left\langle i_{x}{}^{*}\right\rangle =\frac{\rho c_{f}\varepsilon_{b}}{\tan\phi}\left[\begin{array}{l}\left\langle \tilde{u}^{3}\right\rangle \cos\alpha+\left\langle \tilde{u}^{2}\right\rangle \left(u+2u\cos^{2}\alpha+2v\sin\alpha\cos\alpha\right)\\ -\dfrac{\tan\beta}{\tan\phi\cos\gamma}\left(\left\langle \left|\tilde{u}\right|^{3}\right\rangle +3\left\langle \left|\tilde{u}\right|\tilde{u}\right\rangle \left(u\cos\alpha+v\sin\alpha\right)\right)\end{array}\right] \tag{3.31}$$

$$\left\langle i_y{}^*\right\rangle = \frac{\rho c_f \varepsilon_b}{\tan\phi}\left[\begin{array}{l}\left\langle \tilde{u}^3\right\rangle \sin\alpha + \left\langle \tilde{u}^2\right\rangle\left(v + 2v\sin^2\alpha + 2u\sin\alpha\cos\alpha\right)\\ +\dfrac{\tan\gamma}{\tan\phi}\left(\left\langle\left|\tilde{u}\right|^3\right\rangle + 3\left\langle\left|\tilde{u}\right|\tilde{u}\right\rangle\left(u\cos\alpha + v\sin\alpha\right)\right)\end{array}\right] \tag{3.32}$$

The above formulations are valid for any wave and any current as long as the wave is stronger than the current. Assuming that only longshore currents exist, i.e. $u=0$, results in:

$$\left\langle i_x{}^*\right\rangle = \frac{\rho c_f \varepsilon_b}{\tan\phi}\left[\begin{array}{l}\left\langle \tilde{u}^3\right\rangle \cos\alpha + 2\left\langle \tilde{u}^2\right\rangle v\sin\alpha\cos\alpha\\ -\dfrac{\tan\beta}{\tan\phi\cos\gamma}\left(\left\langle\left|\tilde{u}\right|^3\right\rangle + 3\left\langle\left|\tilde{u}\right|\tilde{u}\right\rangle v\sin\alpha\right)\end{array}\right] \tag{3.33}$$

$$\left\langle i_y{}^*\right\rangle = \frac{\rho c_f \varepsilon_b}{\tan\phi}\left[\begin{array}{l}\left\langle \tilde{u}^3\right\rangle \sin\alpha + \left\langle \tilde{u}^2\right\rangle v\left(1 + 2\sin^2\alpha\right)\\ +\dfrac{\tan\gamma}{\tan\phi}\left(\left\langle\left|\tilde{u}\right|^3\right\rangle + 3\left\langle\left|\tilde{u}\right|\tilde{u}\right\rangle v\sin\alpha\right)\end{array}\right] \tag{3.34}$$

For weak longshore currents one can write the relation

$$\frac{\left\langle\left|\tilde{u}\right|\tilde{u}\right\rangle}{\left\langle\tilde{u}^3\right\rangle} \propto \frac{v}{u_m} \ll 1 \tag{3.35}$$

This brings forth further simplifications to Equations (3.33) and (3.34).

$$\left\langle i_x{}^*\right\rangle = \frac{\rho c_f \varepsilon_b}{\tan\phi}\left[\left\langle \tilde{u}^3\right\rangle \cos\alpha + 2\left\langle \tilde{u}^2\right\rangle v\sin\alpha\cos\alpha - \frac{\tan\beta}{\tan\phi\cos\gamma}\left\langle\left|\tilde{u}\right|^3\right\rangle\right] \tag{3.36}$$

$$\left\langle i_y{}^*\right\rangle = \frac{\rho c_f \varepsilon_b}{\tan\phi}\left[\left\langle \tilde{u}^3\right\rangle \sin\alpha + \left\langle \tilde{u}^2\right\rangle v\left(1 + 2\sin^2\alpha\right) + \frac{\tan\gamma}{\tan\phi}\left\langle\left|\tilde{u}\right|^3\right\rangle\right] \tag{3.37}$$

Noting from Figure (3.2) that $\tan\beta = -\dfrac{\partial h}{\partial x}$ and $\tan\gamma = \dfrac{\partial h}{\partial y}$, Equations (3.34) and (3.35) can be rewritten as

$$\left\langle i_x^{\ *}\right\rangle = \frac{\rho c_f \varepsilon_b}{\tan\phi}\left[\left\langle \tilde{u}^3\right\rangle \cos\alpha + 2\left\langle \tilde{u}^2\right\rangle v \sin\alpha\cos\alpha + \frac{\left\langle \left|\tilde{u}\right|^3\right\rangle}{\tan\phi\cos\gamma}\frac{\partial h}{\partial x}\right] \tag{3.38}$$

$$\left\langle i_y^{\ *}\right\rangle = \frac{\rho c_f \varepsilon_b}{\tan\phi}\left[\left\langle \tilde{u}^3\right\rangle \sin\alpha + \left\langle \tilde{u}^2\right\rangle v\left(1+2\sin^2\alpha\right) + \frac{\left\langle \left|\tilde{u}\right|^3\right\rangle}{\tan\phi}\frac{\partial h}{\partial y}\right] \tag{3.39}$$

The volumetric sediment transport rate $\vec{q}$ is related to the immersed weight sediment transport rate $\vec{i}$ by the relation

$$\vec{q} = \frac{\vec{i}}{\rho g\left(s-1\right)\left(1-p\right)} \tag{3.40}$$

where s is the specific gravity of the sediment, and p is the porosity of the bed. The longshore and cross-shore components of the volumetric sediment transport then are

$$\left\langle q_x^{\ *}\right\rangle = K\left[\left\langle \tilde{u}^3\right\rangle \cos\alpha + 2\left\langle \tilde{u}^2\right\rangle v \sin\alpha\cos\alpha + \frac{\left\langle \left|\tilde{u}\right|^3\right\rangle}{\tan\phi\cos\gamma}\frac{\partial h}{\partial x}\right] \tag{3.41}$$

$$\left\langle q_y^{\ *}\right\rangle = K\left[\left\langle \tilde{u}^3\right\rangle \sin\alpha + \left\langle \tilde{u}^2\right\rangle v\left(1+2\sin^2\alpha\right) + \frac{\left\langle \left|\tilde{u}\right|^3\right\rangle}{\tan\phi}\frac{\partial h}{\partial y}\right] \tag{3.42}$$

where $K = \dfrac{c_f \varepsilon_b}{g\tan\phi\left(s-1\right)\left(1-p\right)}$.

3.2. Derivation of Expressions for Velocity Moments

3.2.1. Velocity Moments Based on Second-order Stokes Waves

In order to calculate the sediment transport rates, we need to evaluate the velocity moments in the equations above. As mentioned in the previous section, a pure sinusoidal wave causes the wave-induced component of the cross-shore sediment transport to vanish. As a result the gravity-induced component of the cross-shore sediment transport carries sediments in the offshore direction until the bed slope becomes zero. In this model, the mechanism pushing the sediment onshore is the wave skewness. Since under a nonlinear wave, the transport under the wave crest in the onshore direction is greater than the transport under the trough in the offshore direction, the model calculates net onshore sediment movement on a horizontal bottom. Comparison of the horizontal velocities under a linear and second-order Stokes wave is shown in Figure 3.4.

From the discussion above, it follows that a nonlinear wave theory is necessary. The second-order Stokes wave is chosen as the wave theory. However, it should be noted that Stokes expansion method is not valid for shallow water. The range of validity is defined as the region where Ursell Number, $U_R<26$ (Dean and Dalrymple, 1984). The Ursell Number is defined as

$$U_R = \frac{L^2 H}{h^3} \tag{3.43}$$

where L is the wave length, H is the wave height, and h is the water depth.

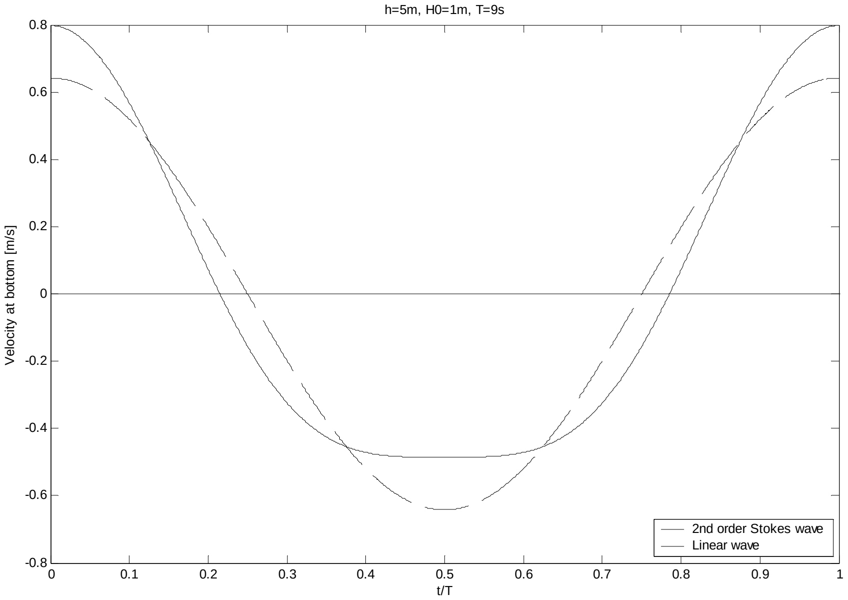

Figure 3.4. Comparison of horizontal bottom velocity profile under a linear wave and a second-order Stokes wave

For the depths considered, a higher order Stokes approximation could be a more appropriate wave representation. However for simplicity, a second-order Stokes wave is assumed.

The horizontal wave orbital velocity at the bottom under a second-order Stokes wave is defined as

$$\begin{aligned}\tilde{u}_b(t) &= \frac{H\omega}{2}\frac{\cos\omega t}{\sinh kh} + \frac{3H^2\omega k}{16}\frac{\cos 2\omega t}{\sinh^4 kh} \\ &= u_m \cos\omega t + \frac{3u_m^2}{4C\sinh^2 kh}\cos 2\omega t \\ &= a_1 \cos\omega t + a_2 \cos 2\omega t\end{aligned} \tag{3.44}$$

where

$$a_1 = u_m \tag{3.45}$$

$$a_2 = \frac{3u_m^2}{4C\sinh^2 kh} \tag{3.46}$$

$$u_m = \frac{H\omega}{2\sinh kh} \tag{3.47}$$

$\omega = 2\pi/T$, $k = 2\pi/L$ and C is the wave celerity from the linear wave theory. The dispersion equation for the linear wave theory is also valid for the second-order Stokes approach.

$$\omega^2 = gk\tanh kh \tag{3.48}$$

In the range of validity of second-order Stokes approach, the velocity moments $\left\langle \tilde{u}_b^2 \right\rangle$ and $\left\langle \tilde{u}_b^3 \right\rangle$ are computed to be:

$$\left\langle \tilde{u}_b^2 \right\rangle = \frac{a_2^2}{2}\left(A^2+1\right) \tag{3.49}$$

$$\left\langle \tilde{u}_b^3 \right\rangle = \frac{3}{4}a_2^3 A^2 \tag{3.50}$$

where $A = \frac{a_1}{a_2}$.

The moment $\left\langle \left|\tilde{u}_b\right|^3 \right\rangle$ is calculated numerically.

3.2.2. Approximation to the Velocity Moments Based on Linear Wave Theory

Guza and Thornton (1985) noticed that the dependency of the even velocity moments are not critically affected by the wave asymmetry. The error associated with the employment of the linear versions of the even moments is acceptable.

$$\left\langle \tilde{u}_b^2 \right\rangle = \frac{a_1^2}{2} \tag{3.51}$$

$$\left\langle \left|\tilde{u}_b\right|^3 \right\rangle = \frac{4a_1^3}{3\pi} \tag{3.52}$$

Stive (1986), based on the work of Flick et al. (1981), says that the odd velocity moments vanish in the surf zone. Starting from this, we can say that $\left\langle \tilde{u}_b^3 \right\rangle = 0$, for $U_R > 26$, where Equation (3.50) is not valid. In fact, this does not have much importance for this study since the focus of this study is the offshore zone beyond the breaking bar.

3.3. Summary of Primitive Equations for Nonlinear Waves with Significant Incidence Angles and Weak Longshore Currents

For this general case, it is not convenient to get a single formula giving the change of water depth in time due to the complexity of each term constituting the formulation. Even if such a complex expression is evaluated, it would not be easy to draw conclusions just by looking at it nor would it be easy to code such an expression to solve it numerically. Rather, solving a set of equations is better. The first of the governing equations is the conservation of sediment mass

$$\frac{\partial h}{\partial t} = \frac{\partial q_x}{\partial x} + \frac{\partial q_y}{\partial y} \tag{3.53}$$

The transport rates and the velocity moments, needed to evaluate these transport rates, are summarized in Equation (3.54).

$$\left\langle q_x^{\ *}\right\rangle = K\left[\left\langle \tilde{u}^3\right\rangle \cos\alpha + 2\left\langle \tilde{u}^2\right\rangle v \sin\alpha\cos\alpha + \frac{\left\langle \left|\tilde{u}\right|^3\right\rangle}{\tan\phi\cos\gamma}\frac{\partial h}{\partial x}\right]$$

$$\left\langle q_y^{\ *}\right\rangle = K\left[\left\langle \tilde{u}^3\right\rangle \sin\alpha + \left\langle \tilde{u}^2\right\rangle v\left(1+2\sin^2\alpha\right) + \frac{\left\langle \left|\tilde{u}\right|^3\right\rangle}{\tan\phi}\frac{\partial h}{\partial y}\right]$$

$$\left\langle \tilde{u}_b^2\right\rangle = \frac{a_2^2}{2}\left(A^2+1\right) \tag{3.54}$$

$$\left\langle \left|\tilde{u}_b\right|^3\right\rangle = \frac{1}{T}\int_t^{t+T}\left|\tilde{u}_b(t)\right|^3 dt$$

$$\left\langle \tilde{u}_b^3\right\rangle = \frac{3}{4}a_2^3 A^2$$

3.4. Derivation of a Combined Governing Equation for Quasi-linear Shore-normal Waves

In order to get a simple governing equation, some additional assumptions can be made. With the assumption of shore-normal waves, no ambient longshore currents, and small longshore bottom slope Equations (3.39) and (3.40) reduce to

$$\left\langle q_x^{\ *}\right\rangle = K\left[\left\langle \tilde{u}^3\right\rangle + \frac{\left\langle \left|\tilde{u}\right|^3\right\rangle}{\tan\phi}\frac{\partial h}{\partial x}\right] \tag{3.55}$$

$$\left\langle q_y^{\ *}\right\rangle = K\frac{\left\langle \left|\tilde{u}\right|^3\right\rangle}{\tan\phi}\frac{\partial h}{\partial y} \tag{3.56}$$

However, these assumptions might be more proper for a section going through the middle of the pit.

By noting that the ratio $\left\langle \tilde{u}_b^3\right\rangle \big/ \left\langle \left|\tilde{u}_b\right|^3\right\rangle$ is called the wave skewness, ψ, of the oscillatory wave motion, Equation (3.52) is rewritten as

$$\left\langle q_x^{\ *}\right\rangle = K\left\langle \left|\tilde{u}\right|^3\right\rangle\left[\psi + \frac{1}{\tan\phi}\frac{\partial h}{\partial x}\right] \tag{3.57}$$

Inserting the transport equations into the continuity equation, Equation (3.50) results in

$$\frac{\partial h}{\partial t}=K\frac{\partial}{\partial x}\left[\left\langle\left|\tilde{u}\right|^{3}\right\rangle\left(\psi+\frac{1}{\tan\phi}\frac{\partial h}{\partial x}\right)\right]+K\frac{\partial}{\partial y}\left[\frac{\left\langle\left|\tilde{u}\right|^{3}\right\rangle}{\tan\phi}\frac{\partial h}{\partial y}\right] \tag{3.58}$$

Based on the work of Guza and Thornton (1985), as discussed previously, the linear even velocity moments are employed. Substitution of the velocity moments into the equation above gives the relation between the change of depth and the wave conditions to be as

$$\frac{\partial h}{\partial t}=\frac{4K}{3\pi\tan\phi}\left[u_m^3\left(\frac{\partial^2 h}{\partial x^2}+\frac{\partial^2 h}{\partial y^2}\right)+\left(\frac{\partial u_m^3}{\partial x}\frac{\partial h}{\partial x}+\frac{\partial u_m^3}{\partial y}\frac{\partial h}{\partial y}\right)\right]+\frac{9K}{16}\frac{\partial}{\partial x}\left(\frac{u_m^4}{C\sinh^2 kh}\right) \tag{3.59}$$

or

$$\frac{\partial h}{\partial t}=\frac{4K}{3\pi\tan\phi}\vec{\nabla}\cdot\left(u_m^3\vec{\nabla}h\right)+\frac{9K}{16}\frac{\partial}{\partial x}\left(\frac{u_m^4}{C\sinh^2 kh}\right) \tag{3.60}$$

However, further simplification of the formula could not be achieved and an analytical solution for the problem could not be found.

3.5. Remarks on the Equilibrium Beach Profile and Wave Skewness

In order to investigate the bathymetric changes due to the presence of the pit only, the initial beach profile is taken as the EBP proposed by Bailard and Inman (1981). In fact, any other choice of the initial profile would result in an ambient transport, even if there is no pit, because there is a unique profile at which any cross-shore sediment transport equation predicts zero transport. Any initial profile other than the inherent EBP will be shaped until the profile adjusts itself to the inherent EBP. Any observation made during this period would include the effect of the ambient transport too. However, it is doubtful if the ultimate EBP can be ever reached as the sediment supply or the geologic properties of the region may not allow it.

The EBP proposed by Bailard and Inman (1981) is obtained by setting the cross-shore sediment transport equation equal to zero. For an arbitrary wave angle with a longshore current, the EBP is obtained from Equation (3.31).

$$\tan\beta = \frac{\left\langle \tilde{u}_b^3 \right\rangle \cos\alpha + \left\langle \tilde{u}_b^2 \right\rangle \sin 2\alpha}{\left\langle \left|\tilde{u}_b\right|^3 \right\rangle + 3\left\langle \left|\tilde{u}_b\right| \tilde{u}_b \right\rangle v \sin\alpha} \cos\gamma \tan\phi \qquad (3.61)$$

For the simplest case where there is no steady current and the wave approach angle is zero, the EBP is given by

$$\tan\beta = \tan\phi \frac{\left\langle \tilde{u}_b^3 \right\rangle}{\left\langle \left|\tilde{u}_b\right|^3 \right\rangle} = \psi \tan\phi \qquad (3.62)$$

The EBP is mainly a function of the wave parameters. Equations (3.61) and (3.62) suggest that the local equilibrium beach slope changes according to the water depth, and wave and current parameters. However, this formulation predicts no relation between the EBP and the sediment size. The only term related to the sediment is the internal friction angle, and it is mainly a function of sediment sphericity and the relative size of the grains in the stack. However, since uniform spherical grains are assumed, sediment does not have an effect on EBP according to this approach.

The evaluated EBP for specific wave conditions exhibits a very steep shallow portion and a very flat deeper portion. Bailard (1981) also points to the unnaturally steep beach slopes predicted by the model for shallow waters. This can be justified by recalling that the Stokes wave theory is not valid in shallow water.

4. NUMERICAL SOLUTION OF THE PIT EVOLUTION PROBLEM

A numerical model is constructed, to simulate the sediment transport at depths of 10-30 meters under moderate wave conditions where the ratio of suspended transport to bed-load transport is small. Thus suspended load is neglected. In this section, the discretization of the differential equations and the boundary conditions are presented.

A simple numerical scheme based on Snell's law and the conservation of energy will be used for the refraction and shoaling of the waves. Bed-load transport in both directions can be calculated for different wave height, period, incidence angle, and weak ambient longshore current combinations. However, since the wave induced currents in the inner shelf vanish, the model does not take them into account.

The present model can not simulate the sediment transport near and within the surf zone. Thus, it is not appropriate for shoreline modeling. However, outside the closure depth, it is expected that the model gives reasonable results.

Finite differencing is employed to solve the equations.

4.1. Governing Primitive Equations in Discretized Form

The definition sketch of a computational cell is shown in Figure 4.1. A staggered grid system, where the cross-shore and longshore transport rates are defined between the depth grids, is employed. The grids are regularly spaced in both directions (Figure 4.2).

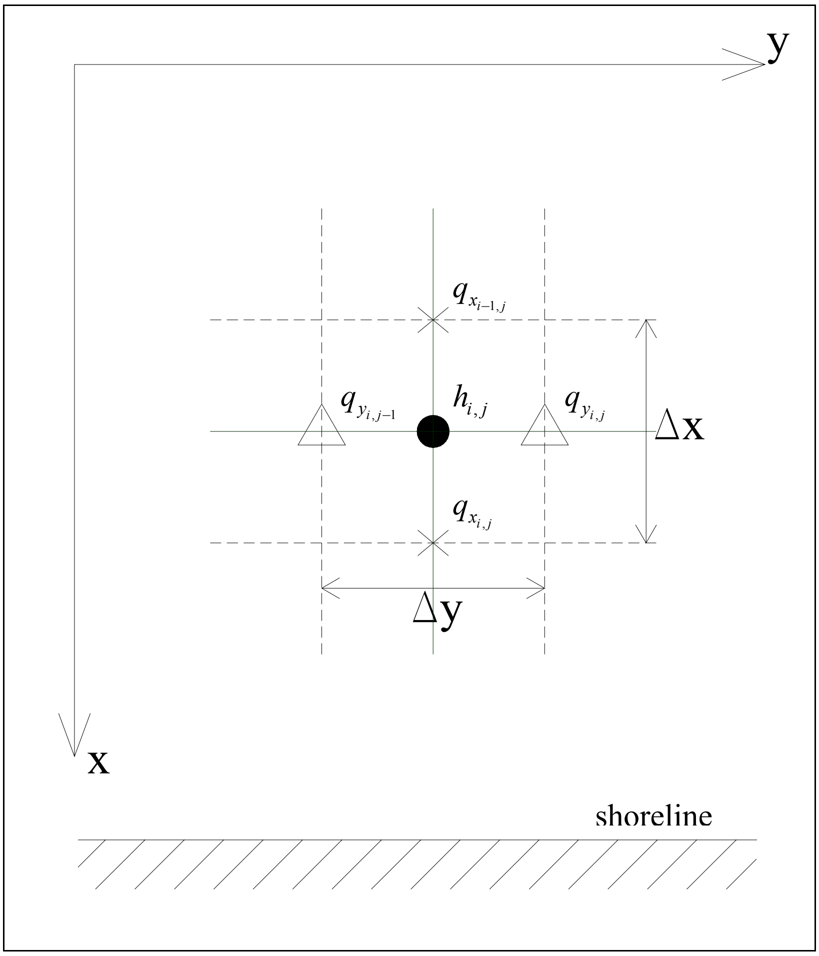

Figure 4.1. Definition of computational grid

The derivatives, except the time derivative, are central differenced, having errors on the order of *O(Δx²)*and *O(Δy²)* in both directions. The time derivative is discretized by forward differencing. The equations are solved explicitly. Thus care has to be taken of the stability issue.

$$\left(\frac{\partial h}{\partial t}\right)_{i,j} = \frac{h_{i,j}^{n+1} - h_{i,j}^{n}}{\Delta t} \tag{4.1}$$

$$\left(\frac{\partial q_x}{\partial x}\right)_{i,j} = \frac{q_{x_{i,j}}^{n} - q_{x_{i-1,j}}^{n}}{\Delta x} \tag{4.2}$$

$$\left(\frac{\partial q_y}{\partial y}\right)_{i,j} = \frac{q_{y_{i,j}}^{n} - q_{y_{i,j-1}}^{n}}{\Delta y} \tag{4.3}$$

$$\left(\frac{\partial h}{\partial x}\right)_{i,j} = \frac{h_{i+1,j} - h_{i-1,j}}{2\Delta x} \tag{4.4}$$

$$\left(\frac{\partial h}{\partial y}\right)_{i,j} = \frac{h_{i,j+1} - h_{i,j-1}}{2\Delta y} \tag{4.5}$$

where h is the water depth, q_x is the rate of time-averaged bed-load sediment transport in the cross-shore direction, and q_y is the rate of time-averaged bed-load sediment transport in the longshore direction. The x-axis shows the shore-normal and y-axis shows the shore-parallel directions. The origin is located in deep water at an appropriate location for the offshore end of the model grid. The shoreline is located at $x=x_s$.

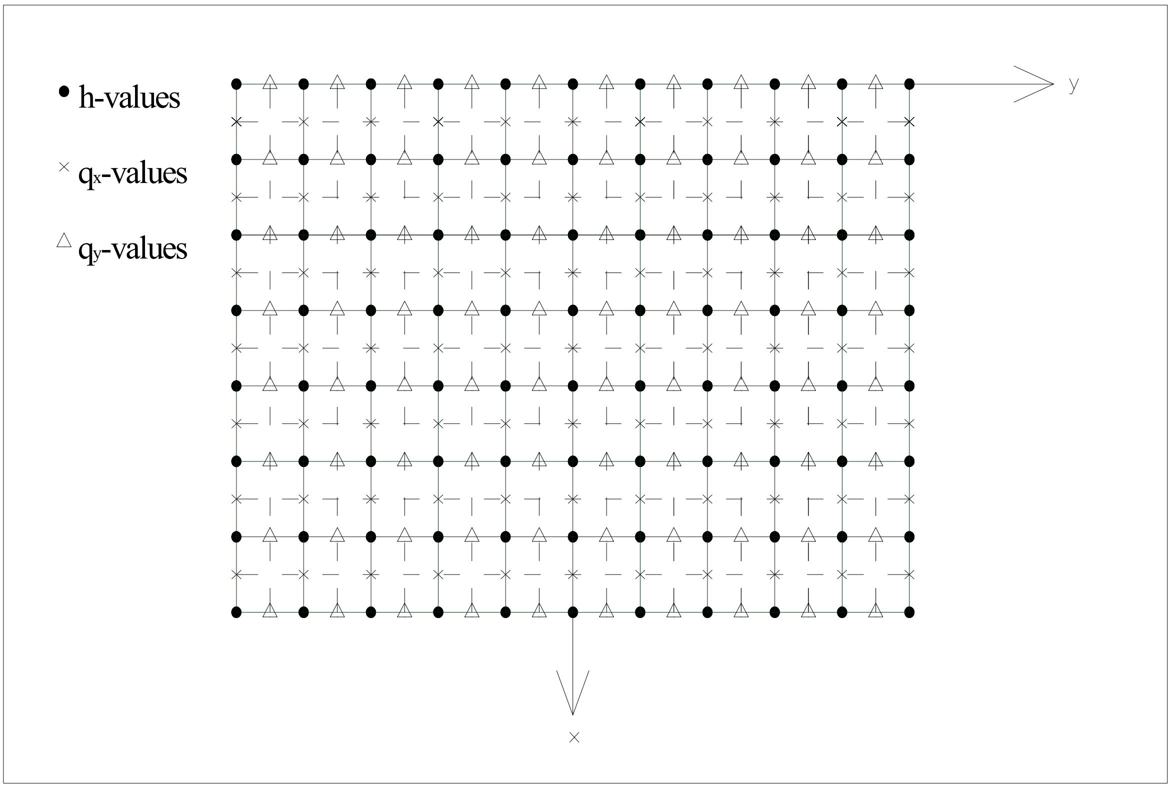

Figure 4.2. Plan view of the discretized computational domain

The velocity moments and the wave angles are computed for grids, where transport rates are defined. The flowchart of the model is shown in Figure 4.3.

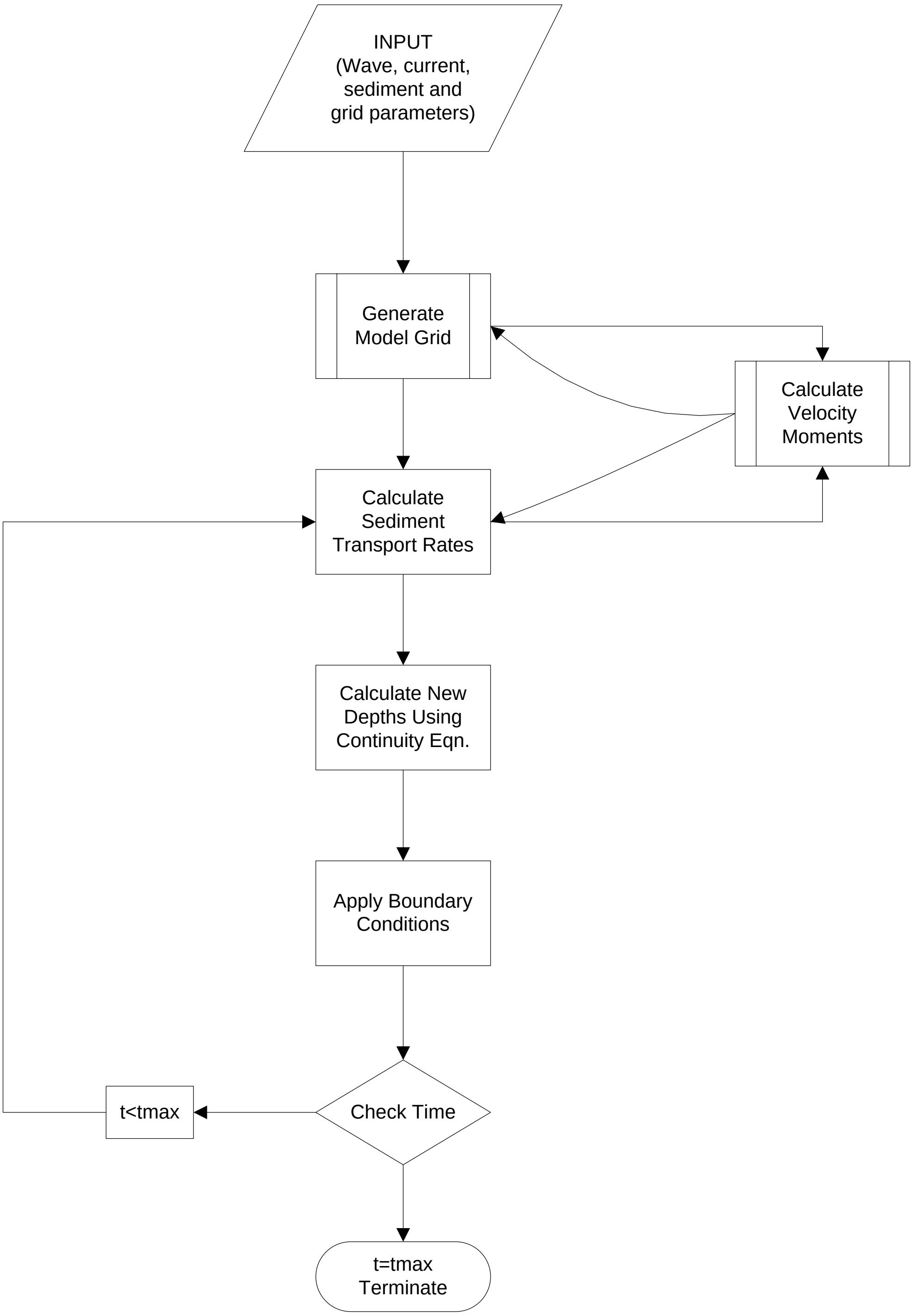

Figure 4.3. Program flowchart

4.2. Transformation of Waves

The conservation of waves equation needs to be solved for the refraction of waves

$$\vec{\nabla} \times \vec{k} = 0 \tag{4.6}$$

For straight and parallel contours, it reduces to the Snell's law.

$$\frac{\sin \alpha}{C} = \frac{\sin \alpha_0}{C_0} \tag{4.7}$$

Local wave angles in this model are calculated using Snell's law.

Conservation of energy equation gives the local wave heights by neglecting energy dissipation due to friction, percolation, and turbulence.

$$\vec{\nabla} \cdot \left(E \vec{C}_g \right) = 0 \tag{4.8}$$

For the case of straight and parallel contours, the shoaling and refraction coefficients are calculated from a simplification of the conservation of energy equation, to determine the local wave heights.

$$H = H_0 \sqrt{\frac{C_0}{2C_g}} \sqrt{\frac{\cos \alpha_0}{\cos \alpha}} \tag{4.9}$$

The model domain is restricted to non-breaking waves (outside the surf zone). Diffraction around the pit is not considered.

To update the velocity field at every time step is thought to be important at depths of interest since the transport rates due to the wave are very small in magnitude. However, it is also important that the wave module of the model works rapidly. Thus employment of a more sophisticated publicly available model that can solve combined refraction-diffraction of waves over irregular topography based on Stokes perturbation method is not preferred

4.3. Representation of the Pit

In this work, the effect of the dredge pit on the shoreline is not examined. However, deformation of the shoreline is an important consequence of dredging. Guidelines proposed by Demir et al. (2004) are employed to compensate for this lack in this work. The guidelines they proposed to reduce the undesired effects of the pit on the shoreline are

- The shore-perpendicular dimension of the pit should be as small as possible.
- The side slopes of the pit should be mild.
- The depth of the pit should be small.
- The increase of the longshore dimension of the pit does not have a crucial effect on the shoreline.

Following the guidelines above, the pit is represented by a change of the depth values at grids corresponding to the dredging depth. Shortly, the model assumes a strip-like pit, parallel to the shoreline as shown in Figure 4.4.

4.4. Boundary Conditions

At the offshore model boundary, the depth is assumed to be constant in time. At the lateral and onshore model boundaries, the bottom slopes in both directions are assumed to be constant throughout the duration of the simulation.

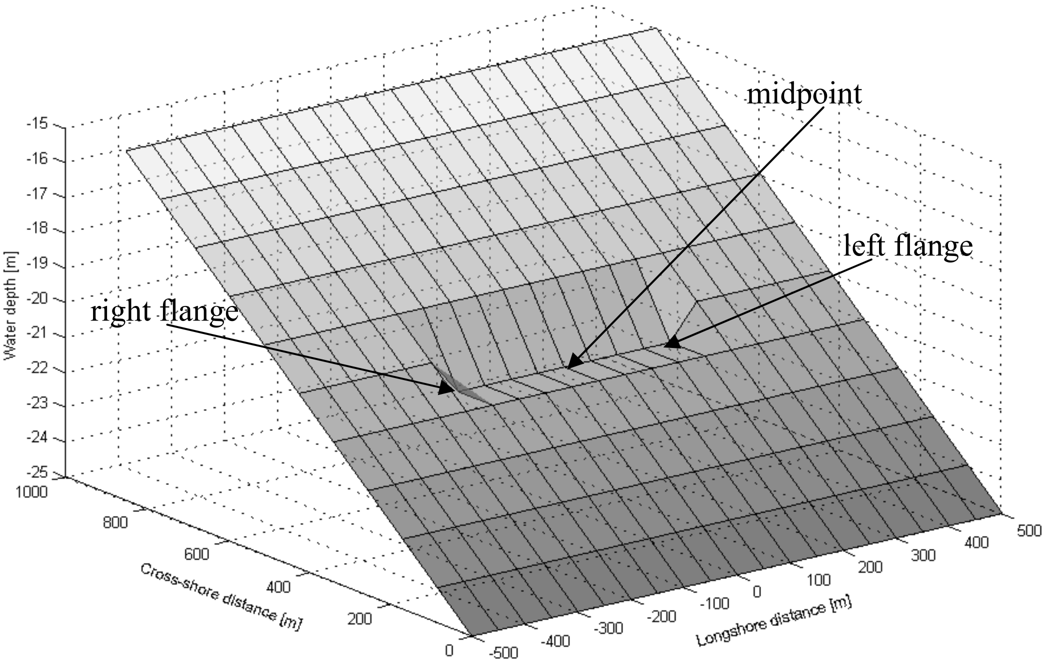

Figure 4.4. Representation of the pit by an increase of the depth at the grids corresponding to the dredging area

5. MODEL OUTCOMES

Discussion of the model outcomes presented in this chapter enables one to get some insight into the backfilling mechanism of a dredge pit in the inner shelf. The model is applied on two distinct cases: a hypothetical pit on a hypothetical bathymetry, which is in equilibrium according to the model of Bailard and Inman (1981) before dredging, and an imaginary pit on the typical bathymetry measured in the Kilyos region.

The dredge pits are investigated for their profile and planform (contour) evolutions, in a time interval of hundred years. The sensitivity of the backfilling of the pit to the wave characteristics and the pit geometry is investigated.

As a quantitative measure of the backfilling, the half life, T_{50}, of the pit is chosen as the representative parameter. The independent non-dimensional parameters are the Ursell number U_r and the relative wave length L_r.

$$U_r = \frac{H_0 L_0^2}{h_d^3} \tag{5.1}$$

$$L_r = \frac{L_0}{h_d} \tag{5.2}$$

In all plots in this section, the origin of the cross-shore direction (x-axis) is translated to coincide with the midpoint of the pit for convenience.

5.1. Hypothetical Case

Relying on the discussion in Section 3.5, the initial bathymetry for the hypothetical case is chosen to be the EBP resulting from Bailard and Inman (1981), Equations (3.58) and (3.59). Chosen monochromatic waves are assumed to attack the beach continuously throughout the model run time. No varying wave climate is employed because the initial bathymetry is a function of the wave properties. The wave heights, which are employed in the model, are shown in Table 5.1. Throughout the analysis, shore-normal waves with a period of 6s are employed. Each wave height represents different hypothetical coastal regions, with varying yearly average wave heights.

Table 5.1. Deep water wave heights, H_0, for which the model was run

	Comb.1	Comb.2	Comb.3
H_0 [m]	1	2	4

Figure 5.1 shows the regional EBP's as a function of deep water wave steepness for the wave conditions specified above.

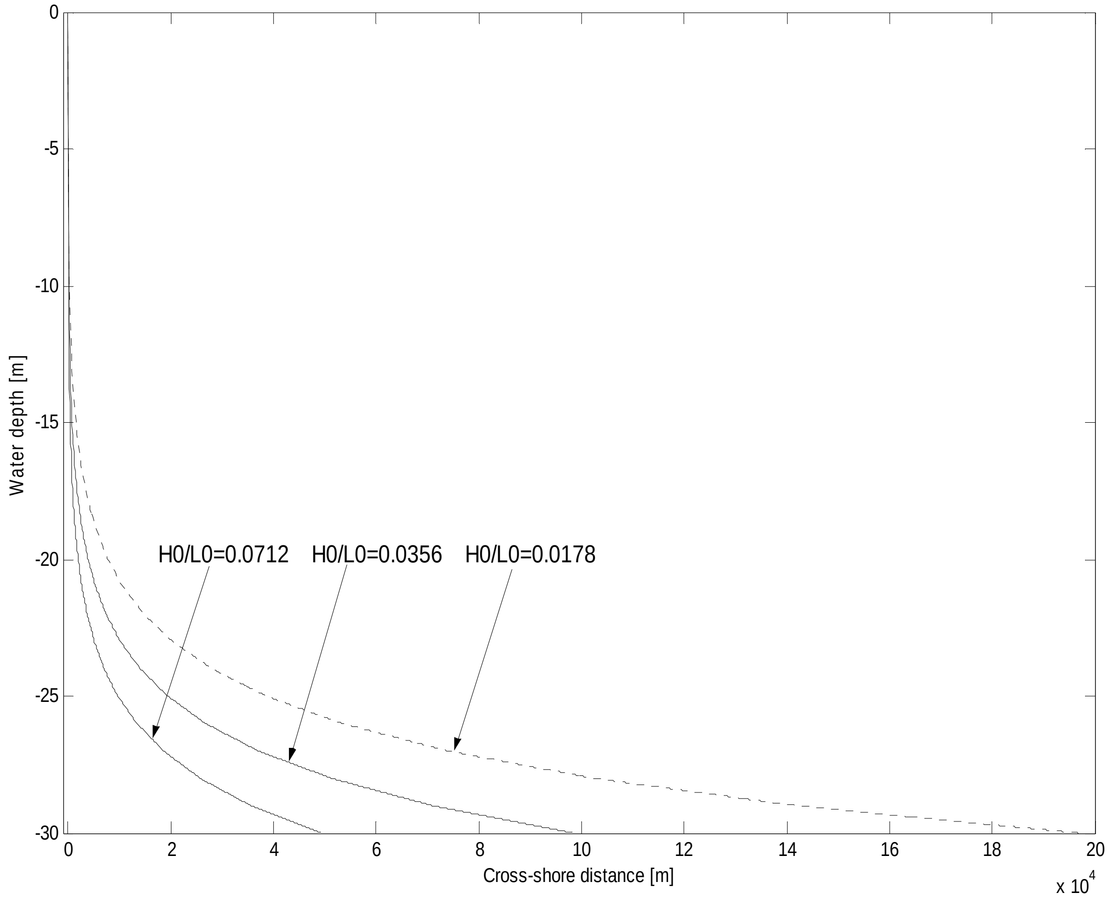

Figure 5.1. The regional EBP's for the three wave combinations in comparison

The longshore stretch of the model beach is twice as the pit length. Cross-shore grid spacing is chosen to accommodate 40 contours between the onshore and offshore depth limits of the model. This is found to be more convenient than specifying a fixed cross-shore grid spacing, since the distance between two specific depth values changes according to the chosen wave conditions, i.e. some EBP's are flatter than others between the same depth limits. Thus, the width of the pit varies depending on the wave conditions, since the pit is represented by a single node in the cross-shore direction. Therefore the width of the pit is equal to twice the cross-shore grid spacing. The longshore grid spacing is 50m throughout the analysis. The dimensions of the pit are given in Table 5.2.

Table 5.2. Dimensions of the model pit and the dredging depths tested

Length of pit [m]	Width of pit [m]	Depth of pit [m]	Dredging Depths [m]
500	18-346	1	15, 17.5, 20

The pits are opened at three different water depths shown in Table 5.3. These depths are not chosen totally arbitrary. The present state of the law allows dredging in waters deeper than 20 m. As mentioned before, according to the studies conducted to investigate the impact of offshore pits on the shoreline, the pit has to be outside of the closure depth to minimize its impact on the shoreline. The closure depth at the area of interest is 10 m Demir et al., 2004).

A time step of 30 days is used.

5.1.1. Planform Evolution

In planform, the pit can be represented by a deformation of the original contour. Thus the time evolution of the dredging contour is investigated. Only the contours, closest to the dredging contour are plotted to asses the impact of the pit on its vicinity.

The following three subsections display the graphical results. A short summary of the results is provided at the end of this section.

5.1.1.1. Under the Attack of Combination 1

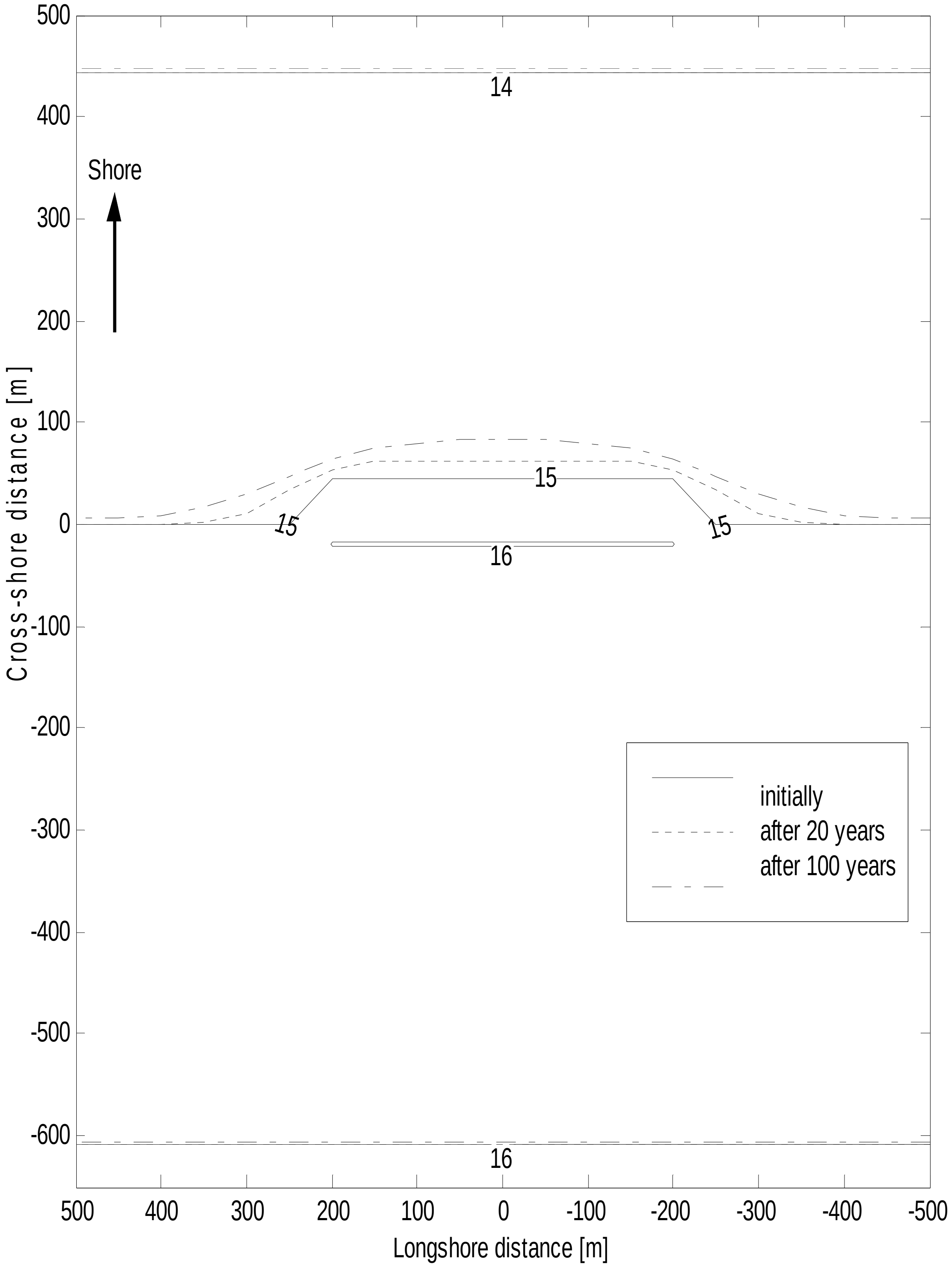

Figure 5.2. Planform evolution at 15m dredging depth in 100 years (U_r=0.94, L_r=3.75)

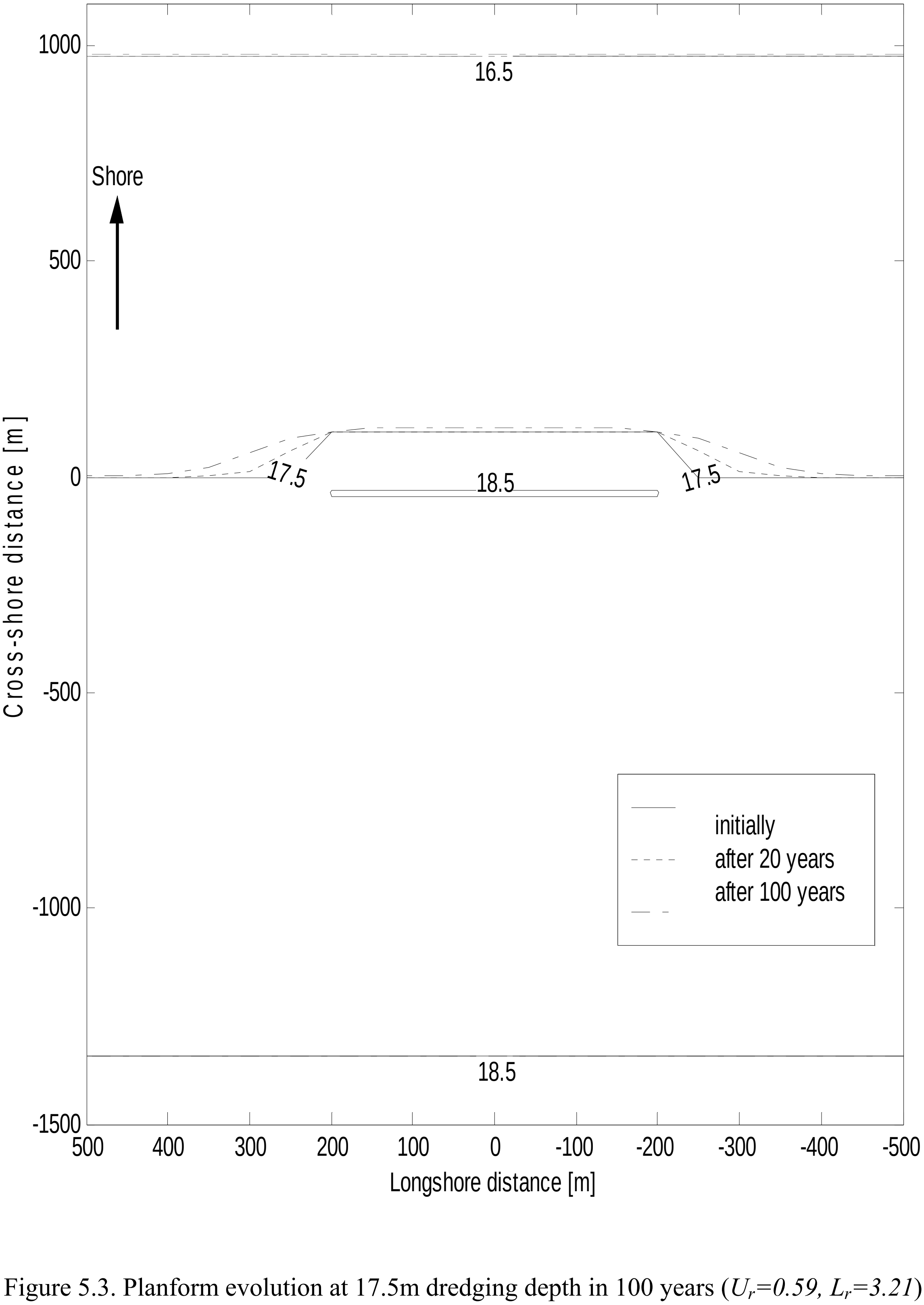

Figure 5.3. Planform evolution at 17.5m dredging depth in 100 years (U_r=0.59, L_r=3.21)

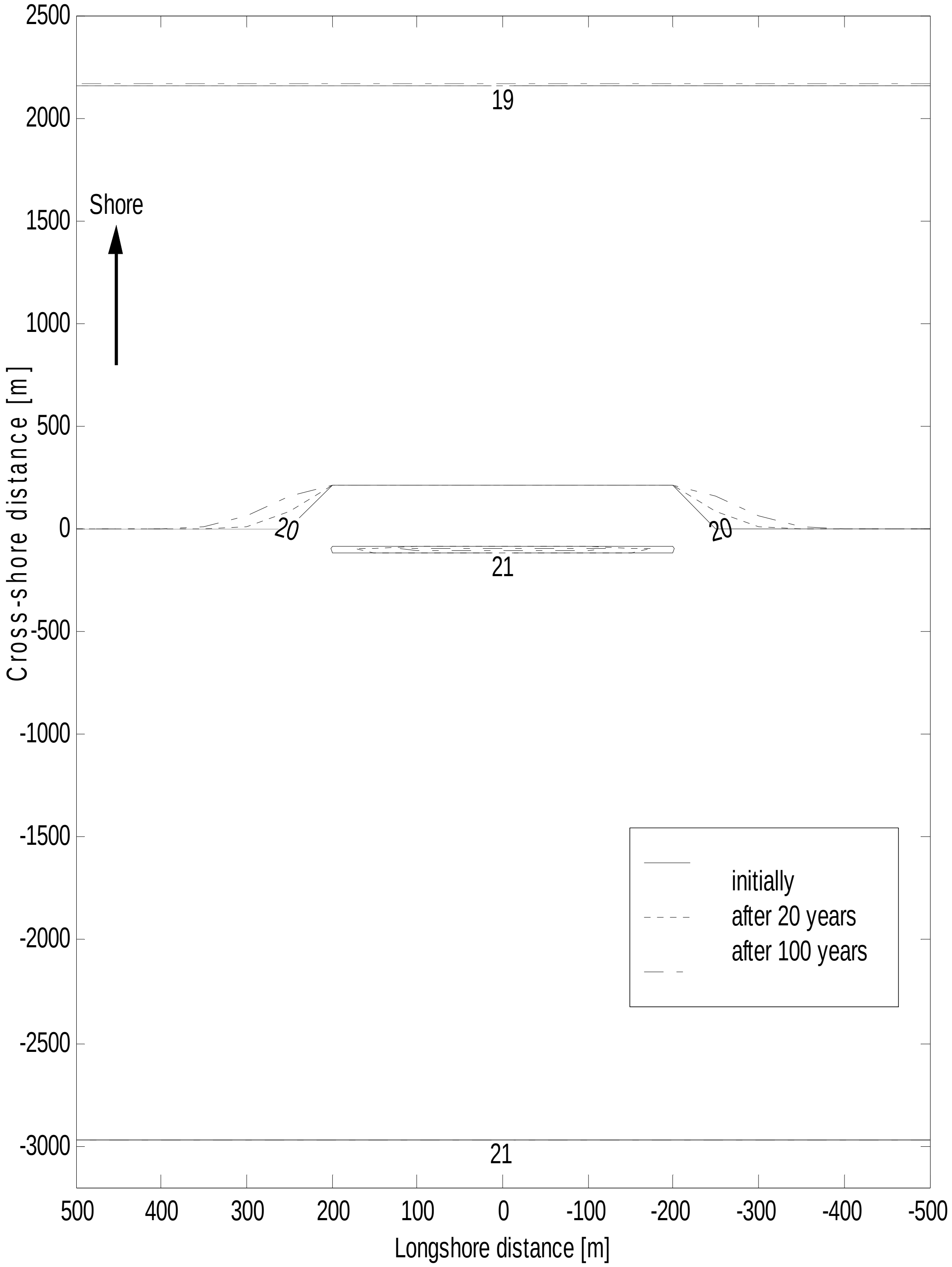

Figure 5.4. Planform evolution at 20m dredging depth in 100 years ($U_r=0.40, L_r=2.81$)

5.1.1.2. Under the Attack of Combination 2

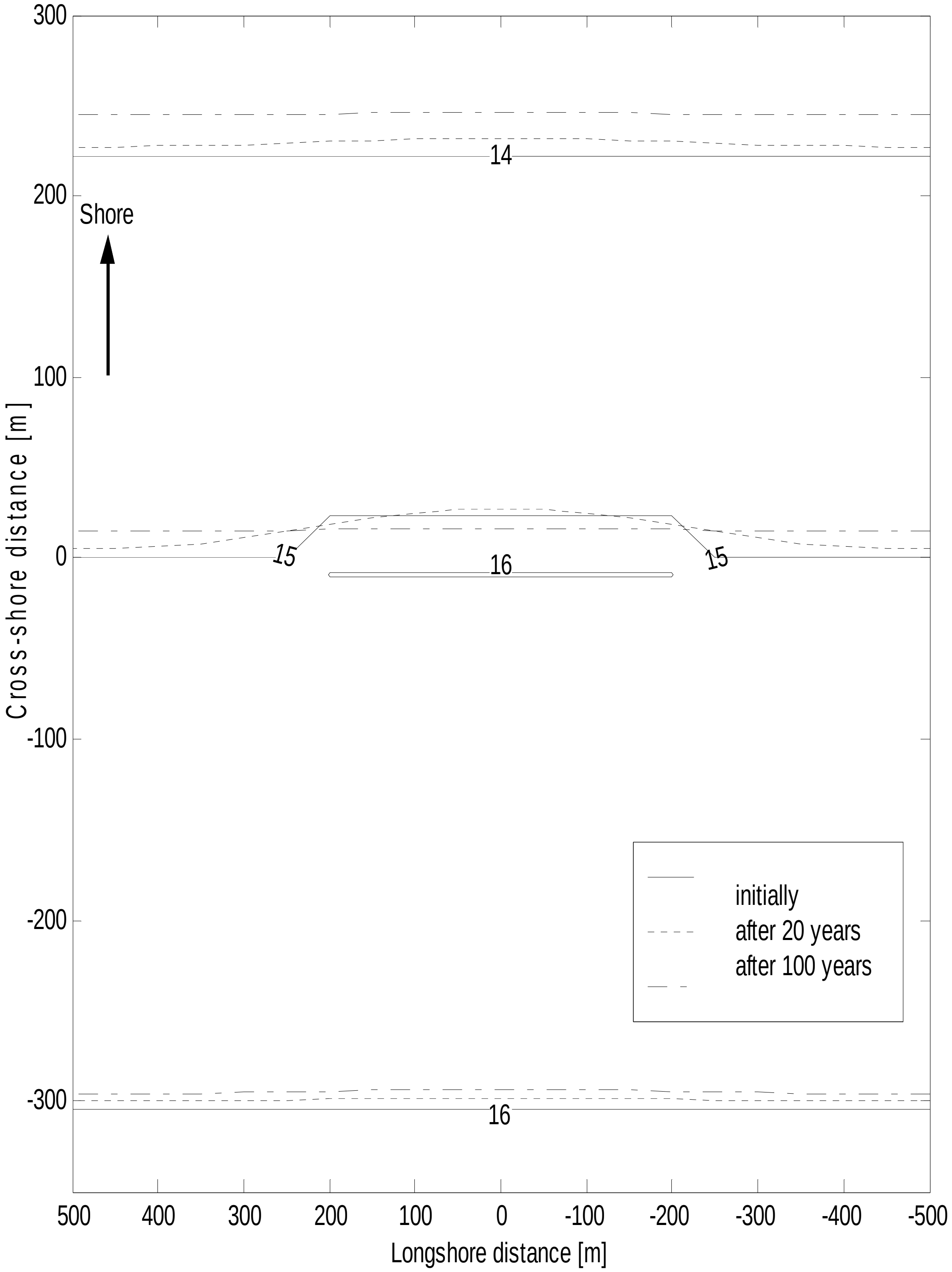

Figure 5.5. Planform evolution at 15m dredging depth in 100 years ($U_r=1.87$, $L_r=3.75$)

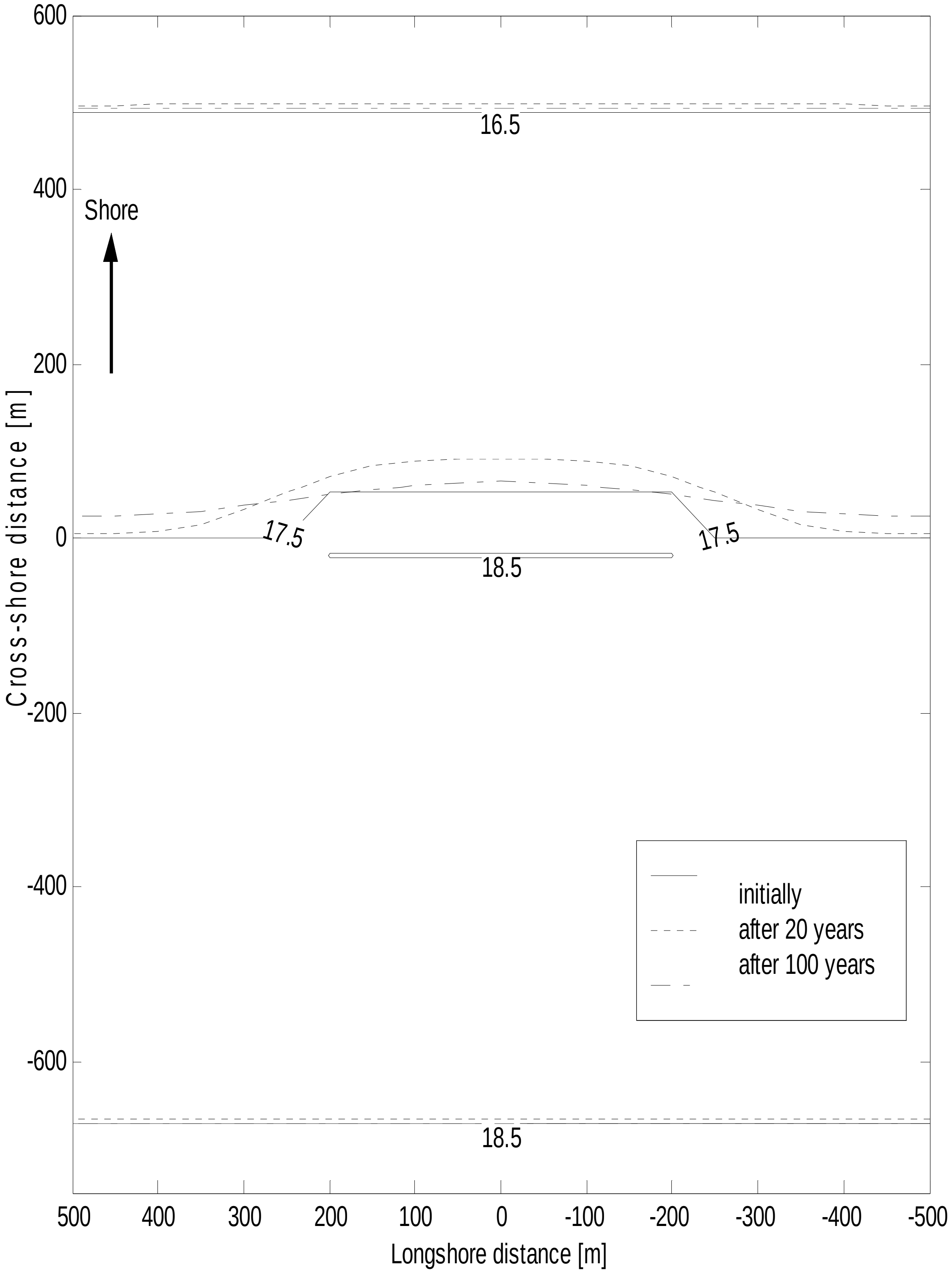

Figure 5.6. Planform evolution at 17.5m dredging depth in 100 years (U_r=*1.18*, L_r=*3.21*)

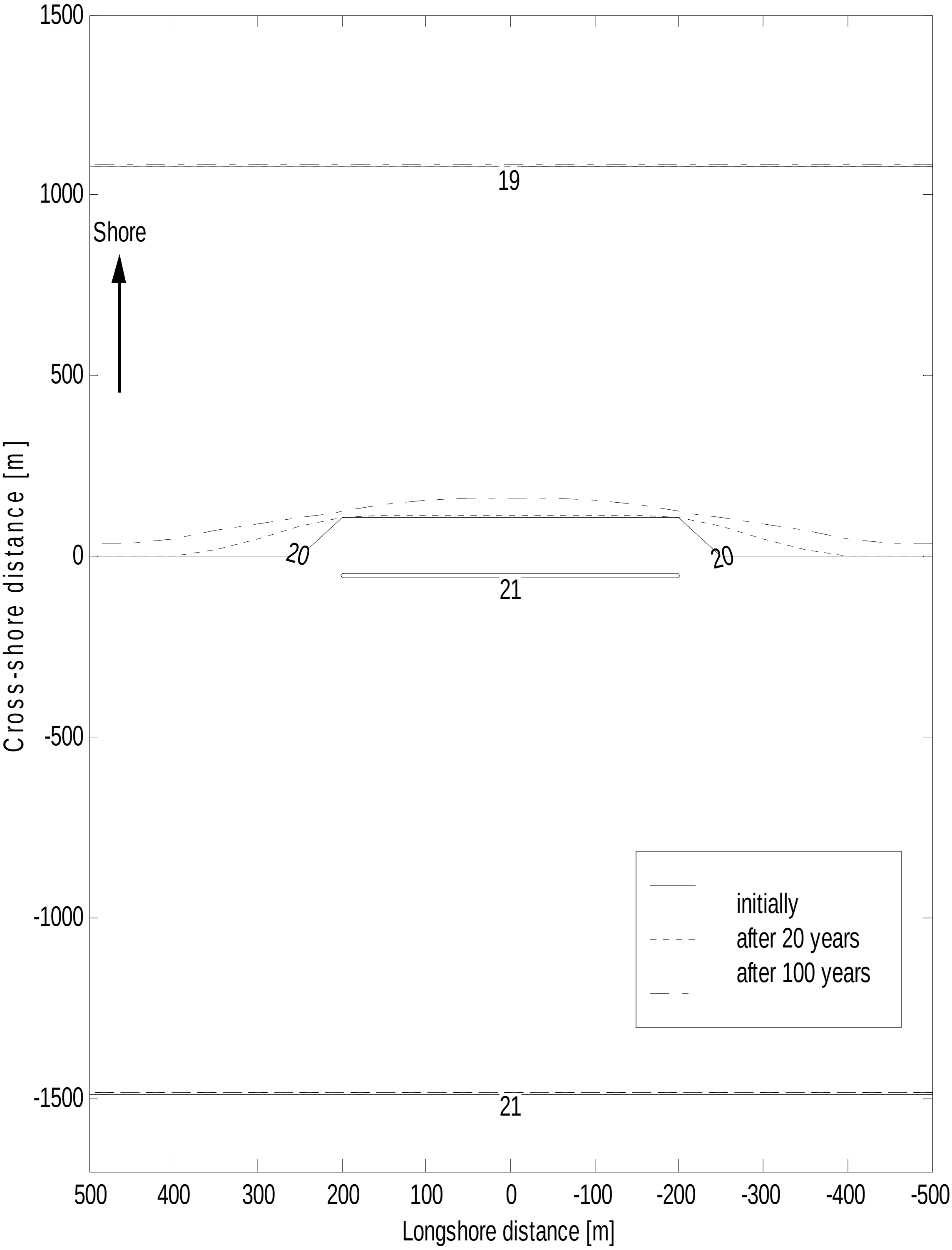

Figure 5.7. Planform evolution at 20m dredging depth in 100 years ($U_r=0.80, L_r=2.81$)

5.1.1.3. Under the Attack of Combination 3

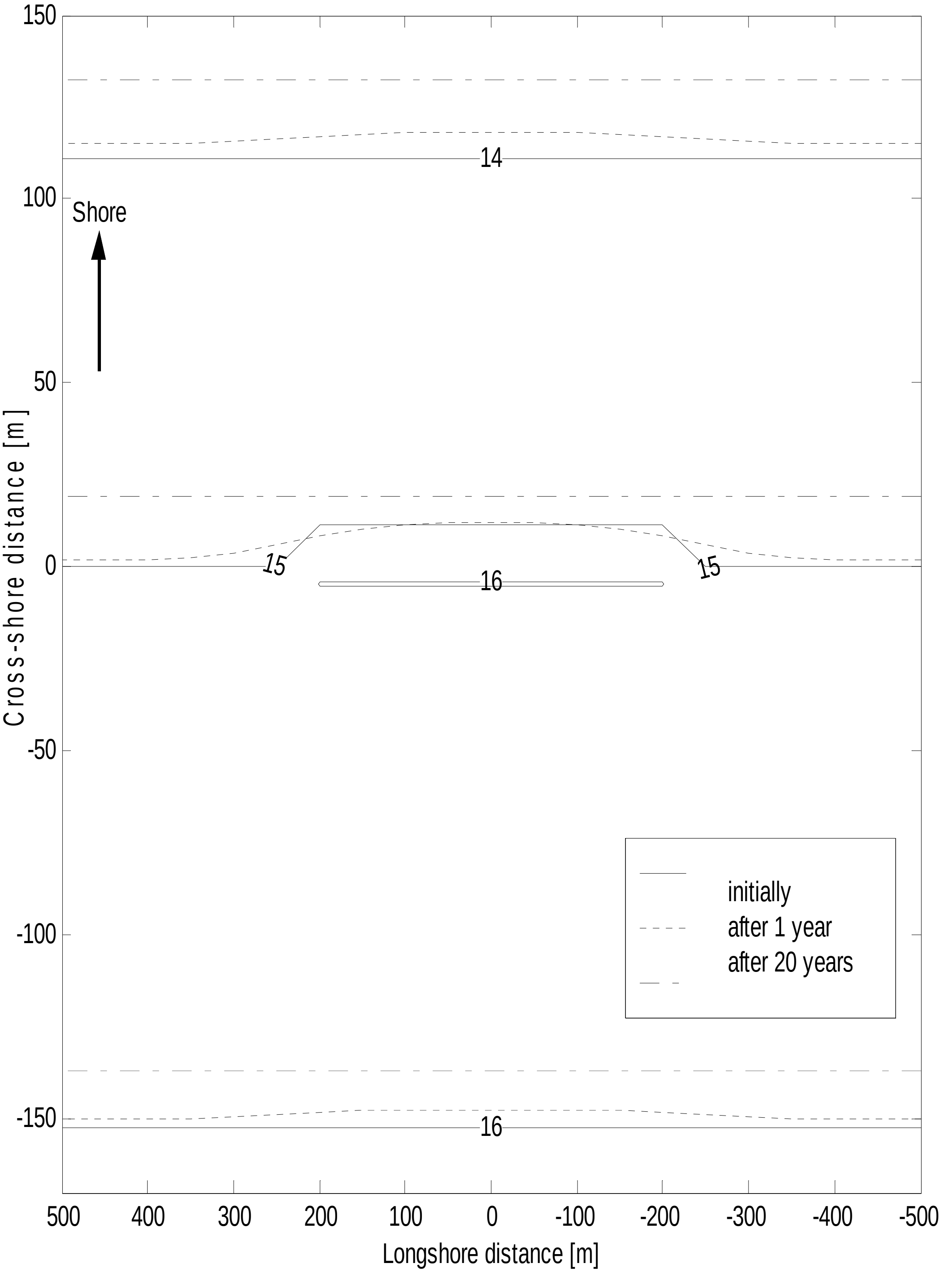

Figure 5.8. Planform evolution at 15m dredging depth in 50 years ($U_r=3.74,\ L_r=3.75$)

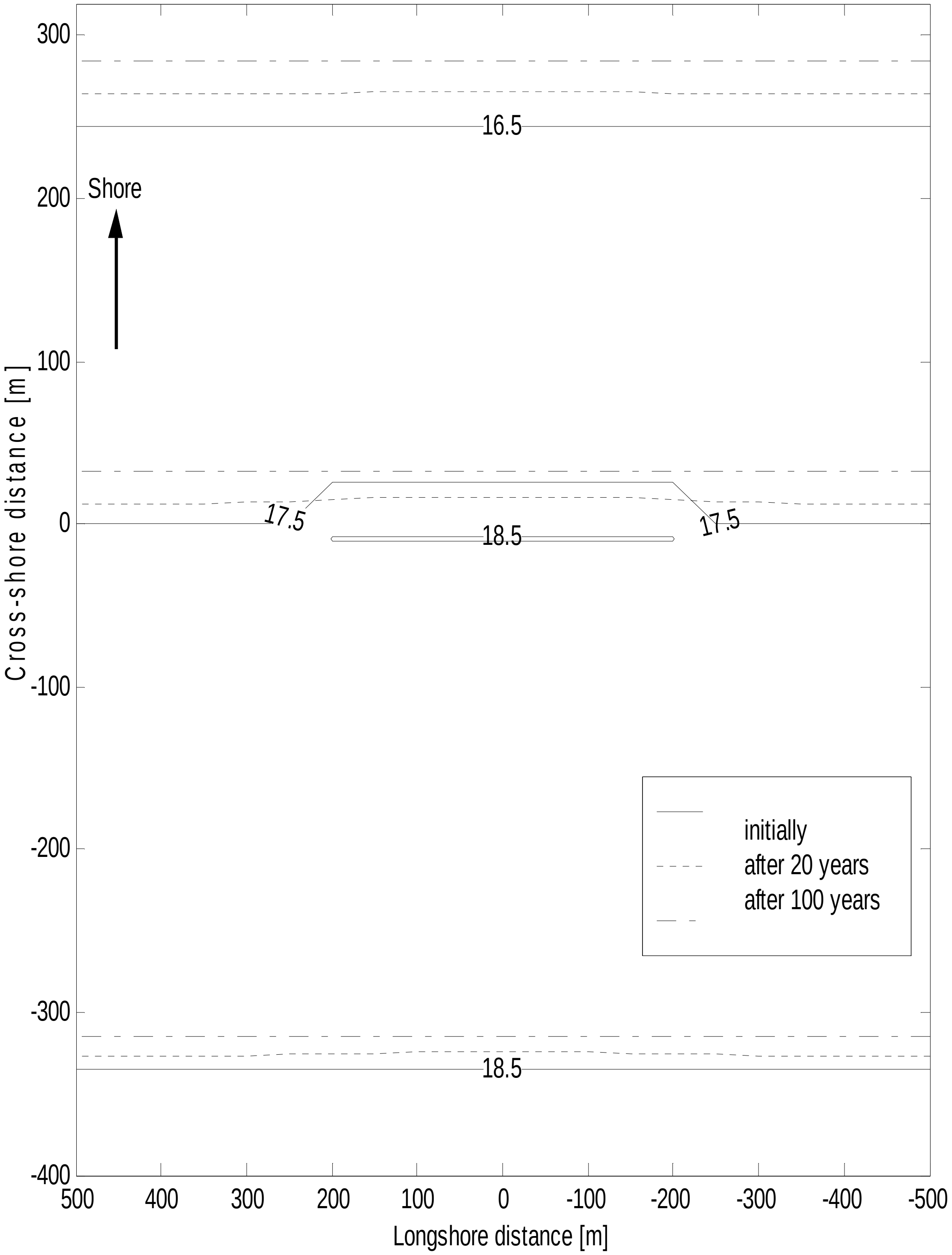

Figure 5.9. Planform evolution at 17.5m dredging depth in 100 years (U_r*=2.36,* L_r*=3.21*)

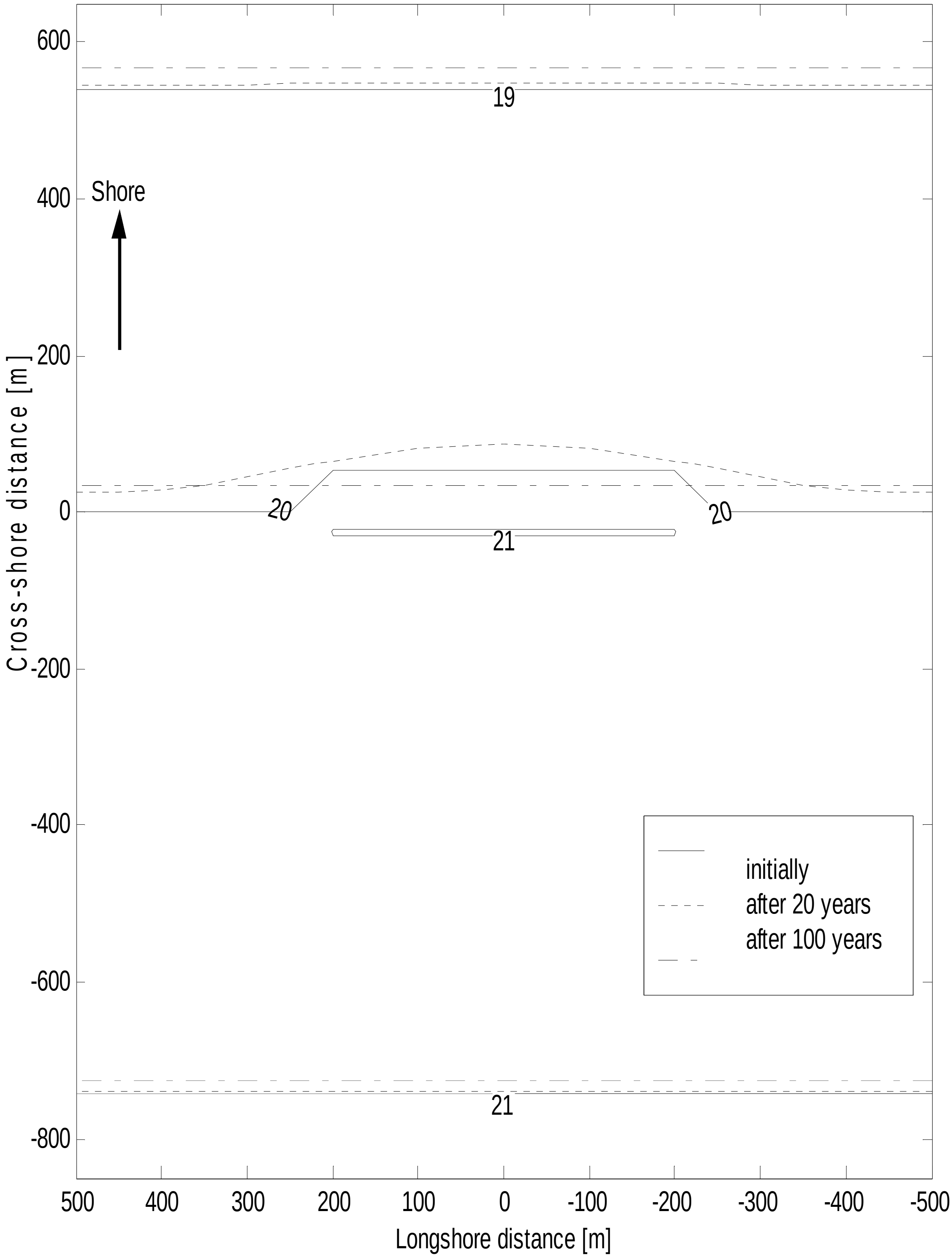

Figure 5.10. Planform evolution at 20m dredging depth in 100 years ($U_r=1.58, L_r=2.81$)

Diffusion of the contour deformation is observed in each case. However, the time scales required for the disappearance of the perturbation is not the same. Shallower dredging depths and more severe wave conditions speed up the process. Recession of the contours is observed in the long run.

5.1.2. Profile Evolution

The following three subsections show the time evolution of the cross-section going through the midpoint of the pit. Only the close proximity of the pit is plotted to emphasize the bathymetric evolution around the pit. The last subsection displays the rate of depth change of the midpoint and the flanges (the outmost nodes in the longshore direction) of the pit.

5.1.2.1. Under the Attack of Combination 1

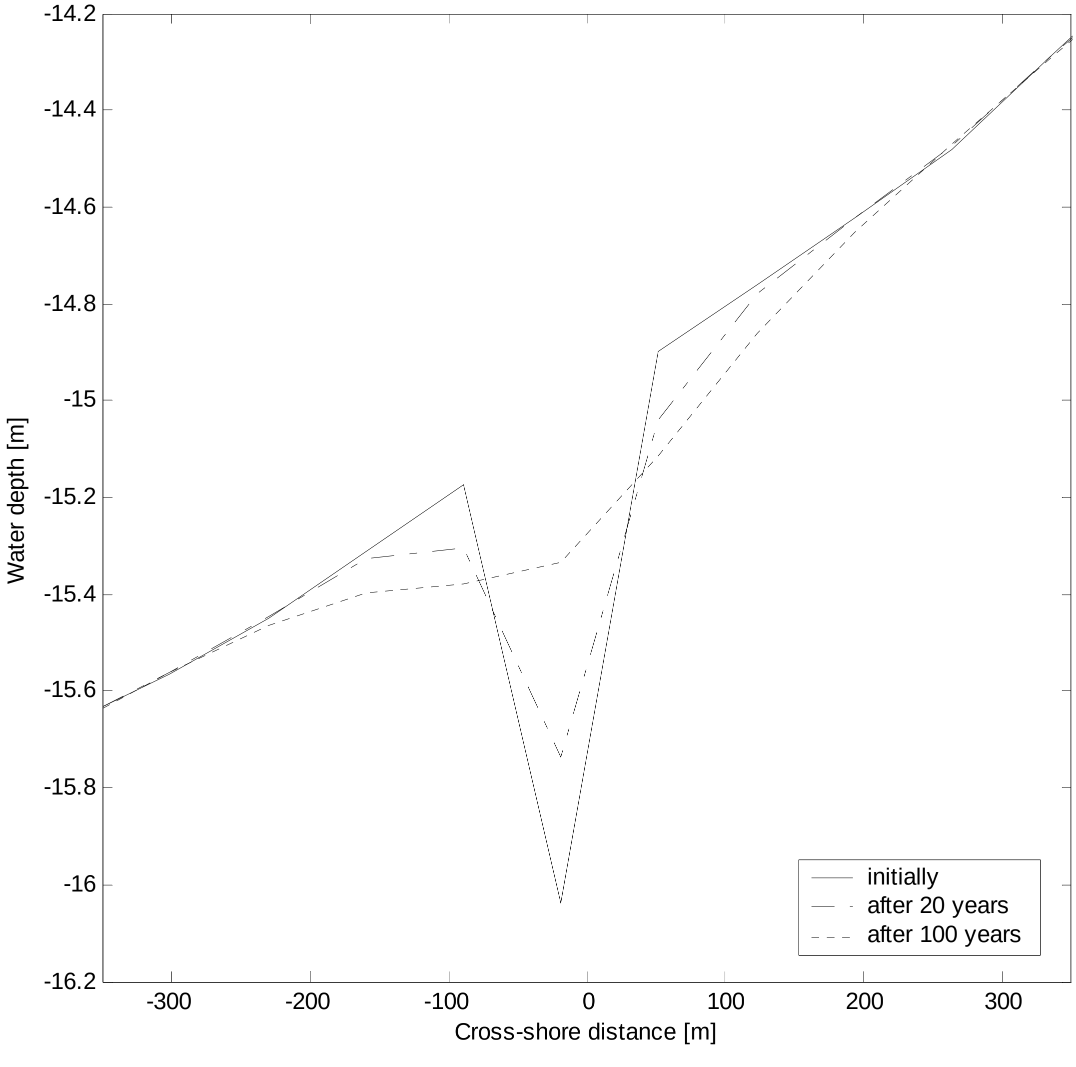

Figure 5.11. Profile evolution at 15m dredging depth in 100 years ($U_r=0.94, L_r=3.75$)

Figure 5.11 shows the cross-shore evolution of the pit dug at the 15 m contour. A depth recovery of 70 per cent is observed at the midpoint during 100 years. The perturbation extends up to 300m in each direction from the midpoint of the pit after 100 years.

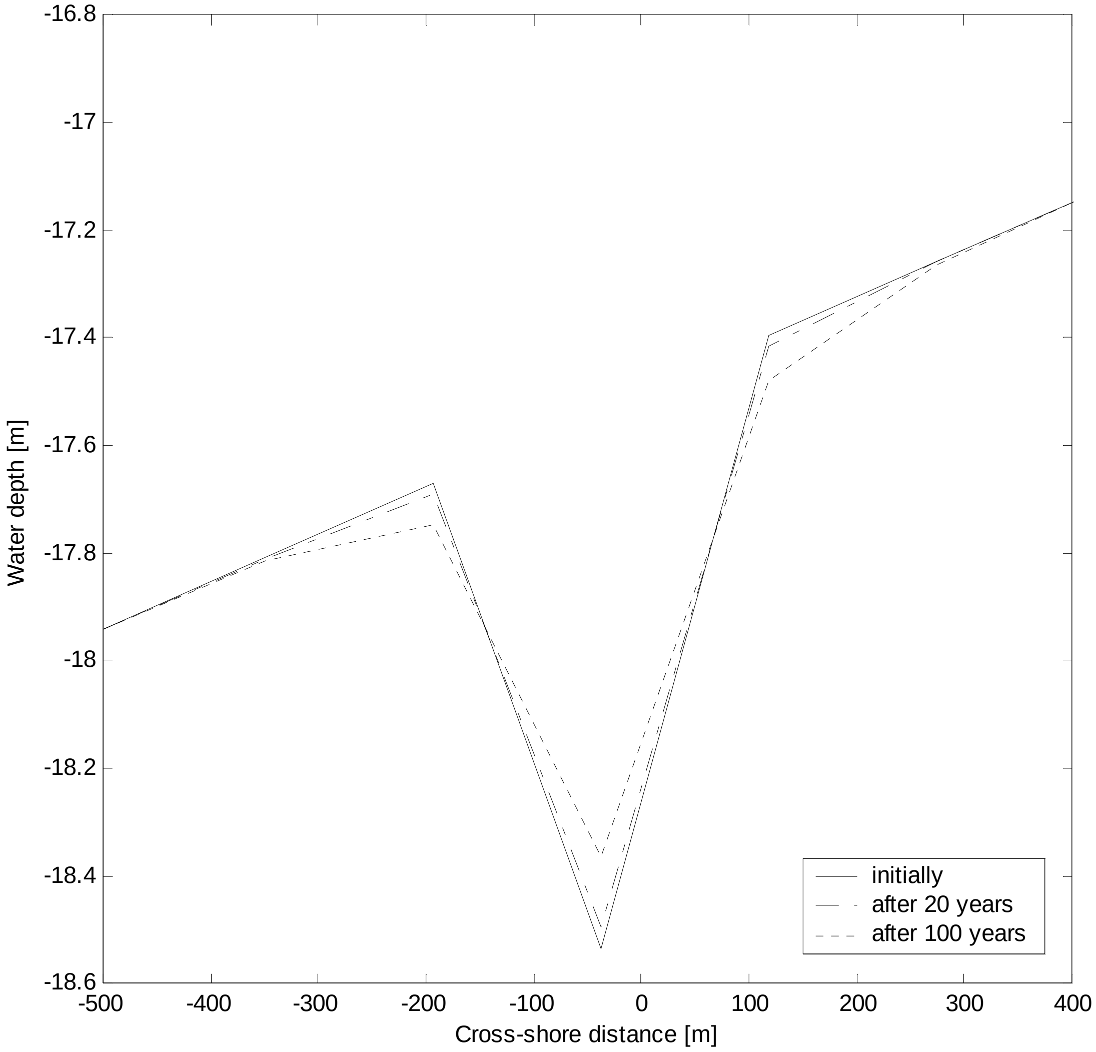

Figure 5.12. Profile evolution at 17.5m dredging depth in 100 years ($U_r=0.59$, $L_r=3.21$)

Figure 5.12 shows the cross-shore evolution of the pit dug at the 17.5 m contour. The midpoint has risen 0.17m during 100 years, i.e. less than 20 per cent. The perturbation extends up to 400m in each direction from the midpoint of the pit after 100 years.

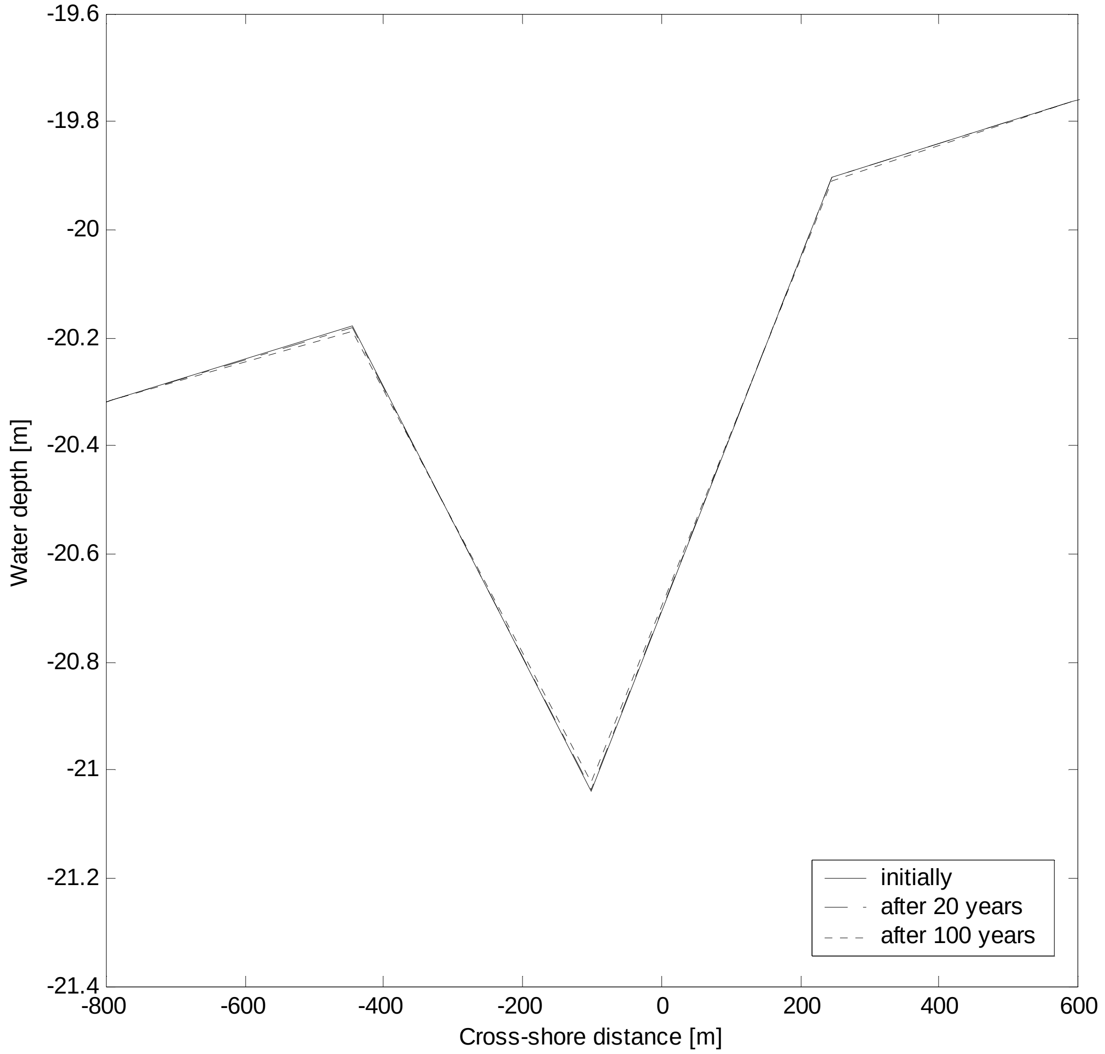

Figure 5.13. Profile evolution at 20m dredging depth in 100 years ($U_r=0.40$, $L_r=2.81$)

Figure 5.13 shows the cross-shore evolution of the pit dug at the 20 m contour. From the figure it is obvious that the cross-section remains stable over 100 years. The transport at this depth is negligible for this wave condition.

5.1.2.2. Under the Attack of Combination 2

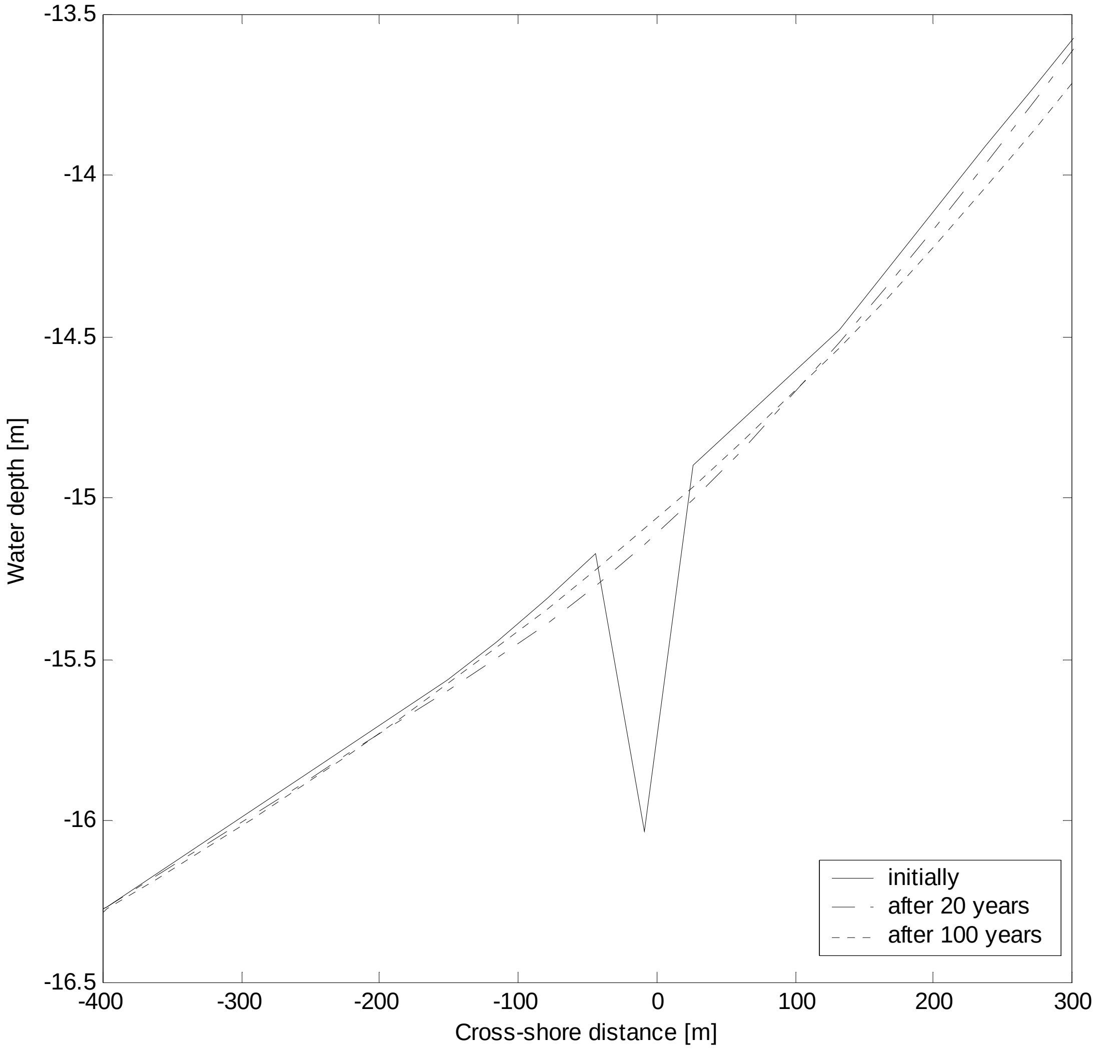

Figure 5.14. Profile evolution at 15m dredging depth in 100 years ($U_r=1.87$, $L_r=3.75$)

Figure 5.14 shows the cross-shore evolution of the pit dug at the 15 m contour. The pit has almost disappeared within 20 years. The onshore neighbors are eroded more than the offshore neighbors. The beach continues to evolve until it reaches its equilibrium values again.

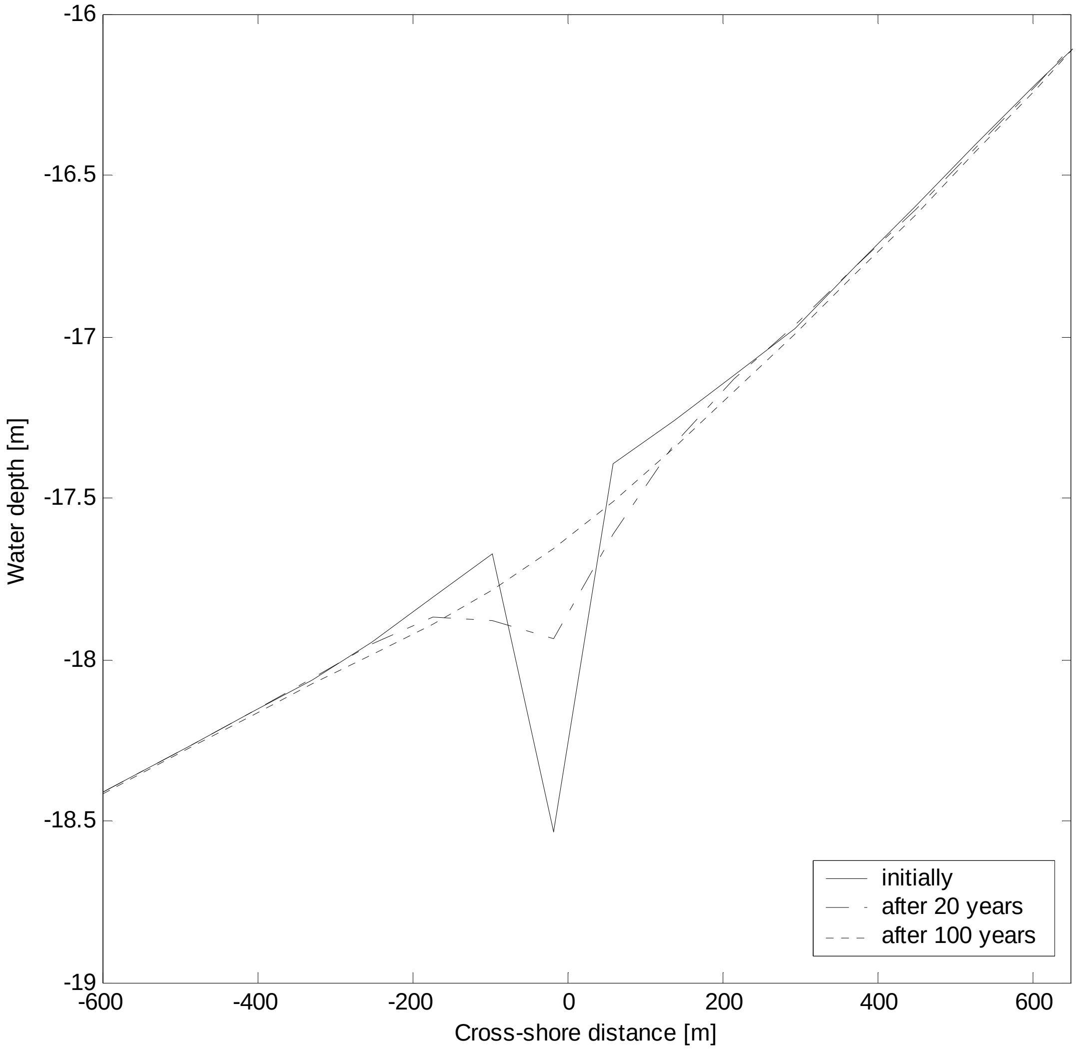

Figure 5.15. Profile evolution at 17.5m dredging depth in 100 years ($U_r=1.18$, $L_r=3.21$)

Figure 5.15 shows the cross-shore evolution of the pit dug at the 17.5 m contour. A depth recovery of 60 per cent is observed at the midpoint during 20 years. Within 100 years the pit has almost disappeared.

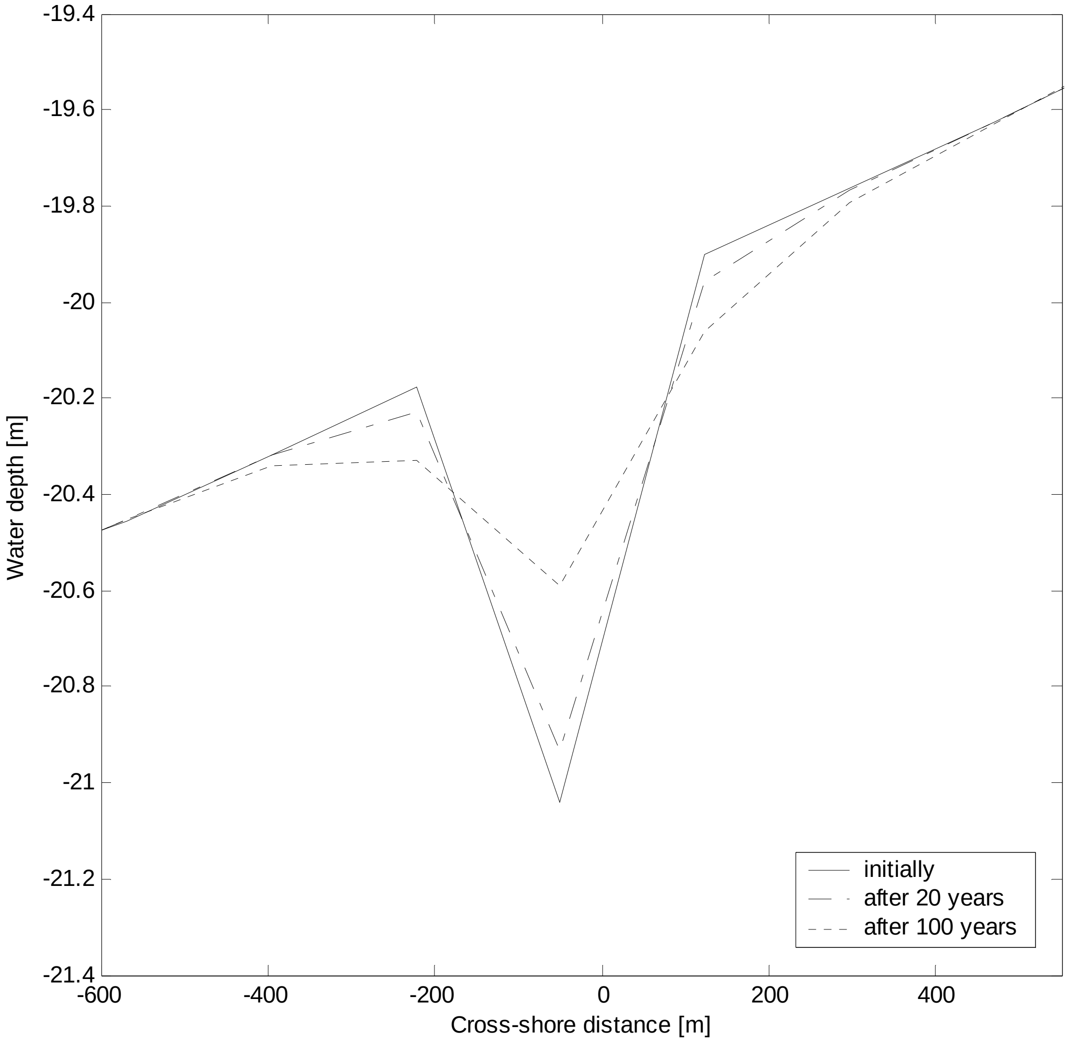

Figure 5.16. Profile evolution at 20m dredging depth in 100 years ($U_r=0.80$, $L_r=2.81$)

Figure 5.16 shows the cross-shore evolution of the pit dug at the 20 m contour. Depth recovery of 45 per cent is observed at the midpoint during 100 years.

5.1.2.3. Under the Attack of Combination 3

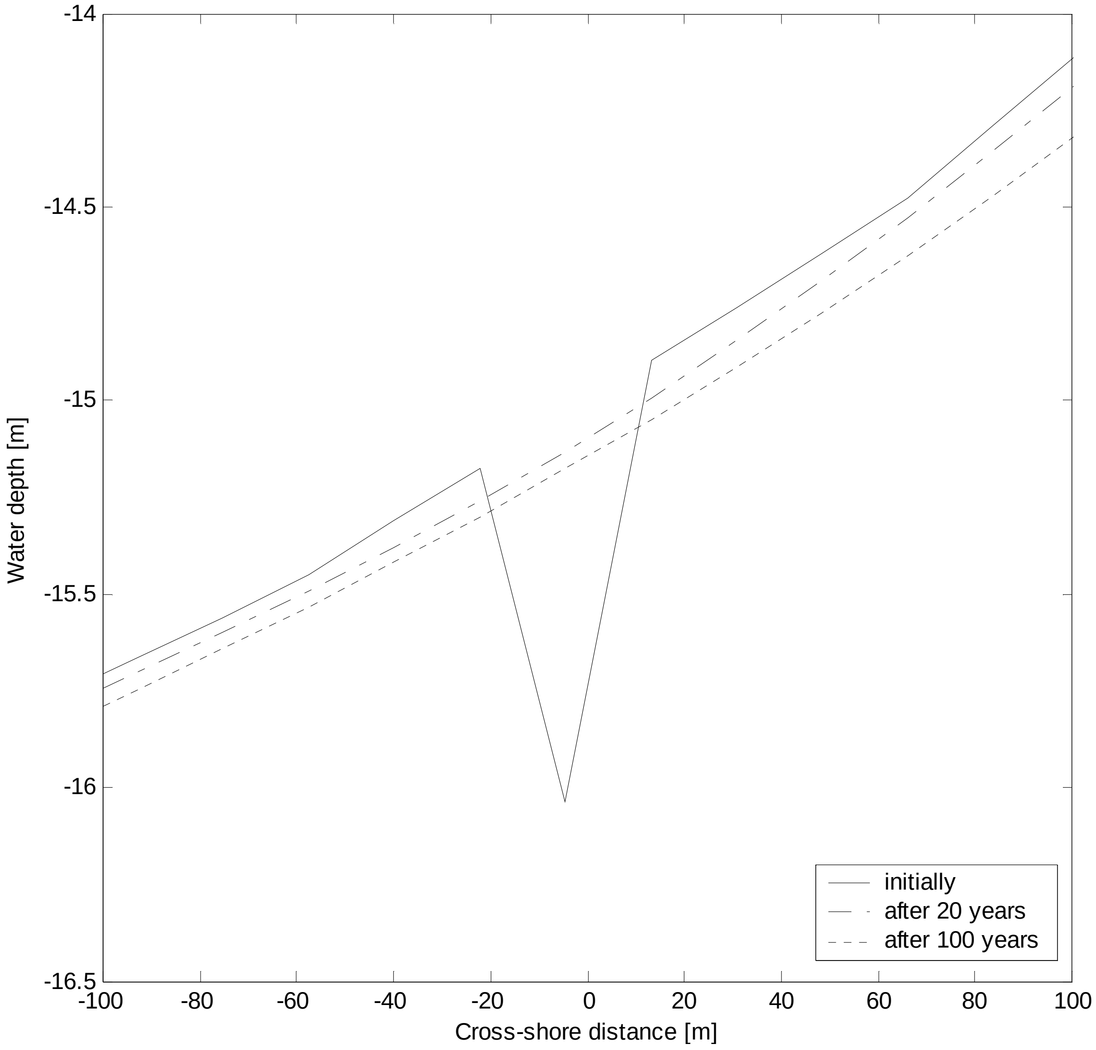

Figure 5.17. Profile evolution at 15m dredging depth in 50 years ($U_r=3.74$, $L_r=3.75$)

Figure 5.17 shows the cross-shore evolution of the pit dug at the 15 m contour. Backfilling occurs very rapidly and the beach almost attains a new equilibrium within 20 years.

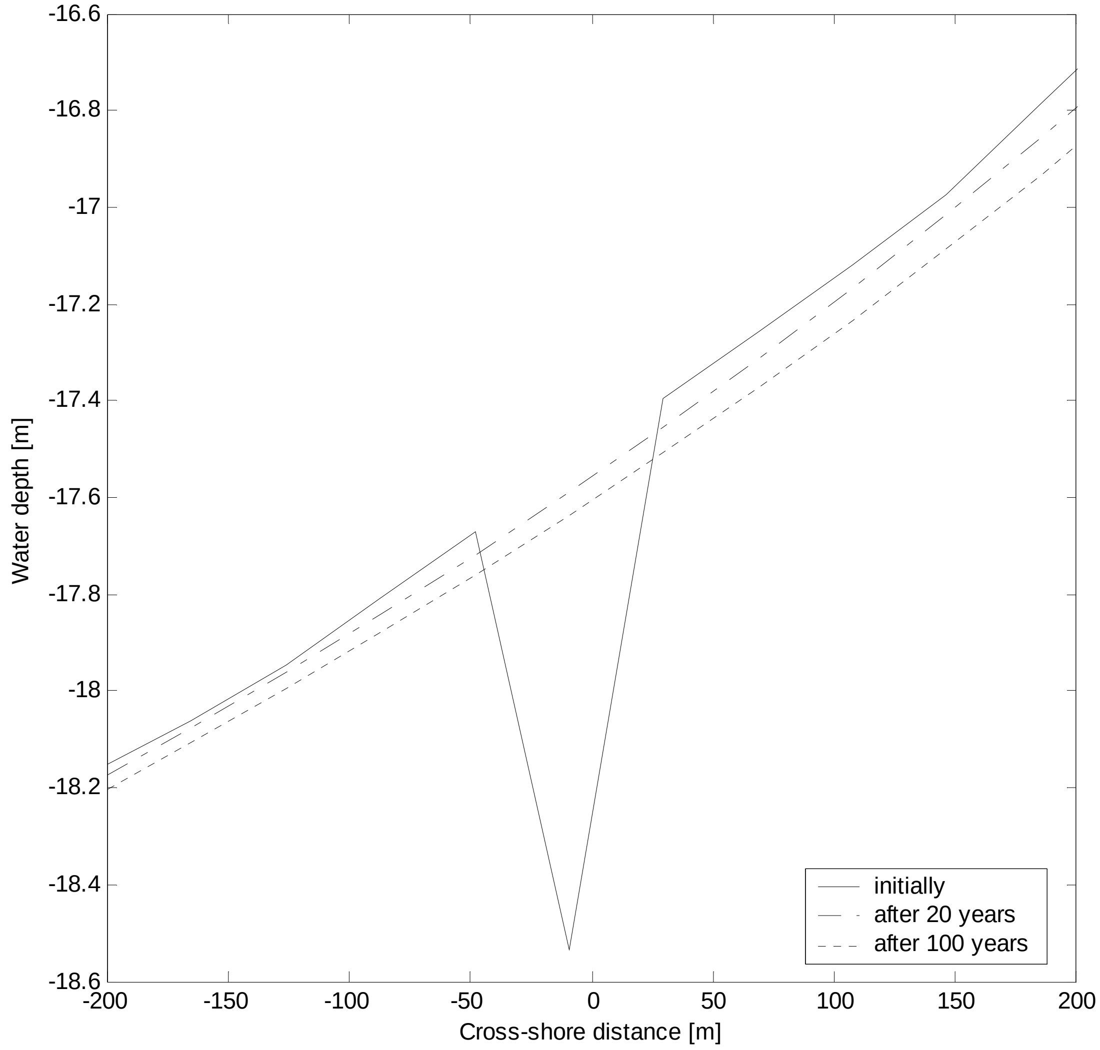

Figure 5.18. Profile evolution at 17.5m dredging depth in 100 years ($U_r=2.36, L_r=3.21$)

Figure 5.18 shows the cross-shore evolution of the pit dug at the 17.5 m contour. The pit recovers before 20 years. Then the profile tries to reach equilibrium.

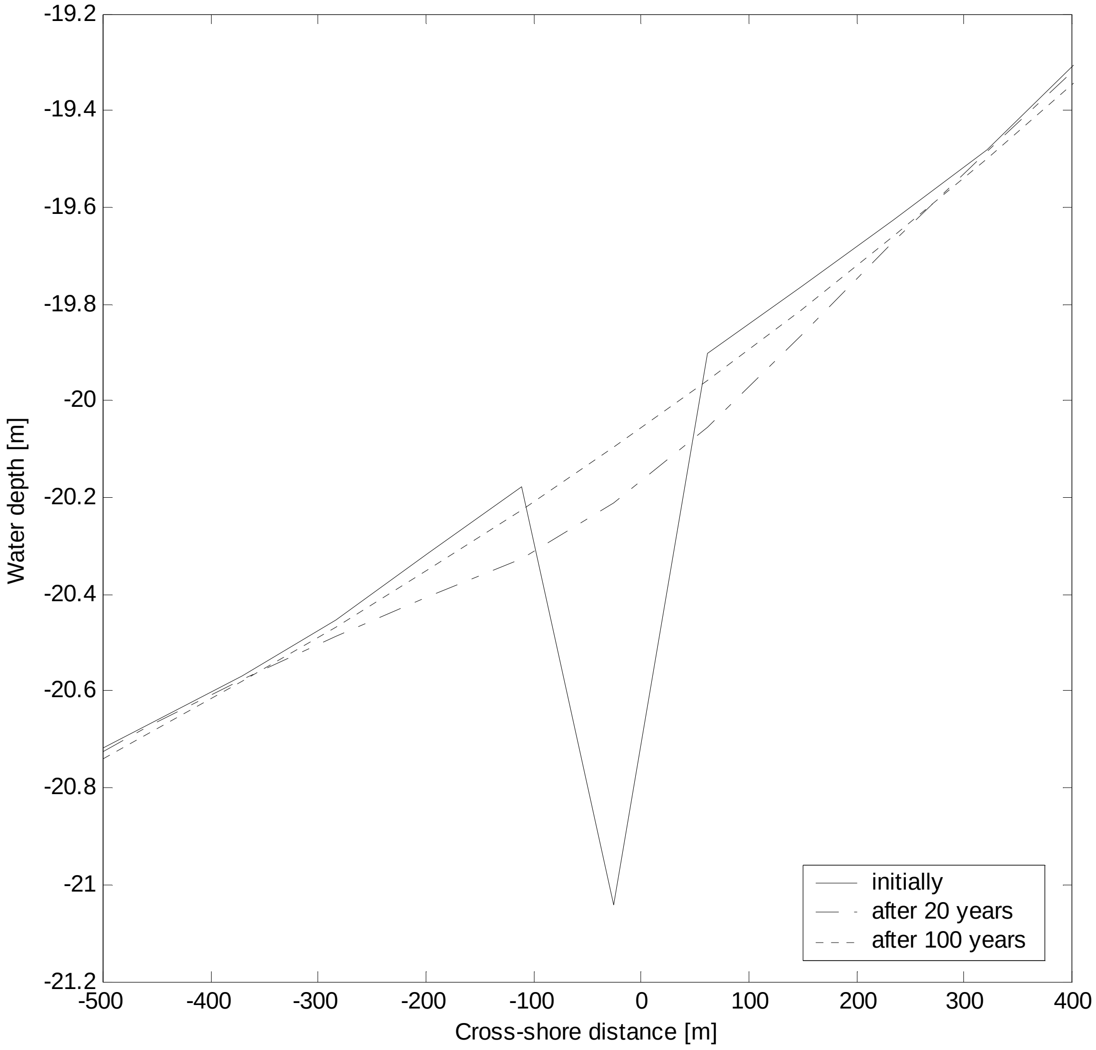

Figure 5.19. Profile evolution at 20m dredging depth in 100 years ($U_r=1.58$, $L_r=2.81$)

Figure 5.19 shows the cross-shore evolution of the pit dug at the 20 m contour. Since the waves are quite high, their effect at the bottom at this depth is immense. The pit recovers very rapidly.

Ursell number seems to be a meaningful choice as a parameter quantifying the backfilling. For Ursell numbers larger than 1.50, the perturbation has disappeared to a large extent in a time interval less than 20 years. However, these results are no sufficient to make any generalizations. A sensitivity analysis should be conducted.

5.1.2.4. Backfilling Rate of the Pit

The time histories of depth changes of the midpoint and of the flanges in time are plotted in this section. Since the waves are shore normal, the contour evolve symmetrically about the midpoint of the pit. In the following figures, the points marked with an arrow indicate the time at which the depths start to increase again. Sediment begins to be transported away from the points under investigation. This is thought to be the result of the background transport. It created by the non-equilibrium beach slopes due to backfilling. At some time the magnitude of the background transport catches up the perturbation transport due to the pit. In the beginning the perturbation transport is larger. As the perturbation fades out, the magnitude of the perturbation transport decreases to the order of the magnitude of the background transport.

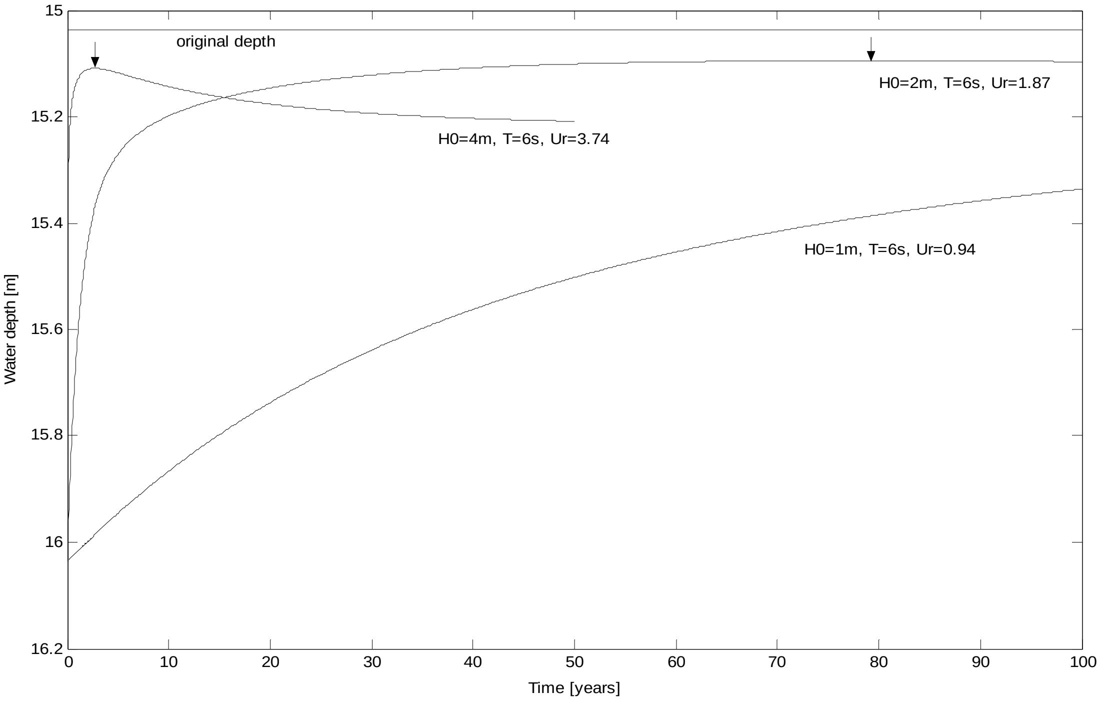

Figure 5.20. Backfilling rate of the middle at 15m dredging depth

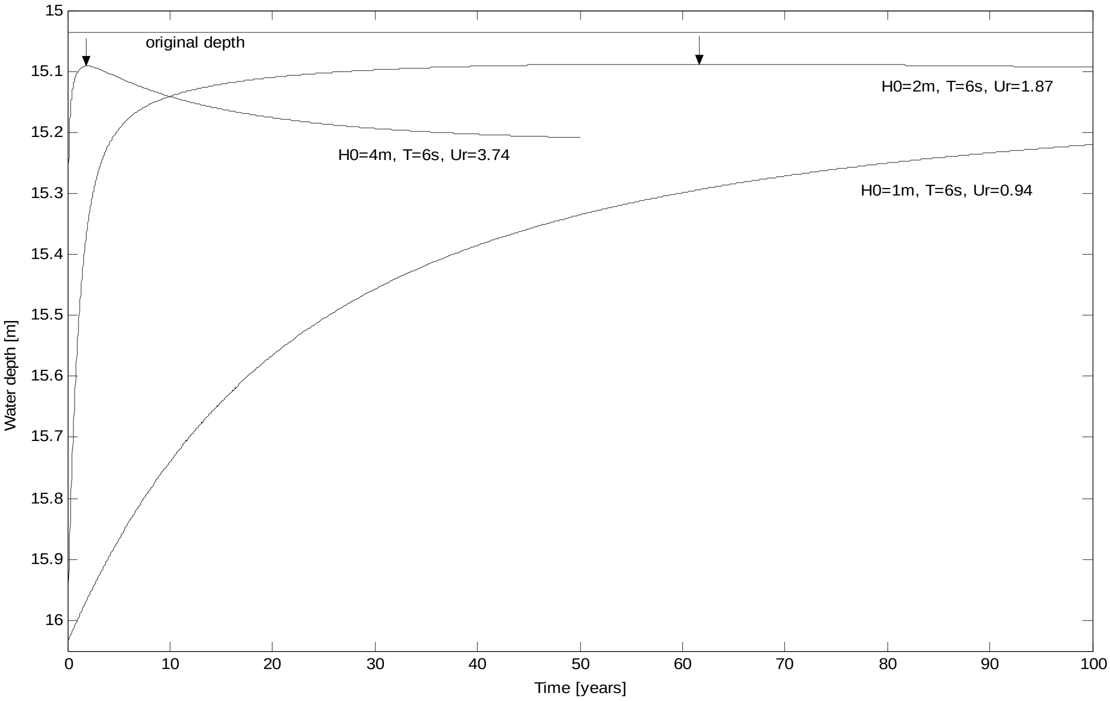

Figure 5.21. Backfilling rate of the flange at 15m dredging depth

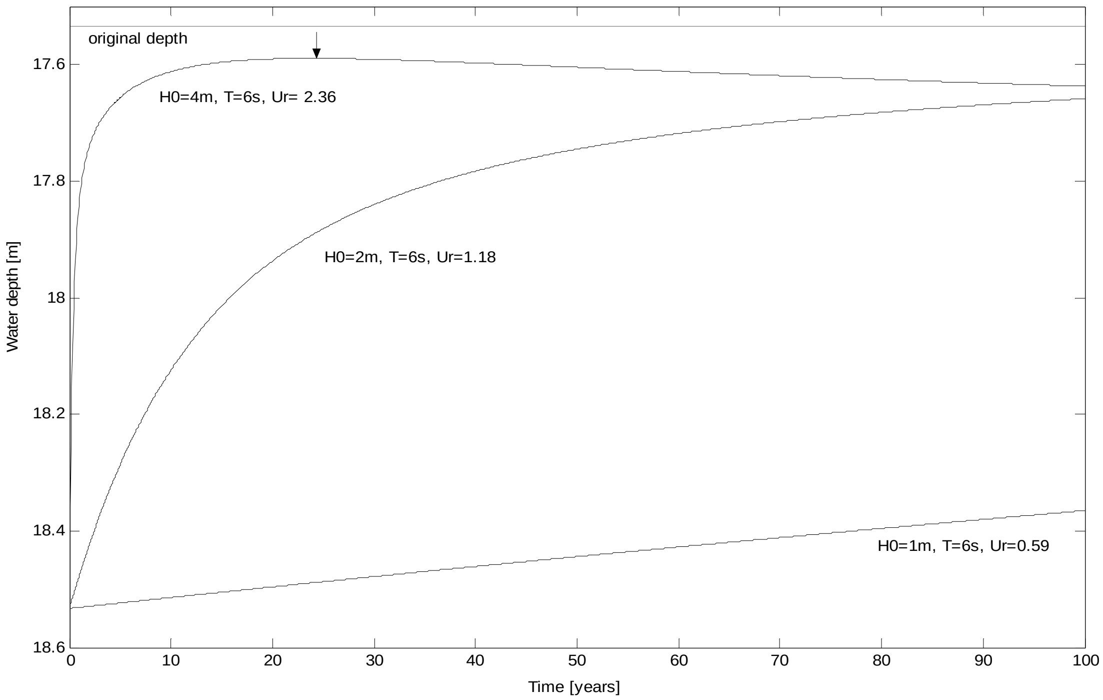

Figure 5.22. Backfilling rate of the middle at 17.5m dredging depth

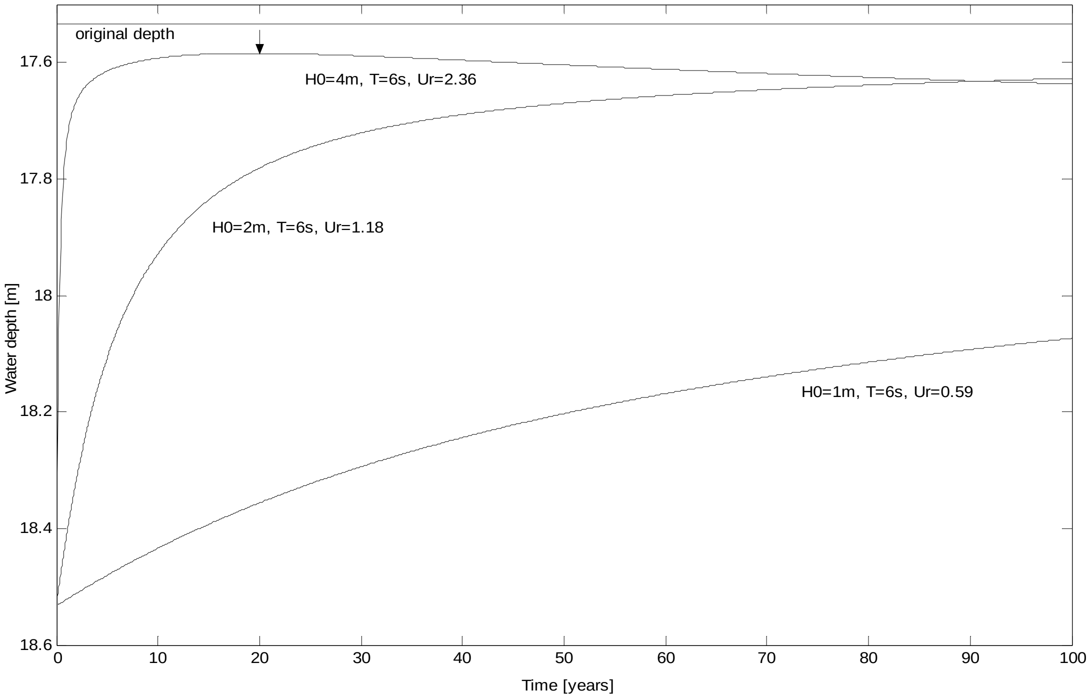

Figure 5.23. Backfilling rate of the flange at 17.5m dredging depth

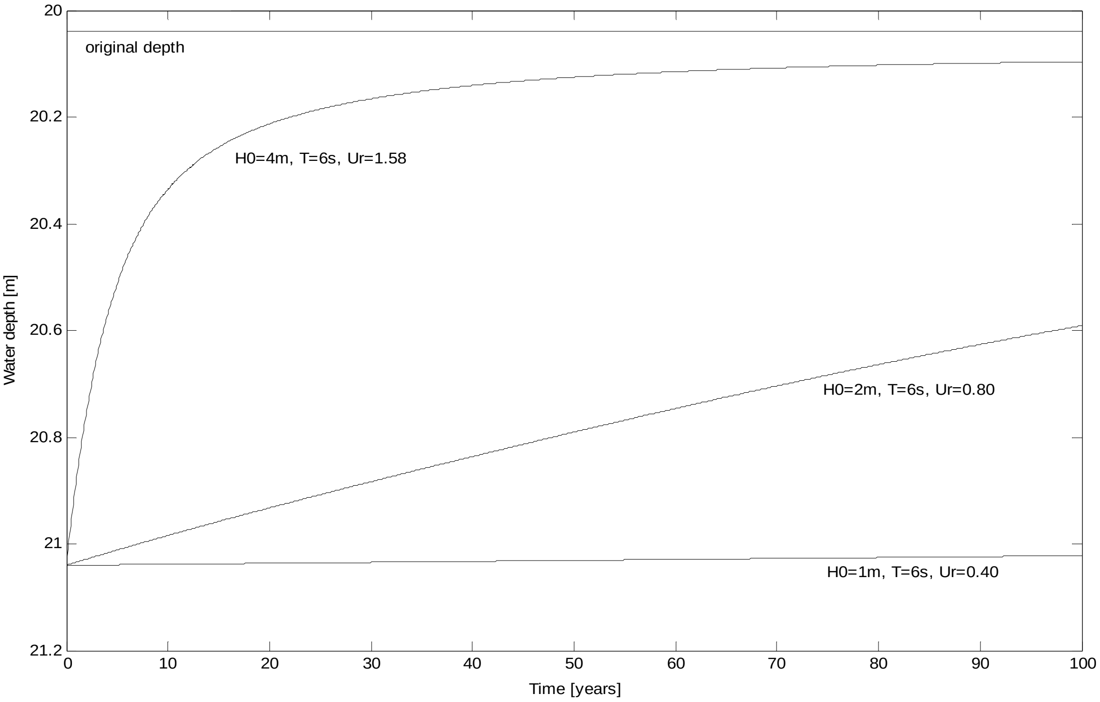

Figure 5.24. Backfilling rate of the middle at 20m dredging depth

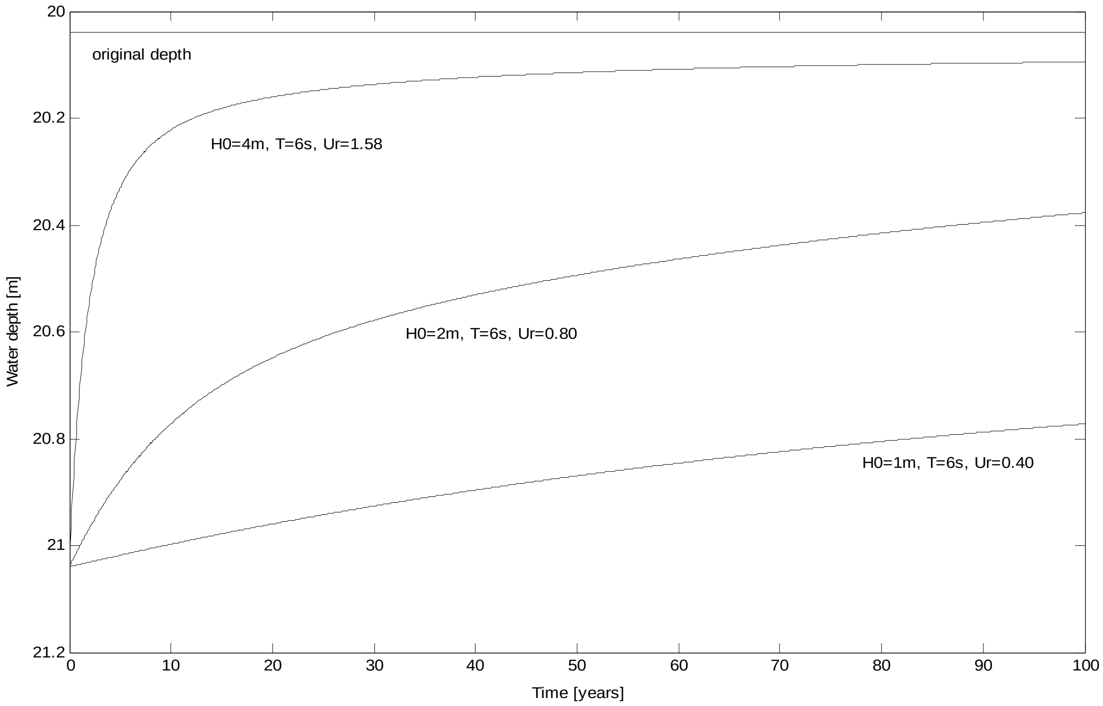

Figure 5.25. Backfilling rate of the flange at 20m dredging depth

5.2. Black Sea Case

To see the evolution of offshore dredge pits in the Southwest Black Sea, the model was applied to a hypothetical pit on a typical offshore bathymetry measured off the Kilyos Coast. The measured bathymetry data at the Boğaziçi University Gümüşdere Campus is employed. The measurements show that the beach profile has a slope of 1/85 offshore of the closure depth between 10-30m contours. A bathymetry with regular cross-shore grid spacing of 85m, corresponding to a depth spacing of 1m, is created. Longshore grid spacing, the stretch of beach modeled, and the model pit dimensions are the same as in the hypothetical case.

The waves are generated randomly, obeying the distribution of the representative wave statistics of Southwest Black Sea given in Table 5.3.

Table 5.3. Representative wind and wave conditions for Kilyos Beach using the analysis of Demir, 2002

Wave No	**Hs (m)**	**T (s)**	**Theta (deg.) geographic**	**Theta (deg.) model**	**Probability of occurrence**
W11	1.0	5.2	20 (NNE)	3	0.3345
W12	1.0	5.2	50 (NE)	33	0.3345
W13	3.0	7.5	23 (NNE)	5	0.0147
W14	3.0	7.5	45 (NE)	28	0.0205
W15	5.0	9.5	23 (NNE)	5	0.0039
W16	5.0	9.5	45 (NE)	28	0.0059
Calm	-	-	-	-	0.2860

In order to get rid of the ambient transport due to the initial slopes, which are not the equilibrium values, the model is run twice: for a bathymetry with a pit, and for a bathymetry without pit. What is plotted in the following figures is the difference between both cases, i.e. in the following figures the observed changes are completely due to the pit. The slope adjustment that occurs after backfilling will not be observed in these cases, as was observed in the previous section.

The time step is taken to be 10 days for the dredging depths of 20m and 25m. However, as the pit is dug at shallower depths, the bottom velocity, i.e. the transport rate, increases rapidly. Due to this sudden increase, the numeric solution starts to oscillate. In order to prevent this failure, the numerical instability, the time step is reduced to 5 days for 15 m dredging depth.

Figures 5.26-5.31 show the evolution of the dredging contour. Figures 5.32-5.37 show the evolution of the cross-section through the midpoint of the pit and the backfilling rate of the midpoint and the flanges.

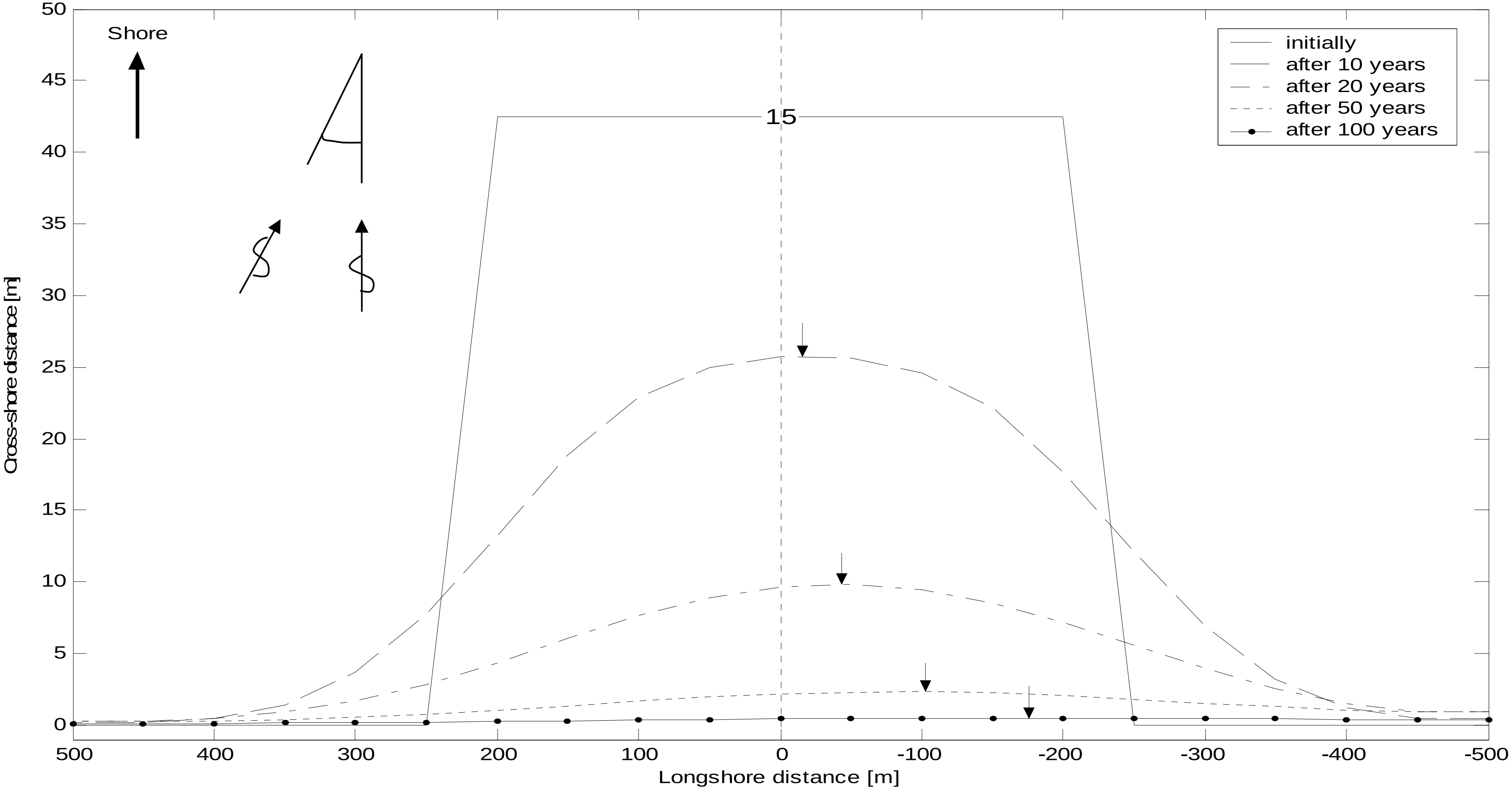

Figure 5.26. Planform evolution of the dredging contour at 15m depth in 100 years

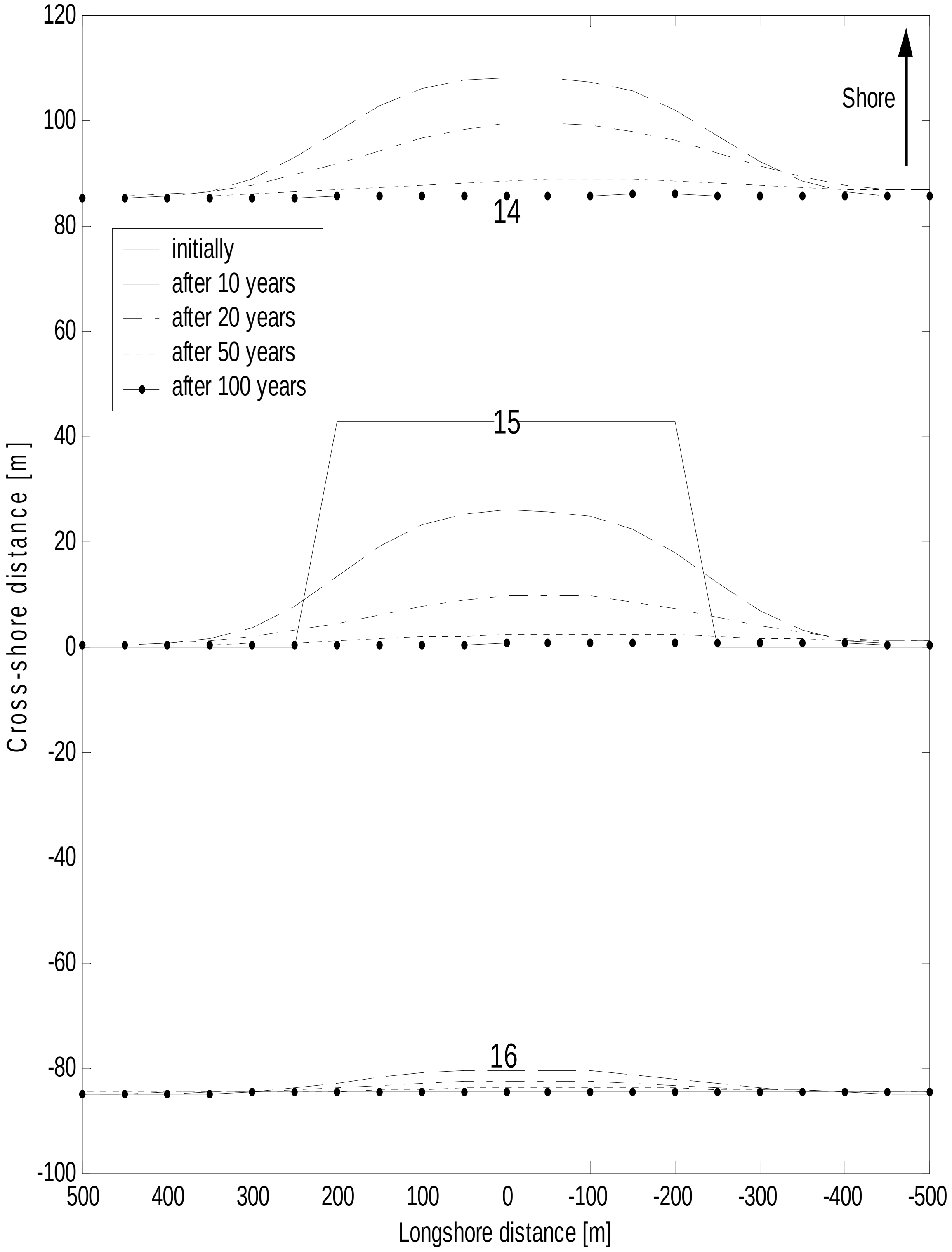

Figure 5.27. Planform evolution around the dredging contour at 15m depth in 100 years

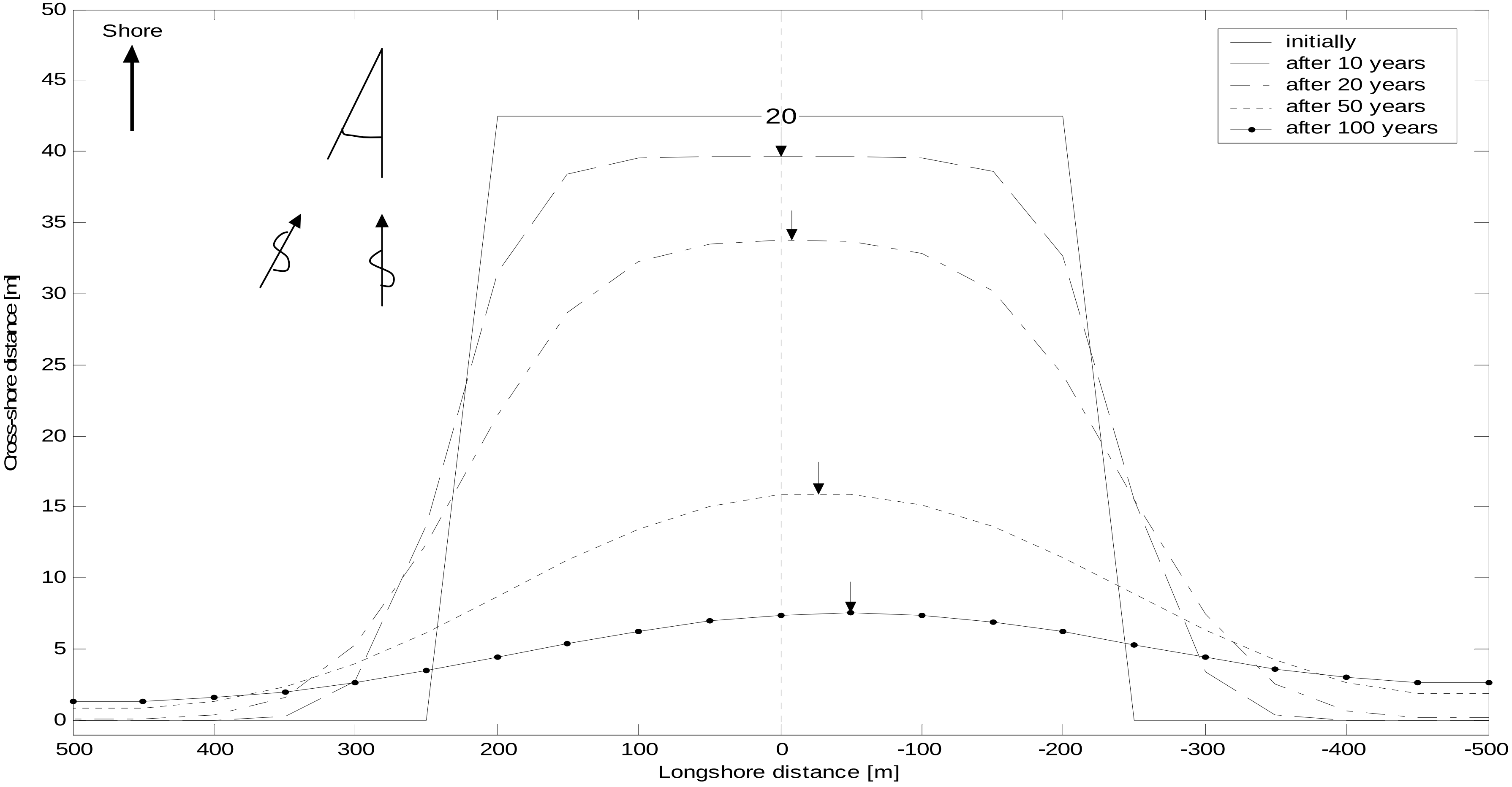

Figure 5.28. Planform evolution of the dredging contour at 20m depth in 100 years

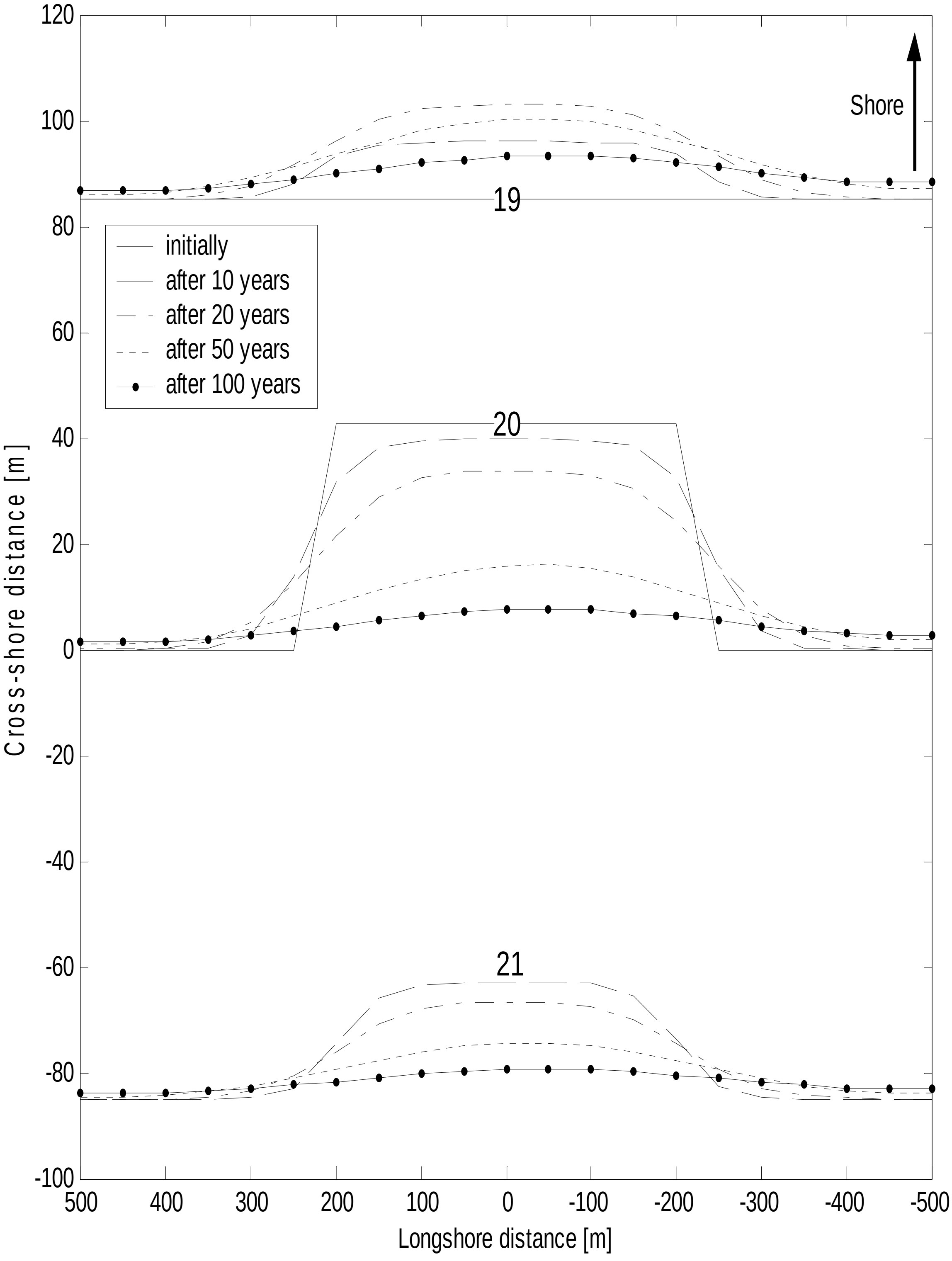

Figure 5.29. Planform evolution around the dredging contour at 20m depth in 100 years

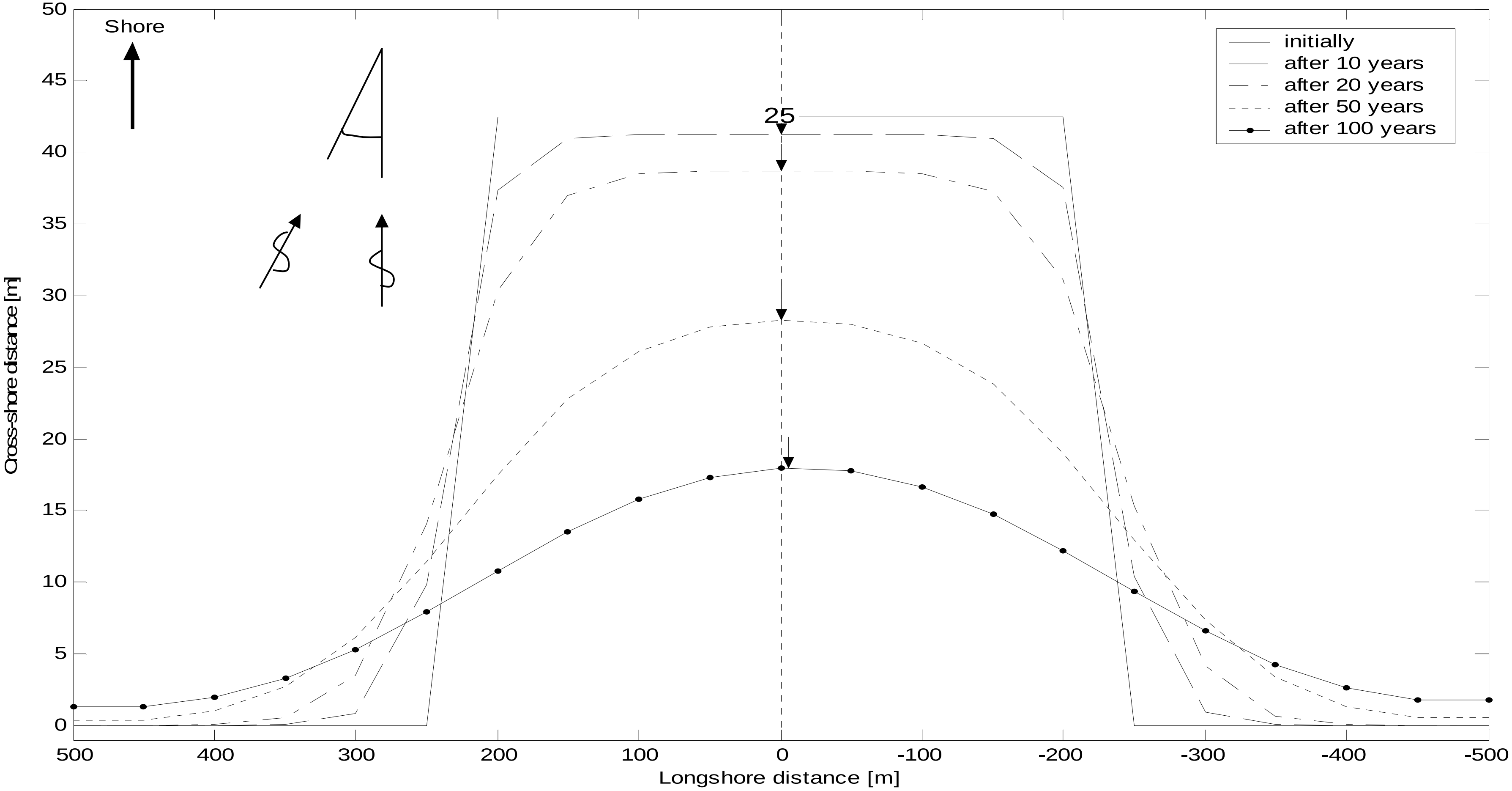

Figure 5.30. Planform evolution of the dredging contour at 25m depth in 100 years

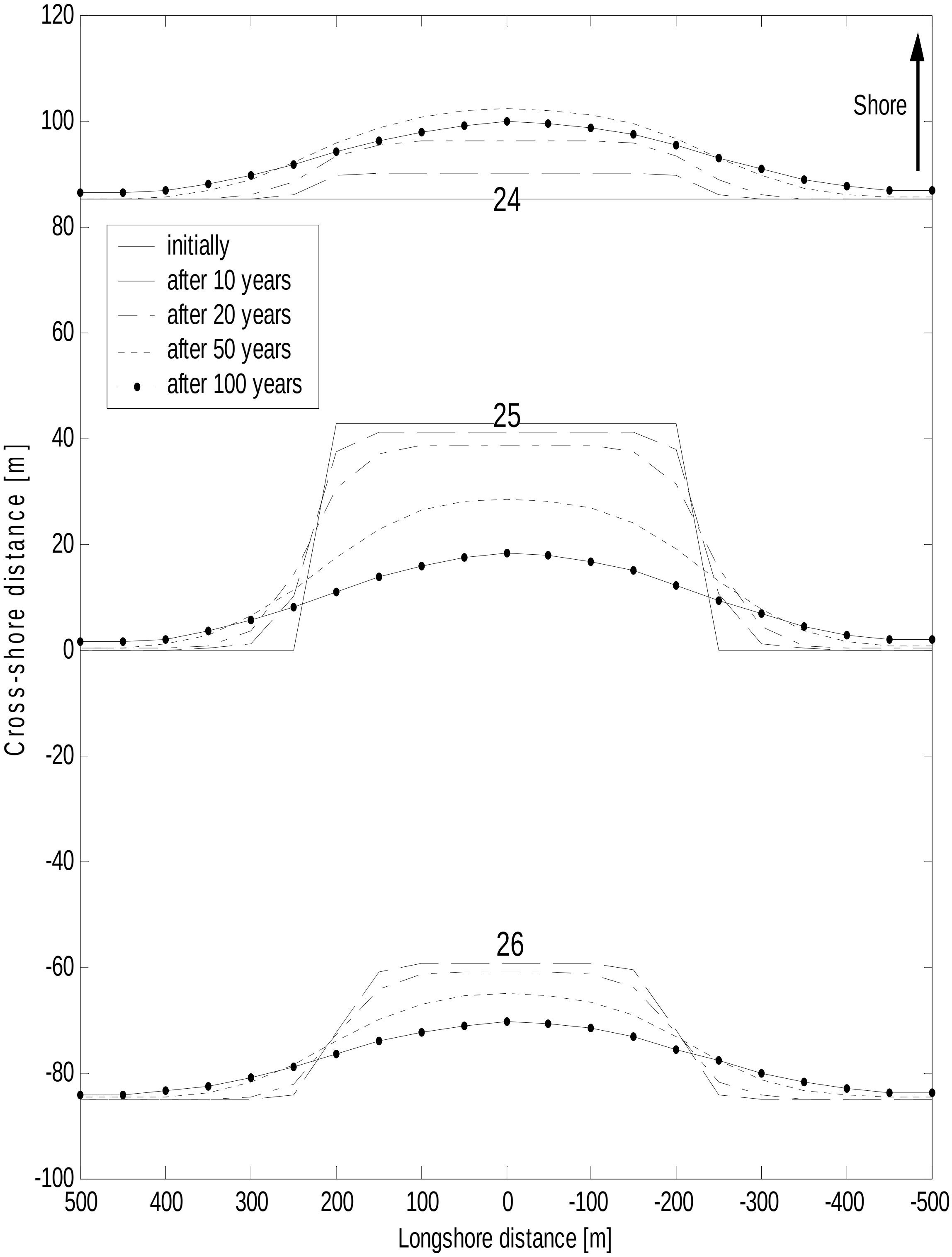

Figure 5.31. Planform evolution around the dredging contour at 25m depth in 100 years

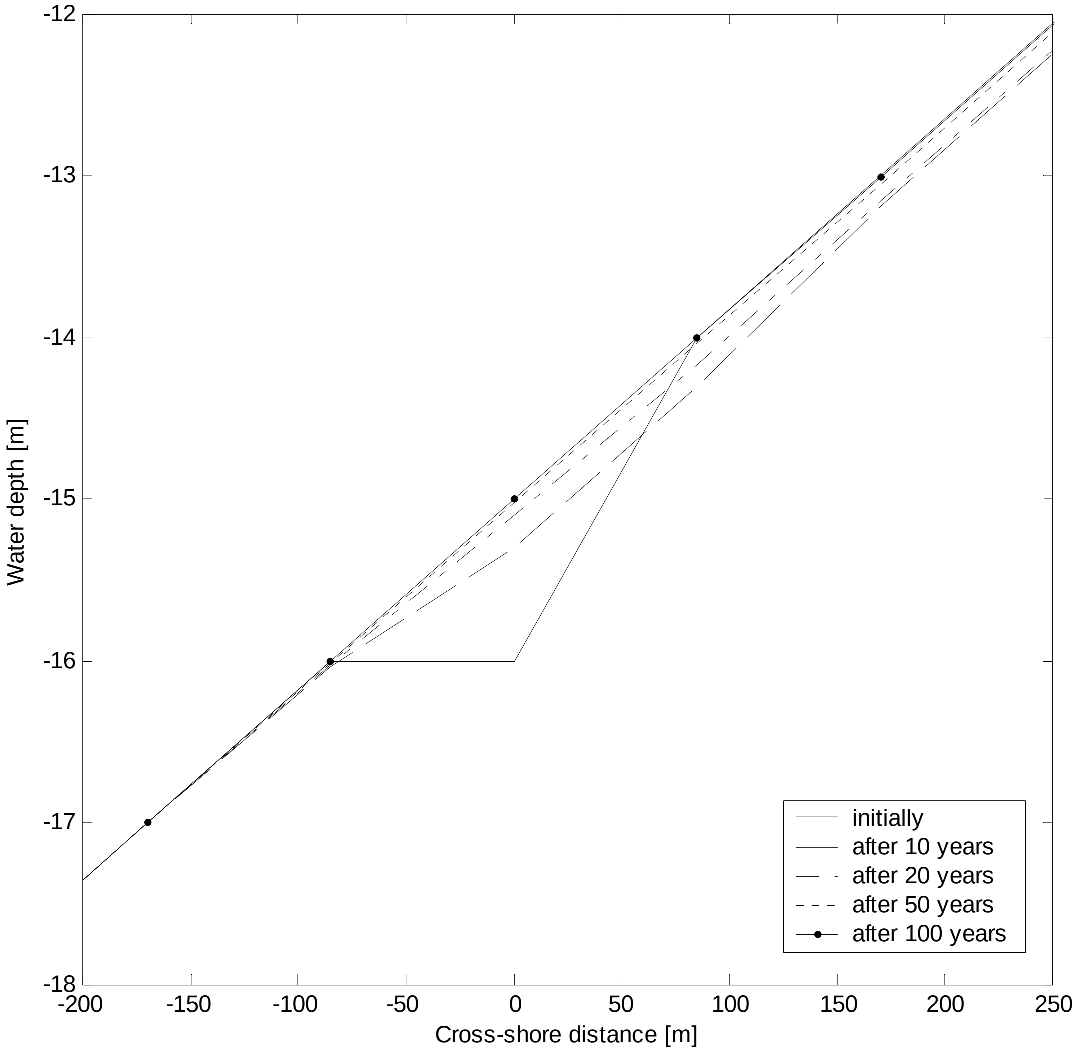

Figure 5.32. Profile evolution at 15m dredging depth in 100 years

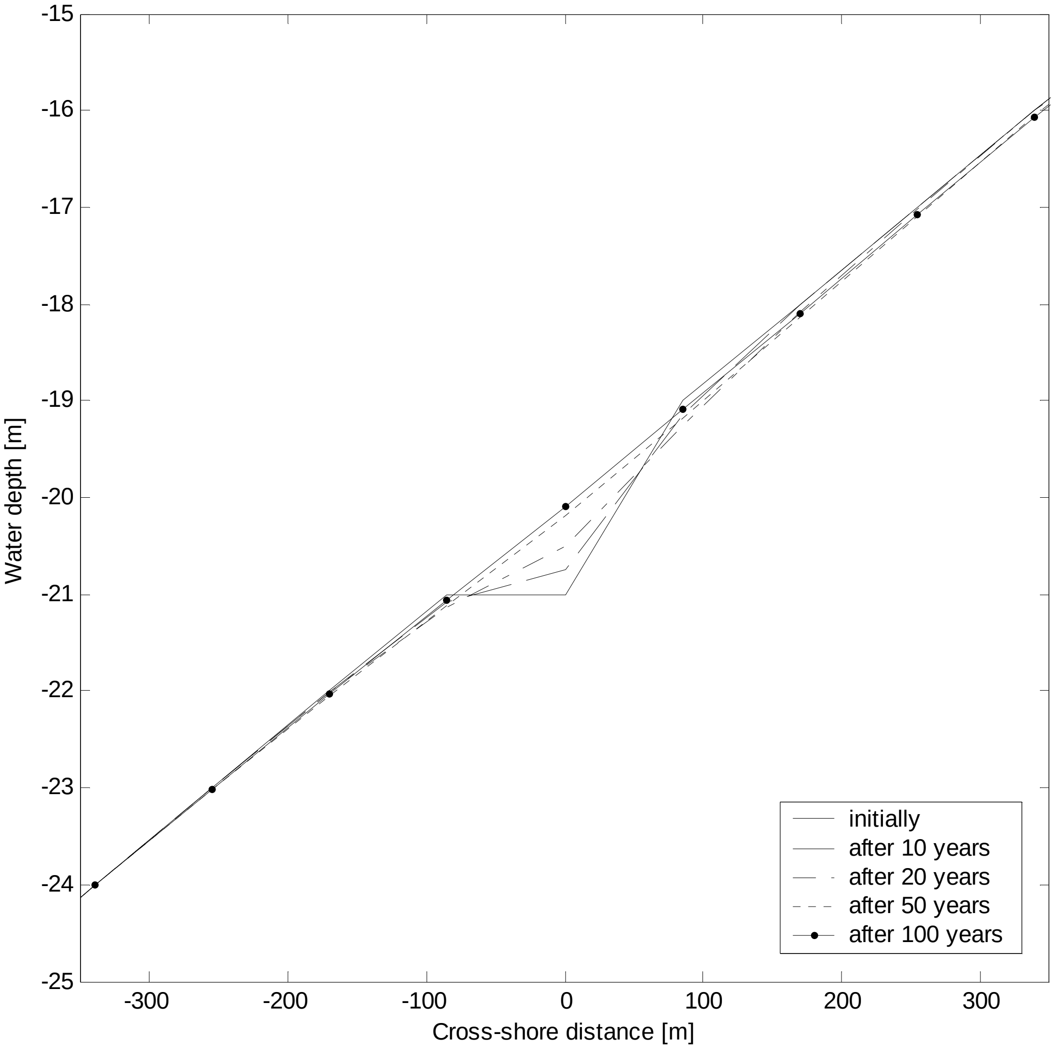

Figure 5.33. Profile evolution at 20m dredging depth in 100 years

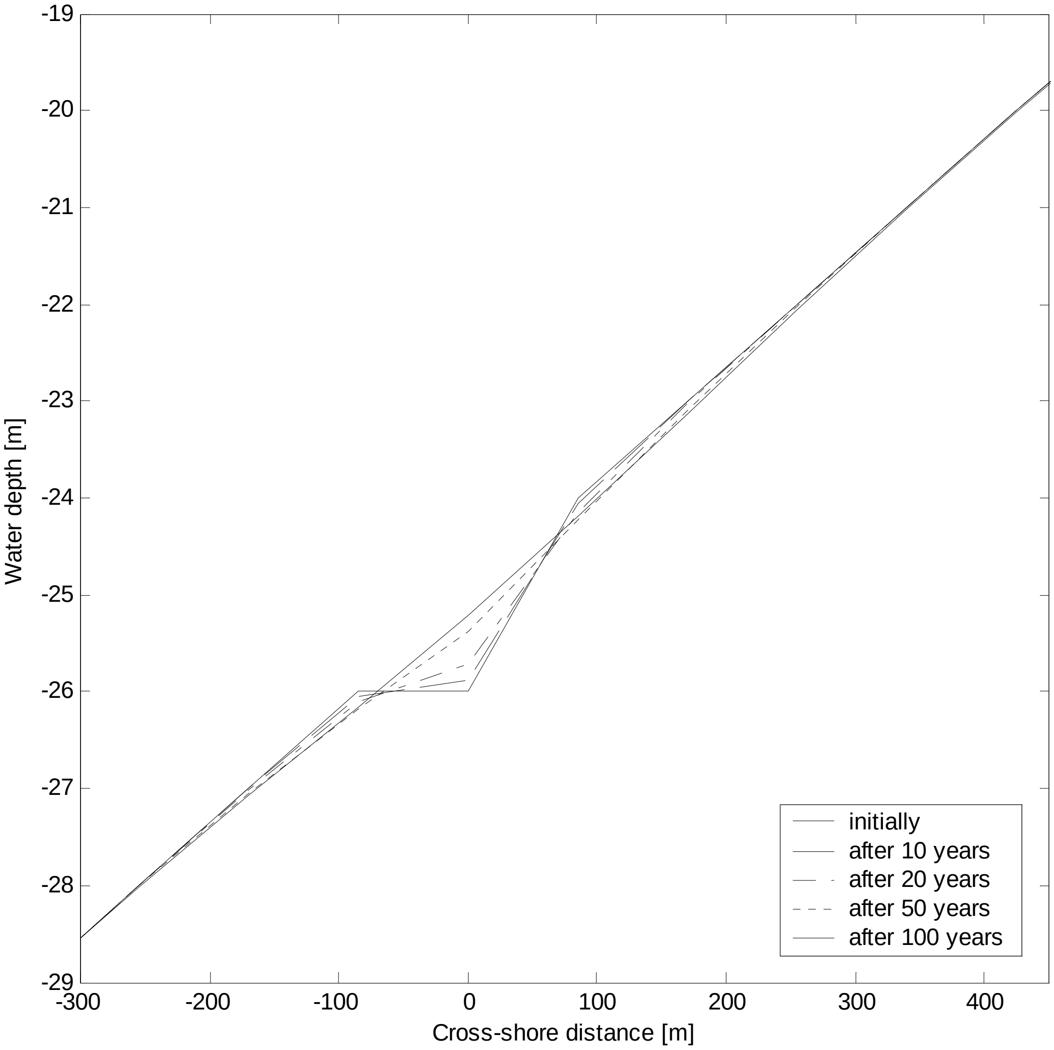

Figure 5.34. Profile evolution at 25m dredging depth in 100 years

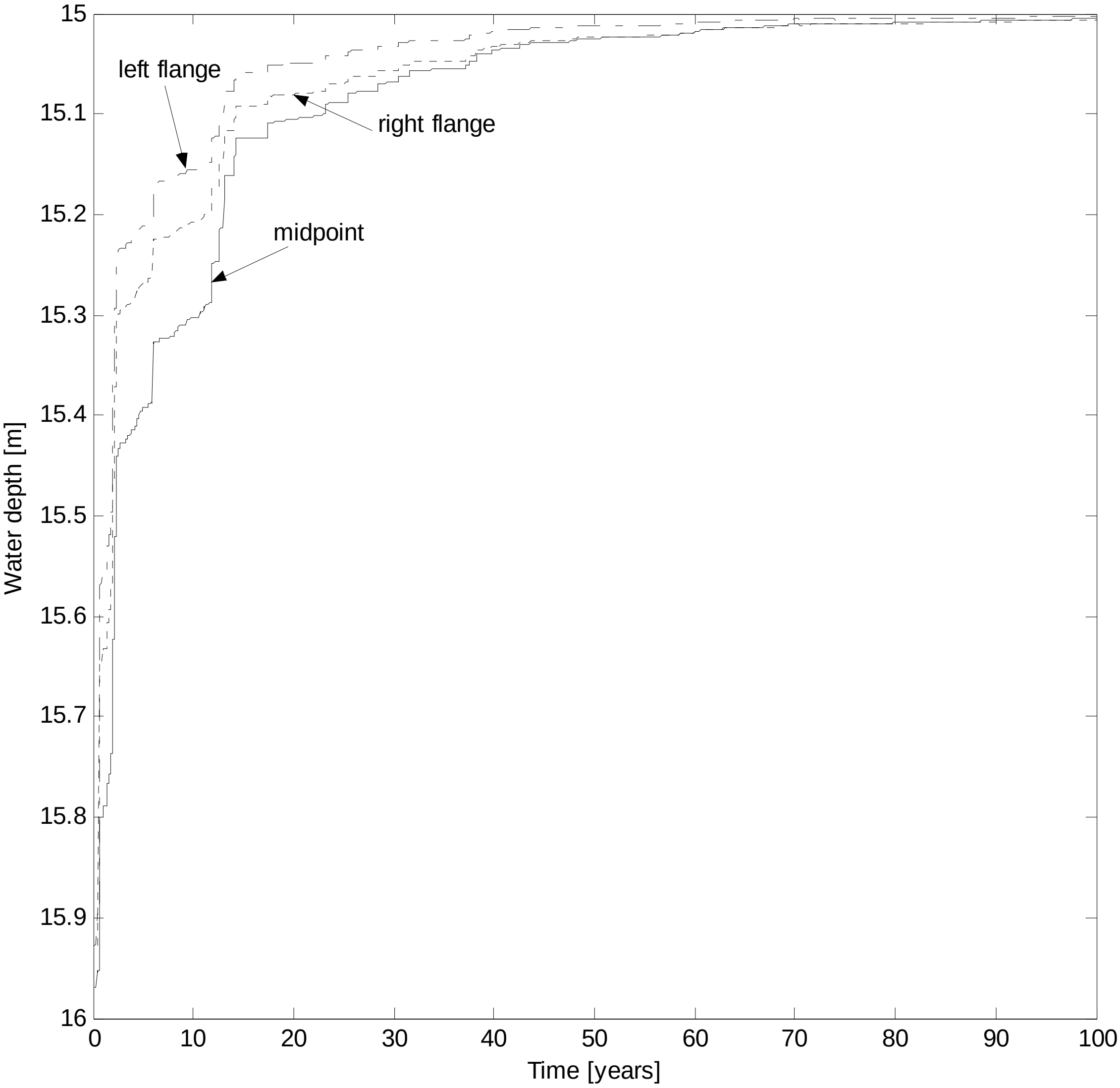

Figure 5.35. Backfilling rate of the midpoint and the flanges at 15 m dredging depth

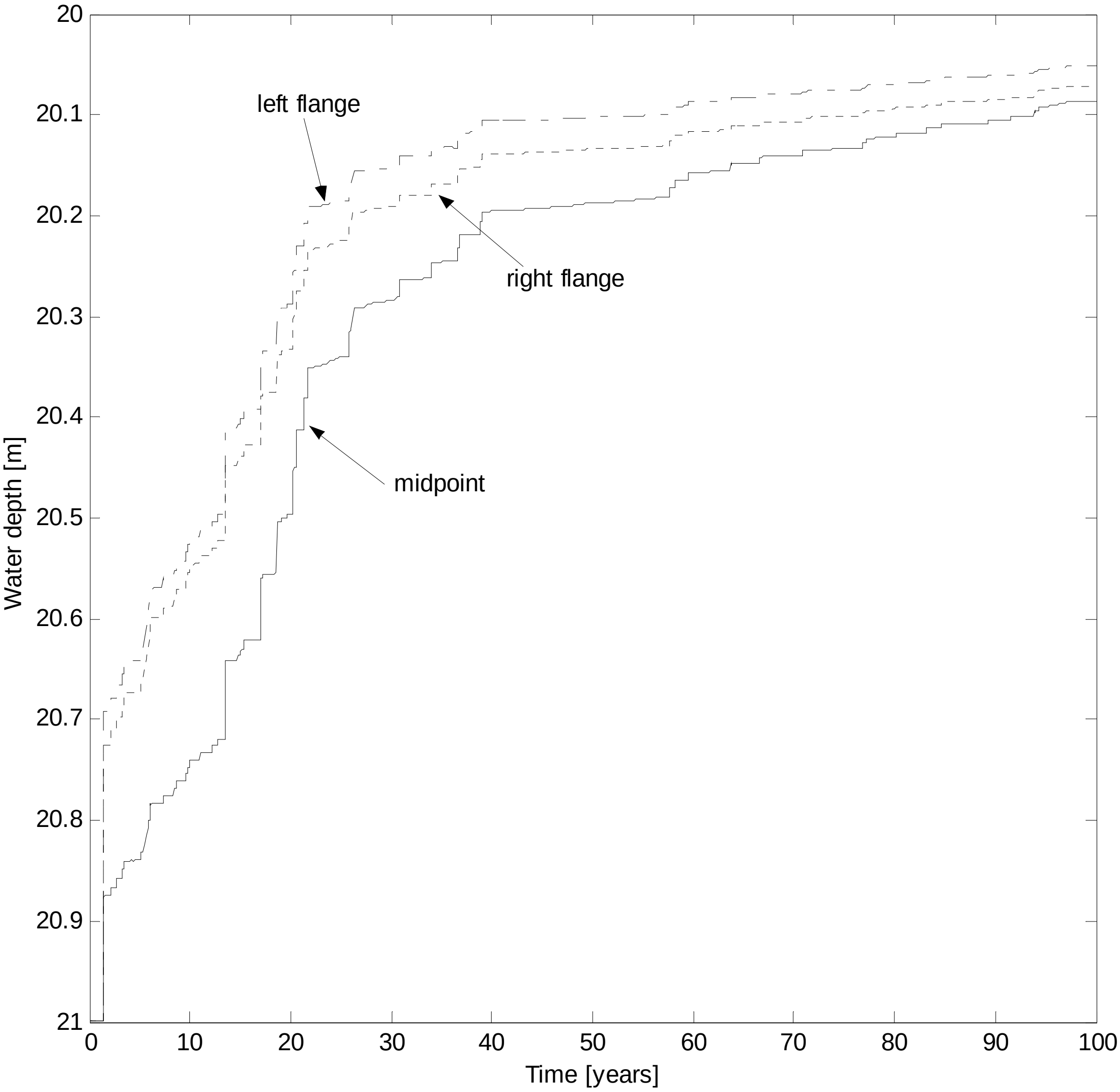

Figure 5. 36. Backfilling rate of the midpoint and the flanges at 20 m dredging depth

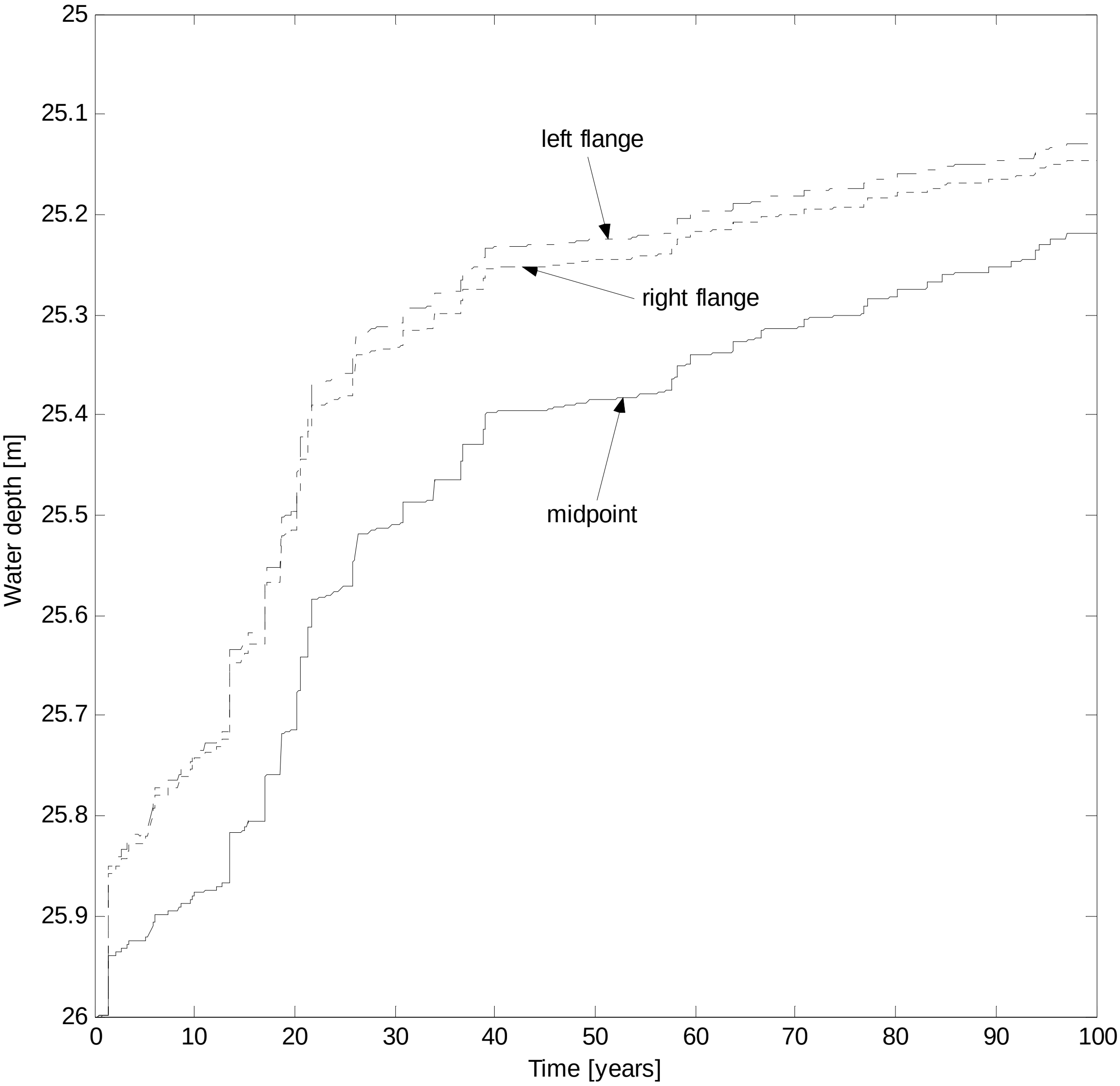

Figure 5.37. Backfilling rate of the midpoint and the flanges at 25 m dredging depth

Under the same wave climate, the rate of the backfilling becomes slower as the pit is dug more offshore. As opposed to the case where the waves are shore-normal, the pit moves in the opposite direction of the wave in the longshore as a result of waves with non-zero incidence. For shore-normal waves the pit diffuses symmetrically. Inspecting the neighboring contours reveals that at 15m dredging depth, the onshore neighbor is eroded substantially whereas the offshore neighbor is not that much eroded. However, at 25m dredging depth both neighbors are eroded almost by the same amount. The explanation for this is that the gradients of the cross-shore sediment transport decay very fast as the water becomes deeper, and after some depth the gradients are on the same order of magnitude on both sides of the pit. At these depths, both sides erode by almost the same amount. This phenomenon can be seen more easily by looking at the profile evolution plots.

5.3. Sensitivity Analysis

In order to make predictions about the time scales of the backfilling some quantitative indicators are needed. The amount of backfilling is represented by the half life, T_{50}, of the pit. It is the time at which the backfilled material within the dredged region reaches fifty per cent of the dredged sediment volume. The half life has to be some function of the wave characteristics, the dredging depth, the pit geometry, the initial bathymetry and the sediment characteristics.

Two different non-dimensional universal parameters are chosen to investigate the dependency of the half life on the wave characteristics and the dredging depth. These are the Ursell number, U_r, and the relative wave length, L_r, which are defined at the beginning of the chapter. All analyses here assume shore-normal waves. Sensitivity of the half life to the wave angle is very small and thus it is neglected. Figure 5.38 and Figure 5.39 show the dependency of the half life on the Ursell number and the relative wave length. The wave parameters and dredging depths used in the analysis are shown in Table 5.4.

Table 5.4. Variables for the analysis

Wave height [m]	Wave period [s]	Dredging depth [m]
1.0	5	15
1.5	6	17.5
2.0	**7**	**20**
3.0	8	22.5
5.0	9	25

The common parameters for the analyses are listed in Table 5.5.

Table 5.5. Bathymetric parameters for Figures 5.38 and 5.39

Beach slope	Length of pit	Width of pit	Depth of pit
1/85	500m	170m	1m

The dependency of the half life on the pit geometry is represented by the flatness of the pit, F_p, which is defined as

$$F_p = \frac{d_p}{\sqrt{L_p^2 + W_p^2}} \tag{5.3}$$

where d_p is the depth of the pit, L_p is the length of the pit and W_p is the width of the pit.

Figure 5.40 shows the dependency of the half life on the flatness of the pit. For this analysis the wave period and the dredging depth are taken to have fixed values that are written in bold case in Table 5.4. The bathymetric parameters for the analysis are listed in Table 5.6.

Table 5.6. Bathymetric parameters for Figure 5.40

Beach slope	Length of pit	Width of pit	Depth of pit
1/85	500m	170m	0.01-5m

The dependency of the half life on the initial bathymetry is not investigated here. The dependency of the half life on sediment size is incorporated in the transport equations indirectly through the empirical relations of the bed-load efficiency and the drag coefficient. They are functions of the sediment size, wave conditions and the water depth. Due to their empirical character, they are taken to have fixed values at all depths and at all wave conditions throughout the analyses ($\varepsilon_b=0.013, c_f=0.05$).

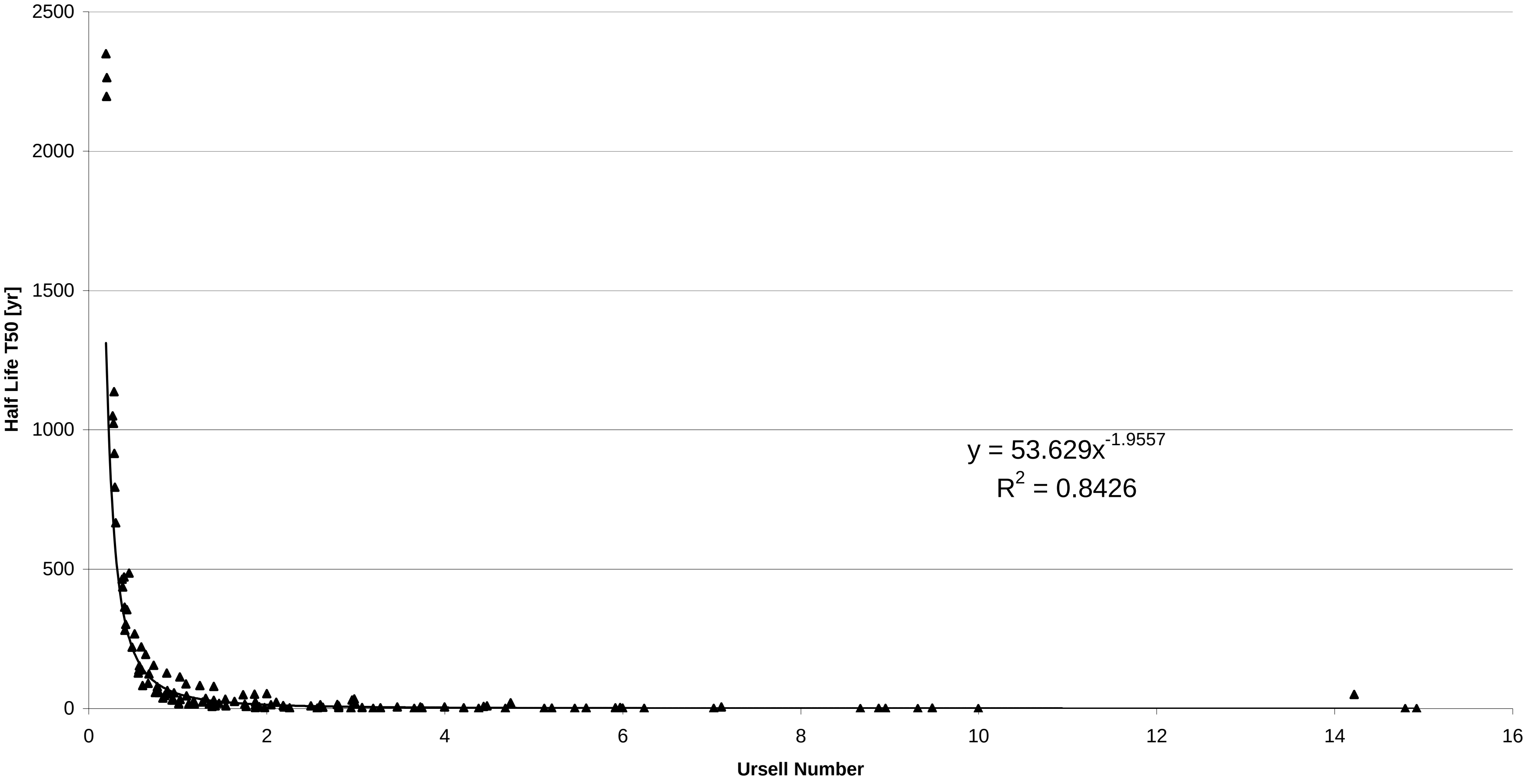

Figure 5.38. Half life of the pit as a function of the Ursell number

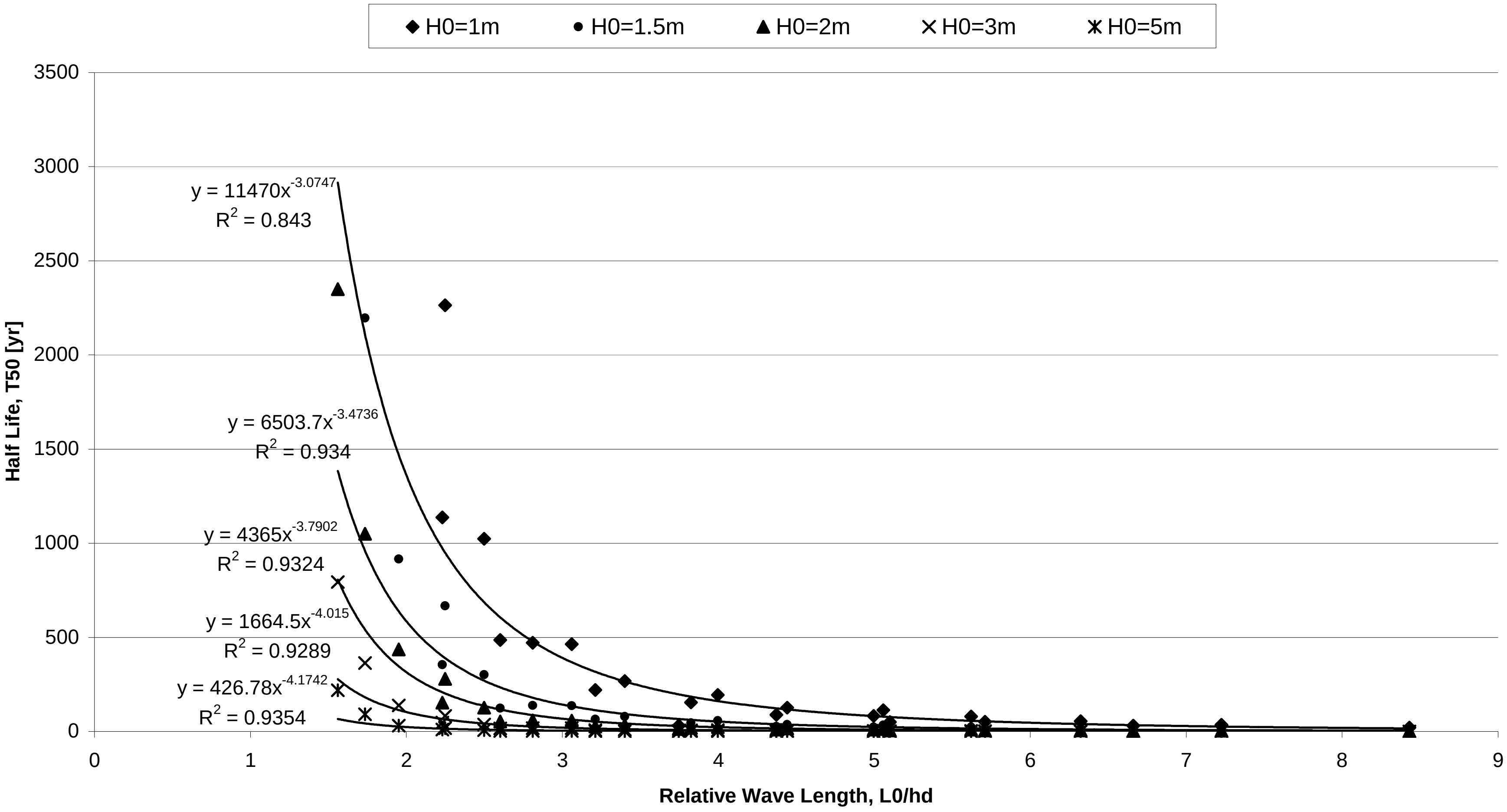

Figure 5.39. Half life of the pit as a function of the relative wave length

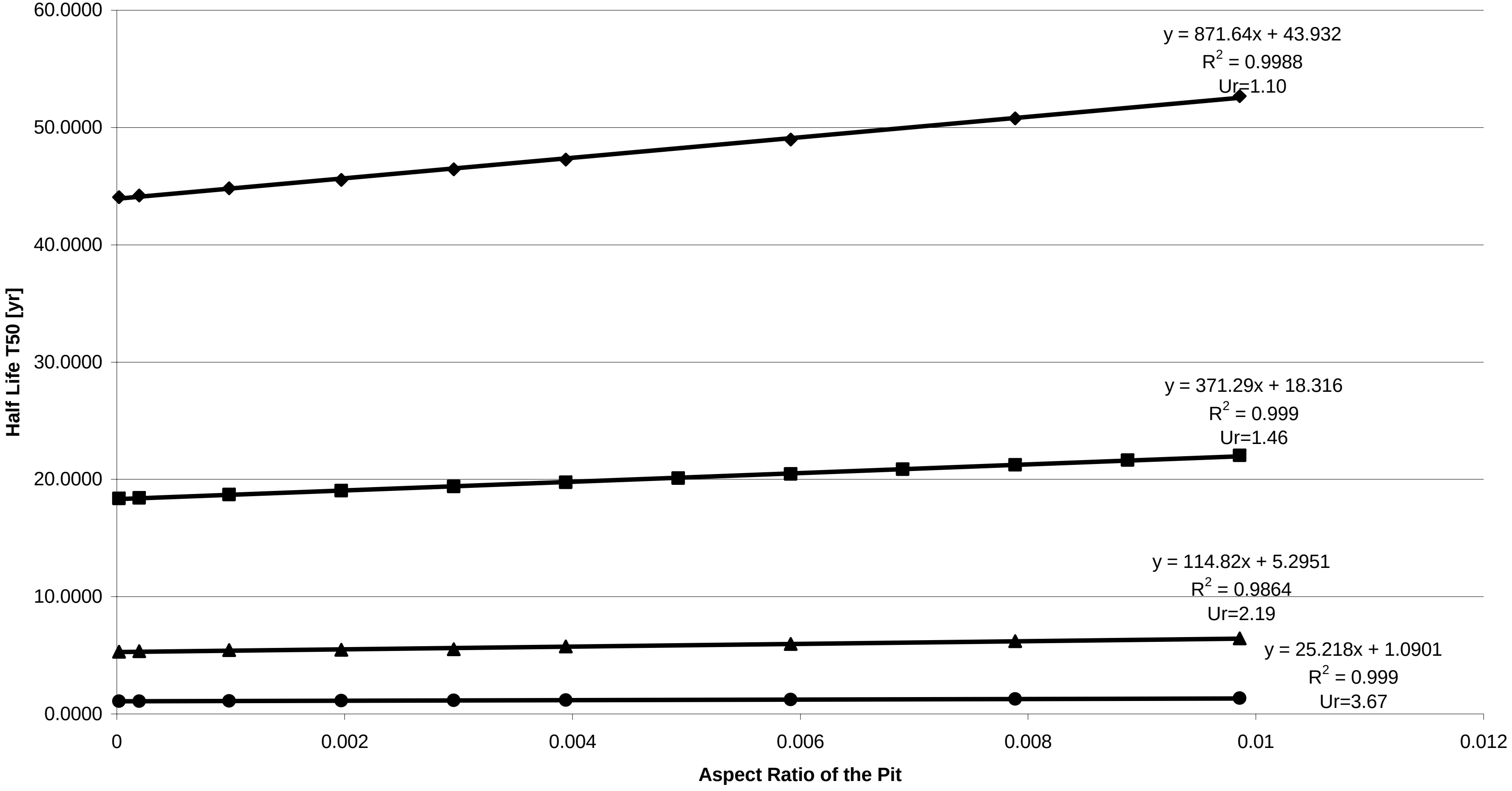

Figure 5.40. Half life of the pit as a function of the aspect ratio of the pit

5.4. Summary of Results

The perturbation in the dredge contour diffuses both in longshore and cross-shore directions. The rate of diffusion varies with wave characteristics and the dredging depth. The sensitivity analyses reveal that Ursell number, U_r; and relative wave length, L_r, are important parameters to control the half life of the pit, T_{50}. The relations between the half life and these parameters are power functions with negative exponents. The exponent and the coefficient vary depending on other model parameters indicating that these two are not the only parameters that control the process. However, the analytical dependency is unknown at this point, and the knowledge is limited to the range of numerical values investigated in the sensitivity analysis. Flatness of the pit affects the half life in a linear fashion. The effect of the magnitude of the wave angle on the half life is negligible.

The sediment transport is composed of two parts: the perturbation transport due to the pit only and the background transport due to the non-equilibrium bottom slopes. The sensitivity analysis is done in such a way where the effect of the background transport is filtered out from the results. However, the background transport is part of the total picture, which will be observed in practical applications. As the perturbation fades out, the magnitude of the perturbation transport decreases to the order of the magnitude of the background transport and at some point in time the background transport catches up with the perturbation transport. That point is identical in the test runs as the peak point in Figures 5.20-5.25. Due to the presence of the background transport, the dredging contour does not come to its original position before dredging. It moves onshore unless there is a sediment influx into the system.

The longshore extent of visible contour deformation is around a half of the pit length in each direction. The same extent in the cross-shore direction depends on the wave characteristics and the dredging depth.

For shore-normal waves, the diffusion of the dredging contour is symmetrical around the center axis of the pit. For oblique waves, the pit migrates in the direction of the wave. Oblique waves disturb the symmetry of the cross-shore transport but not the longshore transport. The updrift side of the pit rises more rapidly than the leeward side so that the pit migrates alongshore, towards the wave.

For Black Sea conditions simulated as randomly varying wave heights, periods, angles, and durations, the results indicate that the half life of the dredge pit is on the order of decades. On the other hand, the test runs using steady monochromatic waves with height similar to the average Black Sea conditions, predict much longer half lives. Under a realistic wave climate, i.e. random waves of different wave height, period, wave angle, and duration, the important waves that cause most of the backfilling are not the average waves but the seldom large waves associated with severe weather conditions.

6. CONCLUSIONS

The planform and profile evolutions of a dredge pit at the inner shelf are investigated under linear and nonlinear waves. A new transport model is developed based on Bailard and Inman (1981) by including the effect of a longshore bottom slope. Bed-load transport is assumed to dominate at water depths far beyond the surf zone. The model assumes weak longshore current relative to the wave orbital velocity, non-breaking waves, plane bed, constant drag coefficient, constant bed-load efficiency, quasi-steady sediment transport, and cohesionless bed-load sediment transport.

A non-linear wave theory is needed. The velocity induced component of the sediment transport vector vanishes when linear wave theory is employed. This means that the sediment is transported only offshore. The model could not be simplified to an analytically solvable level. Thus the primitive equations are solved numerically for a three-dimensional dredged bathymetry.

Three different cases are investigated. The first is a pit on a bathymetry, which was in equilibrium before dredging. The bathymetry is subjected to the continuous attack of a monochromatic wave. The second is an imaginary pit on a measured bathymetry in the southwestern Black Sea that was under the attack of the typical wave spectrum for this region. The third case is a sensitivity analysis conducted on a planar beach attacked by monochromatic waves.

Pits dredged at the inner shelf (10m-30m water depth) are filled back with sand. This sand is transported from both adjacent areas in the longshore and on/offshore sides of the pit by asymmetric waves. Oblique waves causes the pit to migrate alongshore in the wave direction.

The rate of backfilling is quantified by a parameter called the “half life, T_{50}” of the pit. It is defined as the time at which the backfilled material within the original limits of dredged region reaches fifty per cent of the dredged sediment volume Half life is found to be a function of the non-dimensional parameters the Ursell number, U_r, the relative wave length, L_r, and the flatness of the pit, F_p. However, an analytical relation could not be established. Half life is found to be inversely proportional to the Ursell number and the relative wave length, and it is linearly proportional to the flatness of the pit.

The waves which cause most of the backfilling are not the yearly average waves but the more seldom higher waves. Thus the local wave climate at the project site should be thoroughly analyzed before dredging. Based on this analysis, the dredging depth should be chosen carefully to satisfy the desired project half life. The presence of the pit induces a perturbation transport and thus backfilling is inevitable at the inner shelf. However, the timescale for the backfilling will vary greatly depending on the wave climate at the project site. As the pit fills from the surrounding, the dredging contour moves onshore. The extent of visible contour deformation depends on the pit location and the wave parameters. The sensitivity analyses presented in this thesis seems to be very promising. The Ursell number is an important parameter to predict the evolution of a dredge pits. However, additional work is required to define this relationship more accurately.

APPENDIX A: MATLAB CODES

```
clear all
close all
tic

%CONSTANTS

g=9.81;         % gravitational acceleration, [m/s^2]
ro=1000;        % density of water, [kg/m^3]
kappa=0.78;     % breaker index
Cf=0.025;       % drag coefficient
epsb=0.13;      % bed load efficiency according to Bagnold
p=0.4;          % porosity of bottom
s=2.65;         % specific gravity of sediment
phi=32;         % angle of repose of sand
D=0.3;          % mean diameter of sand

%INPUT

H0in=[1.04, 1.04, 3.02, 3.02, 5.02, 5.02];
Tin=[5.2, 5.2, 7.5, 7.5, 9.5, 9.5];
alfa0in=[3, 33, 5, 28, 5, 28];
vam=0;
hpit=20;
b=15:25;
moff=1/85;
dt=5*86400;       % time step, [s]
daysim=3600;      % simulation duration (real-time), [days]
tp=10;
dh=0.5;
ymax=1000;
dy=50;
dpit=1;
lp=500;
pr=[0.4685, 0.4685, 0.0205, 0.0288, 0.0055, 0.0082];

% DATA MANIPULATION

dx=dh/moff;
phi=phi/180*pi;                  % angle of repose, [rad]
alfa0in=alfa0in./180*pi;
K=Cf*epsb/g/tan(phi)/(s-1)/(1-p);    % transport coefficient
daycont=dt/86400;                % data storage interval (real-time), [days]
dayplot=tp*360:tp*360:daysim;       % plot time (real-time), [days]
```

```
tmax=daysim*24*3600;                % simulation duration (real-time), [s]
nt=daysim*24*3600/dt;              % max # of time steps
tplot=dayplot*24*3600/dt;          % time step of plot
klimachange=nt*cumsum(pr);

%BATHYMETRY

yin=-ymax/2:dy:ymax/2;
ny=length(yin);
ip=round((ny/2)-lp/2/dy+1):round((ny/2)+lp/2/dy-1);

[x0,h0,jp]=batkar(moff,dh,dx,hpit,dpit,ny,ip);

[ny,nx0]=size(x0);

y0=flipud(repmat(yin',1,nx0));

ib1=min(ip);
ib2=max(ip);
im=(ib1+ib2)/2;

xs=(x0(:,1:nx0-1)+x0(:,2:nx0))/2;
ys=(y0(1:ny-1,:)+y0(2:ny,:))/2;
h=h0;

warning off MATLAB:divideByZero

d=waitbar(0,'Bekle bi!');
x=x0;
y=y0;
nx=nx0;
hc1(1)=h0(ib1,jp);
hcm(1)=h0(im,jp);
hc2(1)=h0(ib2,jp);

figure(1)
contour(y,max(max(x0))-x,h,b),hold on
figure(2)
plot(max(max(x0))-x((ny+1)/2,:),-h((ny+1)/2,:)),hold on
for it=1:1
   waitbar(it/nt)

   H0=H0m(it);
   T=Tm(it);
   alfa0=alfa0m(it);
   om=2*pi./T;

   hqx=griddata(x,y,h,xs,y(:,1:nx-1));
```

```
   hqy=griddata(x,y,h,x(1:ny-1,:),ys);
   hgam=griddata(x,y,h,xs(1:ny-1,:),ys(:,1:nx-1));

   % wave angles
   alfaqx=asin(tanh(disperse(T,hqx)).*sin(alfa0));
   alfaqy=asin(tanh(disperse(T,hqy)).*sin(alfa0));

   % slopes
   gama=zeros(ny,nx-1);
   gama(2:ny-1,:)=-atan((hgam(2:ny-1,:)-hgam(1:ny-2,:))/dy);
   gama(1,:)=gama(2,:);
   gama(ny,:)=gama(ny-1,:);
   dhdx=-(h(:,2:nx)-h(:,1:nx-1))/dx;
   dhdy=-(h(2:ny,:)-h(1:ny-1,:))/dy;

   % velocity moments
   [u3qx,uA3qx,u2qx]=moments(H0,T,hqx);
   [u3qy,uA3qy,u2qy]=moments(H0,T,hqy);
%
%    % wave induced current
%    vqx=current(H0,T,alfa0,xs,hqx,moff,Cf);
%    vqy=current(H0,T,alfa0,x,hqy,moff,Cf);
%
%    %total current
%    vtqx=vam+vqx;
%    vtqy=vam+vqy;

%    % sediment transport rates
%    qx=K*(u3qx.*cos(alfaqx)+u2qx.*vtqx.*sin(2*alfaqx)-
uA3qx.*dhdx./tan(phi)./cos(gama));
%
qy=K*(u3qy.*sin(alfaqy)+u2qy.*vtqy.*(1+2*(sin(alfaqy)).^2)+uA3qy.*dhdy/tan(phi));
%
    % sediment transport rates
   qx=K*(u3qx.*cos(alfaqx)-uA3qx.*dhdx./tan(phi)./cos(gama));
   qy=K*(u3qy.*sin(alfaqy)+uA3qy.*dhdy/tan(phi));

   hn=zeros(ny,nx);
   hn(2:ny-1,2:nx-1)=h(2:ny-1,2:nx-1)+dt*((qx(2:ny-1,2:nx-1)-qx(2:ny-1,1:nx-
2))/dx+(qy(1:ny-2,2:nx-1)-qy(2:ny-1,2:nx-1))/dy);
   hn(:,1)=h0(:,1);%+(hn(:,2)-h(:,2));
   hn(:,nx)=h0(:,nx);%+(hn(:,nx-1)-h(:,nx-1));
   hn(1,:)=hn(2,:);
   hn(ny,:)=hn(ny-1,:);

   [av ro]=find(hn<0);
   if isempty(av)
      h=hn;
```

```
   else break, end

   hc1(it+1)=hn(ib1,jp);
   hcm(it+1)=hn(im,jp);
   hc2(it+1)=hn(ib2,jp);
   hdiff(it+1)=abs(hn(im,jp)-hn(ib1,jp));

   for zz=1:length(dayplot)
      if it==tplot(zz)
         time=it*dt/86400/360;
         figure(1)
         contour(y,max(max(x0))-x,h,b),hold on
         figure(2)
         plot(max(max(x0))-x((ny+1)/2,:),-h((ny+1)/2,:)),hold on
         for j=1:nx
            for i=1:ny
               kk(i,j)=(i-1)*nx+j;
               hp(kk(i,j))=h(i,j);
               xp(kk(i,j))=x(i,j);
               yp(kk(i,j))=y(i,j);
            end
         end
         fid = fopen(sprintf('%3.0f_years.txt',time),'w+');
         for i=1:nx*ny
            fprintf(fid,' %9.4f %9.4f %9.4f\n',yp(i),xp(i),hp(i));
         end
         fclose(fid);
      end
   end

end
close(d)
t=toc/60

fid = fopen(sprintf('evolution in %3.0f_years.txt',time),'w+');
for i=1:length(hcm)
   fprintf(fid,' %9.4f %9.4f %9.4f %9.4f\n',hc1(i),hcm(i),hc2(i), hdiff(i));
end

fclose(fid);

figure(1)
[C,hh]=contour(y,max(max(x0))-x,h,b);
clabel(C,hh);
ylabel('Cross-shore distance [m]')
xlabel('Longshore distance [m]')
title(sprintf('Planform evolution in %3.0f years, H0=%1.0f, T=%1.1f',time,H0,T))
```

```
figure(2)
xlabel('Cross-shore distance [m]')
ylabel('Water depth [m]')
title(sprintf('Profile evolution in %3.0f years, H0=%1.0f, T=%1.1f',time,H0,T))


figure
plot([0 (1:nt*dt/3600/24/daycont)*daycont/360],hcm)
hold on
plot([0 (1:nt*dt/3600/24/daycont)*daycont/360],hc1,'r--')
hold on
plot([0 (1:nt*dt/3600/24/daycont)*daycont/360],hc2,'g-.')
hold on
plot([0 (1:nt*dt/3600/24/daycont)*daycont/360],hpit*ones(1,length([0
(1:nt*dt/3600/24/daycont)*daycont/360])),'k')
legend('middle of the pit','left corner of the pit','right corner of the pit','original depth',3)
xlabel('Time [years]')
ylabel('Water depth [m]')
title(sprintf('Time history of backfilling, H0=%1.0f, T=%1.1f',H0,T))
--------------------------------------------------------------------------------------------------------
--------------------------------------------------------------------------------------------------------
function [x,h,hin,jp]=batkar(moff,dh,dx,hpit,dpit,ny,ip)

h=15:dh:35;
lh=length(h);
hi=flipud(h);
x=0:dx:(length(h)-1)*dx;
jp=find(hi==hpit);

x0=repmat(x,ny,1);
h0=repmat(hi,ny,1);
hin=fliplr(h0);
h0(ip,jp)=h0(ip,jp)+dpit;

x=x0;
h=fliplr(h0);
jp=lh-jp+1;
--------------------------------------------------------------------------------------------------------
--------------------------------------------------------------------------------------------------------
function [u3,uA3,u2]=moments(H0,T,h)
kappa=0.78;
g=9.81;
[ny nx]=size(h);
kh=disperse(T,h);
k=kh./h;
Ks=sqrt(2*cosh(kh).^2./(2*kh+sinh(2*kh)));
H=H0*Ks;
[i,j]=find(isnan(H));
```

```
H(i,j)=0;
for ih=1:nx
   for iy=1:ny
      if H(iy,ih)>h(iy,ih)*kappa
         H(iy,ih)=h(iy,ih)*kappa;
      end
   end
end

om=2*pi/T;
C=om./k;
um=om*H./sinh(kh)/2;
a1=um;
a2=0.75*um.^2./(C.*(sinh(kh)).^2);
A=a1./a2;
dt=T/1000;
t=0:dt:T;
for ih=1:nx
   for iy=1:ny
      u=a1(iy,ih)'*cos(om*t)+a2(iy,ih)'*cos(2*om*t);
      uA3(iy,ih)=trapz(((abs(u)).^3)')*dt/T;
   end
end
[iv jv]=find(isnan(uA3));
uA3(iv,jv)=0;

L=g*T^2/2/pi*tanh(kh);
UR=L.^2.*H./h.^3;
[ib ne]=find(UR<26);

u3=zeros(ny,nx);
u3(ib,ne)=0.75*a2(ib,ne).^3.*A(ib,ne).^2;
[iv jv]=find(isnan(u3));
u3(iv,jv)=0;

u2=a2.^2/2.*(A.^2+1);

u3=u3;
uA3=uA3;
u2=u2;
--------------------------------------------------------------------------------------------------------------
--------------------------------------------------------------------------------------------------------------
function[khf]=disperse(T,h)
g=9.81;
err=0.001;%error criteria
om=2*pi/T;
s0=om^2*h./g;
khi=s0./sqrt(tanh(s0));%initial guess (mostly used)
```

```
for iter=1:inf,
   khf=khi-(khi.*tanh(khi)-s0)./(tanh(khi)+(khi./(cosh(khi).^2)));
   if max(max(abs(khi-khf)))<err,break,end
   khi=khf;
end
clear khi s0 err iter
```

REFERENCES

Bagnold, R. A., 1963, "Mechanis of Marine Sedimentation", *The Sea*, Vol. 3, edited by M.N. Hill, Interscience, New York, pp. 507 - 528.

Bagnold, R. A., 1966, "*An Approach to the Sediment Transport Problem From General Physics*", Professional Paper 422-1, U.S. Geological Survey, Washington.

Bailard, J. A., 1981, "An Energetics Total Load Sediment Transport Model For a Plane Sloping Beach", *Journal of Geophysical Research*, Vol. 86, No C11, pp. 10,938 - 10,954, November 20.

Bailard, J. A., and D. L.Inman, 1981, "An Energetics Bedload Model for a Plane Sloping Beach: Local Transport", *Journal of Geophysical Research*, Vol. 86, No C3, pp. 2035 - 2043, March 20.

Dean, R. G., and R. A. Dalrymple, 1984, *Water Wave Mechanics for Engineers and Scientists,* Prentice Hall Inc.

Dean, R. G., and R. A. Dalrymple, 2002, *Coastal Processes with Engineering Applications,* Cambridge University Press.

Demir, H., 2002, *Effecst of DredgedHoles on the Shoreline Change in the Black Sea*, M.S. Thesis, Boğaziçi University.

Demir, H, E. N. Otay, P. A. Work, and O. S. Börekçi, 2004, "Impacts of Dredging on Shoreline Change", *Journal of Waterway, Port, Coastal and Ocean Engineering*, Vol. 130, No 4, pp. 170-178, July 1.

Fredsøe, J., and R. Deigaard, 1992, *Mechanics of Coastal Sediment Transport,* World Scientific Publishing Co. Pte. Ltd.

Inman, D. L., M. H. S. Elwany, and S. A. Jenkins, 1993, “Shorerise and Bar-Berm Profiles on Ocean Beaches”, *Journal of Geophysical Research*, Vol. 98, No C10, pp. 18,181 - 18,199, October 15.

Jensen, J. H., E. Ø. Madsen, and J. Fredsøe, 1999, “Oblique Flow over Dredged Channels. II: Sediment Transport and Morphology”, *Journal of Hydraulic Engineering*, Vol. 125, No 11, pp. 1190-1198, November.

Jensen, J. H., and J. Fredsøe, 2001, “Sediment Transport and Backfilling of Trenches in Oscillatory Flow”, *Journal of Waterway, Port, Coastal and Ocean Engineering*, Vol. 127, No 5, pp. 272-281, September/October.

Kobayashi, N., 1982, “Sediment Transport on a Gentle Slope due to Waves”, *Journal of Waterway, Port, Coastal and Ocean Engineering*, Vol. 108, No WW3, pp. 254-271, August.

Larson, M., N. C. Kraus, and R.A. Wise, 1999, “Equilibrium Beach Profiles under Breaking and Non-breaking Waves”, *Coastal Engineering*, Vol. 36, pp. 59-85.

Perlin, M. and R. G. Dean, 1983, *A Numerical Model to Predict Simulate Sediment Transport in the Vicinity of Coastal Structures*, MR83-10, U.S. Army Corps of Engineers, Coastal Engineering Research Center.

Roelvink, J. A., and M. J. F. Stive, 1989, “Bar-Generating Cross-Shore Flow Mechanisms”, *Journal of Geophysical Research*, Vol. 94, No C4, pp. 4785 - 4800, April 15.

Sand Pit Project, EC Fifth Framework Project No. EVK3-2001-00056, http://sandpit.wldelft.nl

Stive, M. J. F., 2001, “A Model for Cross-shore Sediment Transport”, *20th International Conference on Coastal Engineering*, Taipei, November 9-14 1986.

U.S. Army Corps of Engineers, 2002, *Coastal Engineering Manual*, http://users.coastal.ufl.edu/~sheppard/eoc6430/Coastal_Engineering_Manual.htm

Van Rijn, L. C., 1986, “Sedimentation of Dredged Channels By Currents and Waves”, *Journal of Waterway, Port, Coastal and Ocean Engineering*, Vol. 112, No 5, pp. 541-559, September.

REFERENCES NOT CITED

Bakker, W. T, “ The Dynamics of a Coast With a Groyne System”, *Proceedings of the Eleventh Conference on Coastal Engineering*, pp. 492 - 517, ASCE., 1968.

Inman, D. L., and R. A. Bagnold, “Littoral Processes”, *The Sea*, Vol. 3, edited by M.N. Hill, Interscience, New York, pp. 529 - 553, 1963.

Jensen, J. H., E. Ø. Madsen, and J. Fredsøe, “Oblique Flow over Dredged Channels. I: Flow Description”, *Journal of Hydraulic Engineering*, Vol. 125, No 11, pp. 1181-1189, November, 1999.

Perlin, M., *A Numerical Model to Predict Beach Planforms in the Vicinity of Littoral Barriers*, M.S. Thesis, University of Delaware, 1978.

Ribberink, J. S., and A. A. Al-Salem, “Sediment Transport in scillatory Boundary Layers in Cases of Rippled Beds and Sheet Flow”, *Journal of Geophysical Research*, Vol. 99, No C6, pp. 12,707 - 12727, June 15, 1994.

Roelvink, J. A., and I. Brøker, “Cross-shore Profile Models”, *Coastal Engineering*, Vol. 21, pp. 163 - 191, 1993.

Schoonees, J. S., and A. K. Theron, “Evaluation of 10 Cross-shore Sediment Transport Morphological Models”, *Coastal Engineering*, Vol. 25, pp. 1 - 14, 1995.